The author(s) below used Federal funds provided by the U.S. Department of Defense and prepared the following report:

Document Title:	Material Designs Toward a Synthetic Cannabinoid Sensor
Author(s):	Mark H. Griep, Abby L. West, Michael S. Sellers, Alexis M. Fakner, Joseph Dougherty, John K. Northup, Klaus Gawrisch, Shashi P. Karna
Document No.:	NCJ 249873
Date Received at NCJRS:	May 2016
MIPR Number:	DWAM 3 0521

This report has not been published by the U.S. Department of Defense or the U.S. Department of Justice. To provide better customer service, NCJRS has made this federally funded grant report available electronically.

The views and conclusions contained in this document are those of the authors and should not be interpreted as representing the official policies, either expressed or implied, of the Army Research Office, the Defense Forensic Science Center, U.S. Department of Justice or the U.S. Government.

ARL

NOTICES

Disclaimers

The findings in this report are not to be construed as an official Department of the Army position unless so designated by other authorized documents.

Citation of manufacturer's or trade names does not constitute an official endorsement or approval of the use thereof.

Destroy this report when it is no longer needed. Do not return it to the originator.

ARL-XX-XXXX ● XXX 2016

US Army Research Laboratory

Material Designs Toward a Synthetic Cannabinoid Sensor

by Mark H Griep[1], Abby L West[1], Michael S Sellers[1], Alexis M Fakner[1], Joseph Dougherty[1], John K Northup[2], Klaus Gawrisch[2], Shashi P Karna[1]

[1]*Army Research Laboratory, Weapons and Materials Research Directorate, ATTN: RDRL-WM, Aberdeen Proving Ground, MD 21005*

[2]*National Institute of Health, National Institute on Alcohol Abuse and Alcoholism, Rockville, MD 20852*

Contents

Contents iv

List of Figures vii

List of Tables xii

Acknowledgements 15

Executive Summary 16

Abstract 18

Introduction and Background 19

2. Modeling and Simulation 25

2.1 Overview 25

2.2 Cannabinoid Receptor 2 (CB_2) Homology Model and Simulation 25

2.3 Cannabinoid Ligand Parameterization 26

2.4 Cannabinoid/Conjugate Solubility and Diffusivity 27

2.5 Synthetic Cannabinoid Binding Location and Energy 30

2.6 Optimal Dark Quencher (DQ) Linkage 32

2.7 Simulations of Conjugate Binders 34

3. Synthesis of Materials 37

3.1 Synthesis of Cannabinoid Receptor 2 (CB_2) 37

3.2 Characterization of CB_1 Infections 38

3.3 $G\alpha_{i1}$ Production 39

3.4 Ligand-Dark Quencher Conjugation 40

3.4.1 Virodhamine - QSY-9 Conjugates 45

3.4.2 JWH-073 – QSY-9 Conjugates 49

3.4.3 PEG Spacers 56

3.4.4 Ligand-Dark Quencher Purification 62

3.4.5 Ligand-Dark Quencher Conjugate Characterization 71

4.0 Theoretical QD-Dark Quencher FRET Coupling 80

5.0 QD-CB_2 Conjugates 83

6.0 Hand-Held Platform 85

6.1 Physical Design 85

6.2 Detection Technology Interface 86

6.3 Electronics 87

6.4 Signal Processing 89

6.5 Manufacturing 89

7.0 Synthetic Cannabinoid – Damiana Leaf Extracts 89

7.1 Preparation of Spice-Like Herbal Product 90

7.2 Synthetic Cannabinoid Extraction Studies 91

7.2.1 Extraction Solvent Studies 91

7.2.2 Extraction Time Studies 91

7.3 Liquid Chromatography Coupled Mass Spectrometry Analysis of the Damiana Leaf Extracts 91

7.4 Activation of CB_2 in Presence of Various Solvents 97

8.0 Optical G-Protein Activation Assay 98

8.1 Europium GTP 98

8.1.1 Fluoroanalytical Assay Overview 99

8.1.2 Eu-GTP Synthesis 101

8.1.3 Eu-GTP G-Protein Activation Plate Reader Assay 102

8.2 BODIPY-Fl GTPγS CB_2 106

8.3 BODIPY-Fl GTPγS CB_1 109

9.0 Summary, Conclusions, and Future Direction 111

10.0 Appendix 113

10.1 Cannabinoid Receptor 2 (CB_2) Homology Model Details 113

10.2 CHARMM Parameters (ParamChem) for Select Cannabinoids 116

11.0 References **121**

List of Symbols, Abbreviations, and Acronyms **129**

List of Figures

Fig. 1 Example subset of chemical structures of synthetic cannabinoids. 21

Fig. 2 Fluoroanalytical SC sensor concept 23

Fig. 3 SC bionanoelectronic sensing concept. 24

Fig. 4 [A] Homology model of CB_2, with transmembrane helix 6 (gray) and 7 (yellow) highlighted. [B] In-membrane simulation of CB_2, side-view. [C] In-membrane simulation of CB_2, top-view. [B,C] Simulation box contains water, counter-ions of Na^+ and Cl^-, a 1-Palmitoyl-2-oleoylphosphatidylcholine lipid bilayer, and the CB_2 receptor protein. .26

Fig. 5 Setup of AM2201-H_2O interaction for CHARMM parameterization using VMD's FFTK plugin and Gaussian. Lines in background of molecule represent various water positions around AM2201 27

Fig. 6 Representation of virodhamine endocannabinoid (LEFT) and virodhamine + GLY_4 spacer + QSY-9 dark quencher (RIGHT).....28

Fig. 7 Representation of metabolite JWH-018-npentanoic (LEFT) and metabolite JWH-018-npentanoic + QSY7 dark quencher (RIGHT). 29

Fig. 8 Simulation snapshots of molecules in lipid bilayer with surrounding water. LEFT: Virodhamine endocannabinoid. RIGHT: Virodhamine + GLY_4 linker + QSY-9 dark quencher. 30

Fig. 9 Snapshot of JWH-018 n-pentanoic ligand in CB_2 receptor. *TOP* is extracellular view. 31

Fig. 10 JWH-018 (thick lines) diffusing in a lipid bilayer (thin lines). 32

Fig. 11 JWH-018 *n-pentanoic* (red) and WIN55-212 (blue) in the CB2 receptor. 33

Fig. 12 Alkyl chain (red), indole (yellow), and carbon rings (green). 33

Fig. 13 Artificial configuration of JWH-018 *n-pentanoic/*QSY7 conjugate with 10x PEG spacer bound to CB_2 receptor. A lipid bilayer within 5Å of the CB_2 receptor is shown for perspective. Labels of conjugate components are shown on image. 34

Fig. 14 JWH-018-QSY7 conjugate inserted into binding pocket of CB_2 receptor. QSY7 end extends out of the receptor through TM6/7.....35

Fig. 15 Top view of JWH-018-QSY7 conjugate bound to CB_2 receptor. Water and ions have been removed for clarity, lipid bilayer shown in gray. 36

Fig. 16 Overlay of CB_2 TM6 and 7 for bound JWH-018 *n-pentatnoic* (green) and bound JWH-018-QSY7 conjugate (blue).....36

Fig. 17 Overlay of JWH-018 n-pentanoic (green) and JWH-018-QSY7 conjugate (blue) bound to the CB_2 receptor. Similar atoms on both ligands are highlighted with colored spheres. Estimated difference in binding orientation is ~90 degrees. 37

Fig. 18 Characterization of a urea extracted plasma membrane fraction (CB_1#3) and untreated plasma membrane fraction (CB_1#4). These data show the presence of CB activity based on activation by CP55,940 and also the extraction of endogenous G protein by urea treatment of CB_1#3. 38

Fig. 19 Activation of CB_1 receptor with 30nM, and 100nM CP55,940.....39

Fig. 20 GTPγS analysis of various fractions containing α_{i1} after FPLC phenyl sepharose column purification. The data best fits the sum of two gaussians, showing the presence of both myristolated and non-myristolated α_{i1}. 40

Fig. 21 GTPγS analysis of various pools containing α_{i1} after purification. 40

Fig. 22 Molecular structure of the endocannabinoid virodhamine. 41

Fig. 23 (a.) Molecular structure of NHS-QSY-9 dark quencher and (b.) corresponding absorption spectra. 43

Fig. 24 Direct linkage mechanisms forming Virodhamine-QSY-9 conjugate 43

Fig. 25 Carboxyl and amine functional PEG spacers. 44

Fig. 26 Synthesis route to form ligand-dark quencher conjugate with varying PEG spacer lengths of 1.81nm, 3.36nm, and 4.68nm. Steps involve: (a) Blocking the amine group on the COOH-(PEG)x-NH2 material, (b) linking the functional carboxyl group on the (PEG)x to the Virodhamine amine group through a zer-length heterofunctional linker, (c) removal of the amine blocker on the (PEG)x, and (d) linking the NH2-(PEG)x-Virodhamine conjugate to the NHS-QSY-9 dark quencher. 44

Fig. 27 MS of Virodhamine-QSY-9 conjugate with fragment main peak of 419.4 with added H_2O (1198 + H^+ /3). 45

Fig. 28 LC chromatogram using gradient method 0-100%B in from 0-20 min, with 5mM ammonium formate H_2O as solvent A, and MEOH as solvent B. 46

Fig. 29 GC/MS chromatogram of virodhamine stock solution.....46

Fig. 30 GC/MS chromatogram isolating a 62m/z ion, which possibly relates to ethanolamine. 47

Fig. 31 Mass spectra of elution points yielding potential ethanolamine ions. 47

Fig. 32 Mass spectra from Virodhamine conjugate (top) in comparison to Eicosatetraenoic acid (bottom), a compound similar to arachidonic acid. 48

Fig. 33 Structures of the synthetic cannabinoids (a) WIN 55, 212-2, and (b) Nabilone and the dark quencher (c) QSY-7, amine. 50

Fig. 34 Conjugation products of (a) WIN 55, 212-2 to QSY-7 and (b) Nabilone to QSY-7. (c) Practice reaction between hexylamine and benzophenone...50

Fig. 35 Conjugation products of practice reaction between (a) hexylamine and benzophenone, and (b) hexylamine and cyclohexanone.....51

Fig. 36 (a) JWH–018 parent compound and (b) JWH–018 N-pentanoic acid metabolite. 52

Fig. 37 Conjugation product of practice reaction between hexylamine and 1-pyrenebutryic acid. 52

Fig. 38 Molecular structures of (a) QSY-7, amine and (b) JWH- 018 n-pentanoic acid. 52

Fig. 39 Conjugation product of QSY-7, amine to JWH-018 pentanoic acid. 53

Fig. 40 Mass spectra highlighting the expected mass peak of 1097 g/mol for the conjugate of QSY-7, amine to JWH-018 pentanoic acid. 53

Fig. 41 Liquid chromatograph highlighting the conjugate peak centered at 38 minutes, followed by the excess QSY-7 peak at 41 minutes. 53

Fig. 42 Alternate SC-DQ linkage options. A. JWH-073 butanoic acid metabolite. B. UR-144 pentanoic acid metabolite. Conjugates of JWH-073 butanoic acid (C) and UR-144 pentanoic acid (D) to QSY-7 amine. 54

Fig. 43 Structures and molecular mass of (a) JWH-073 butanoic acid, (b) UR-144 pentanoic acid, (c) JWH-073 conjugated to QSY-7, and (d) UR-144 conjugated to QSY-7. 55

Fig. 44 Mass spectral analysis of JWH-073 and UR-144 conjugates. 56

Fig. 45 Structures of PEG spacers Source: *http://www.piercenet.com/product/carboxy-peg-amine-compounds*. 57

Fig. 46 Structures of SC-DQ conjugates with PEG(4x) linker. 57

Fig. 47 G-protein activation of select ligands and estimated EC_{50} values. 60

Fig. 48 linker G-protein activation of mixed CP55,940/dark quencher conjugate materials. 61

Fig. 49 The peaks observed during the purification of JWH-368:(PEG)4:QSY-7 amine using the optimized gradient (top). A zoomed in view of the top figure showing the peaks collected during that run (middle). The peak indicated with a number 1 represents the JWH-368:(PEG)4:QSY-7 amine conjugate. The peak indicated with a number 2 represents the JWH-368:QSY-7 amine conjugate. The peak indicated with a number 3 represents the JWH-368 compound. The mass spectra of each of the three peaks collected (bottom). 64

Fig. 50 The peaks observed during the purification of JWH-018:(PEG)4:QSY-7 amine using the optimized gradient (top). A zoomed in view of the top figure showing the peaks collected during that run and the associated mass spec data (bottom). The peak indicated with a number 1 represents the JWH-018:(PEG)4:QSY-7 amine conjugate. The peak indicated with a number 2 represents the JWH-018:QSY-7 amine conjugate. 65

Fig. 51 The peaks observed during the purification of JWH-073:QSY-7 amine using the optimized gradient (top). A zoomed in view of the top figure showing the peaks collected during that run (bottom) and the associated

mass spec data. The peak indicated with a box represents the JWH-073:QSY-7 amine conjugate. 66

Fig. 52 LC chromatogram (top) and mass (bottom) of purified the three part conjugate, JWH-368:(PEG)4:QSY-7 amine. The conjugate has a retention time of 28.019 minutes and an observed half mass$^+$ of 632.8 g/mol (expected: 1337 g/mol non-ionized). 67

Fig. 53 LC chromatogram (top) and mass (bottom) of the purified two part conjugate, JWH-368:QSY-7 amine. JWH-368:QSY-7 amine has a retention time of 34.3 minutes and an observed mass$^+$ of 1017.4 g/mol (expected: 1017.8 g/mol non-ionized). 68

Fig. 54 LC chromatogram (top) and mass (bottom) of the purified three part conjugate JWH-018:(PEG)4:QSY-7 amine. JWH-018:(PEG)4:QSY-7 amine has a retention time of 35.602 minutes and an observed half mass$^+$ of 672.0 g/mol (expected: 1344.3 g/mol non-ionized). 69

Fig. 55 LC chromatogram (top) and mass (bottom) of the purified two part conjugate JWH-018:QSY-7 amine. JWH-018:QSY-7 amine has a retention time of 44.494 minutes and an observed mass$^+$ of 1095.4 g/mol (expected: 1095.4 g/mol non-ionized). 70

Fig. 56 Chromatogram (top) and mass (bottom) of the purified JWH-073 n-butanoic acid: QSY-7 amine conjugate. JWH-073:QSY-7 amine has a retention time of 44 minutes and an observed mass$^+$ of 1081.3 g/mol (expected: 1081.42 g/mol non-ionized). 71

Fig. 57 JWH-073:QSY7 amine mass spec data, structure, and NMR analysis, shows >99% purity. 73

Fig. 58 JWH-368:(PEG)$_4$:QSY7 amine mass spec data, structure, and NMR analysis, shows an unexpected molecular weight as well as incorrect structure resonances during NMR analysis. 74

Fig. 59 JWH-018:QSY7 amine mass spec data, structure, and NMR analysis, shows the expected molecular weight, a purity >99%,and structure resonances during NMR analysis consistent with the expected structure. 75

Fig. 60 JWH-018:(PEG)$_4$:QSY7 amine mass spec data, structure, and NMR analysis, shows the expected molecular weight, a purity >99%,and structure resonances during NMR analysis consistent with the expected structure. 76

Fig. 61 JWH-368:QSY7 amine mass spec data, structure, and NMR analysis, shows an unexpected molecular weight as well as incorrect structure resonances during NMR analysis. 77

Fig. 62 Dark Quencher compounds were tested at 1ul volume addition to limit methanol in the activation to 2% in comparison to CP55,940 at 1uM also added as 1ul in methanol. No activation of CB_1 receptor was detected. Concentration of DQ compounds were 1.35uM of DQ1, 0.312uM of DQ3, and 1.374uM of DQ4. 78

Fig. 63 Saturation of CB_1 receptor by CP55,940 was determined by addition of 1 uL volumes of CP55,940 providing the final concentrations indicated. These data were fitted to a single-site binding model to calculate an EC_{50} of 30nM. 79

Fig. 64 Dark Quencher competition for 30 nM CP55,940 dissolved in ethanol. DQ1 was added at 13.5 uM, DQ3 at 3.1 uM and DQ4 at 13.7 uM. Only DQ4 (JWH-018:$(PEG)_4$:QSY-7 amine) shows partial inhibition for CP55,940 activation of CB_1. 80

Fig. 65 Comparison of the QD emission spectrau (green) with the QSY-9 (red) and bR (purple) absorption spectrums. 81

Fig. 66 QD-QSY-9 FRET efficiency versus dipole separation. 82

Fig. 67 Comparison of QD-bR and QD-QSY-9 FRET efficiency....83

Fig. 68 Schematic of CP55,940 displacement with excess ligand-dark quencher conjugate. 84

Fig. 69 Effect of JWH-073 – QSY7 addition to the emission of CB_2 bound QDs. 84

Fig. 70 Virtual rendering of sensor platform body and user interface. 86

Fig. 71 Design of 3D printed disposable cartridge for sensor-chip housing. 87

Fig. 72 The cartridge with test sample injected. Gold object represents sensor chip location. 87

Fig. 73 Electronic wiring diagram. 88

Fig. 74 The physical wiring of the platform. The power source (9V battery) is located in the right of picture and powers the Arduino Uno microprocessor (black and blue board). The white rectangle in the left of the picture is a slot for holding the cartridge and houses the electrical pins to connect to it. 89

Fig. 75 Representative image of damiana leaves (A) and the chemical structure of Win 55, 212-2 (B) utilized in the study. 90

Fig. 76 LCMS Plots of 100% ethanol extracts of damiana leaves. Liquid chromatography spectra of control (A) and Win55, 212-2 doped (B) damiana leaf extracts monitored at 330 nm. Mass Spectral plots of control (C) and Win55, 212-2 doped (D) damiana leaf extracts. 93

Fig. 77 Total extracted mass ion plots at 3.6 minutes of control (A) and Win 55, 212-2 doped (B) damiana leaf extracts with 100 % ethanol. Win55, 212-2 has an expected mass of 427.2 g/mol. 94

Fig. 78 Bar charts of peak area (A) and total mass percentage (B) comparisons of Win 55, 212-2 extraction with 2 % (blue) and 100 % (red) solvent concentration. 95

Fig. 79 Bar charts of peak area (A) and total mass percentage (B) comparisons of Win 55, 212-2 extraction with 30 second (blue) and 1 minute (green) shaking times. 96

Fig. 80 Activations of CB_2 in the presence of varying ligand/solvent extract combinations. 97

Fig. 81 Activation of CB_2 at 5000-fold dilutions of mock Spice extracts. 98

Fig. 82 GPCR Activity Schematic. 100

Fig. 83 Structures of GTP (A) and Eu-chelate (B). 102

Fig. 84 Fluorescence signal from 40nM Eu-GTP with CB_1 receptor, in the presence of varying concentrations of quencher (diCy). The indicated concentrations of diCy were mixed in the presence of CB_1 containing membranes and 100nM Eu-GTP and TRF was measured. 103

Fig. 85 CP55,940 activation of CB_1 receptor detected by TRF enhancement of Eu-GTP. CB_1 receptor containing membranes were mixed with $G\alpha_{i1}$ and $G\beta\gamma$ without and with the addition of CP55,940. Reactions were initiated by the addition of Eu-GTP and TRF monitored for three replicate samples each for 30 minutes. 104

Fig. 86 Serotonin receptor (5HT, 5-hydroxytryptamine receptor) was used in place of CB_1 with THC as the activating ligand. 5HT is not activated by THC and should not show an increase in fluorescence. The graph shows a large increase in fluorescence when THC is added, indicating nonspecific interactions of EuGTP and THC. 105

Fig. 87 $G\alpha_{i1}$ was incubated with EuGTP without a receptor present for one hour. Since $G\alpha_{i1}$ will bind GTP spontaneously at a slow rate, some EuGTP should remain bound after the addition of quencher. 105

Fig. 88 Schematic of GPCR-G protein screening assay for synthetic cannabinoids. 107

Fig. 89 Fluorescence emission of BODIPY FL GTPgS after 10 minute incubation in varying experimental configurations. 108

Fig. 90 Time based 512nm fluorescence monitoring of activated assay versus control. 108

Fig. 91 Timebased 512nm fluorescence monitoring of activated assay components. 109

Fig. 92 Time based 512nm fluorescence monitoring of activated assay components CB_1, $G\alpha_{i1}$, and CP55,940 as the activating ligand. The catalysis can be seen between the activated and inactivated reaction. .110

Fig. 93 BODIPY-Fl GTPγS emission in the presence of various ligands. Serotonin is not a CB activating ligand and was used as a negative control. Approximately a 30% increase in signal can be seen when activated. 110

List of Tables

Table 1. Free energies of solvation and computed $\log P^{1\text{-octanol/water}}$ at 300K. ΔG error computed from the standard deviation of 5 simulations, propagated to give logP error. 29

Table 2. Diffusivity values for cannabinoid in lipid. 29

Table 3. Total interaction energy of select cannabinoids bound to CB2 receptor. ($k_bT=0.593kcal/mol$) 31

Table 4. Top 10 CB_2 receptor residues based on interaction energies for JWH-018 n-pentanoic and WIN55-212 cannabinoids. Common residues are bold, 6 of 10. 31

Table 5. Relative CB2 binding affinity of select cannabinoid molecules versus virodhamine 41

Table 6. Molar equivalents and quantities of reagents used in the synthesis protocol. 58

Table 7. Gradients of solvents used in this study for the HPLC purification of JWH-368:(PEG)4:QSY-7 amine and JWH-368:QSY-7 amine. 62

Table 8. Gradients of solvents used in this study for the HPLC purification of JWH-018:(PEG)4:QSY-7 amine and JWH-018:QSY-7 amine. 62

Table 9. Gradients of solvents used in this study for the HPLC purification of JWH-073:QSY-7 amine. 63

Table 10. Expected masses of compounds used in this study. 63

Table 11 Comparison of bR and QSY-9 FRET parameters. 83

Table 12. Quenching effects of dark quencher addition to QD-CB2 conjugate. ..85

Table 13. Fluorescence emission comparisons at 5, 10, 15, and 20 minute timepoints. 109

INTENTIONALLY LEFT BLANK.

Acknowledgements

We would like to acknowledge the insightful input and support of our colleagues at the U.S. Defense Forensic Science Center including Drs. Jeff Salyards, Rick Tontarski, Jason LeBlanc, Brigid O'Brien, and Toni Diegoli. We would also like to thank Mr. Kirk Hines and Dr. Alexei Yeliseev for their aid on this effort. Additionally, this project was supported in part by an appointment to the Internship/Research Participation Program at the U.S. Army Research Laboratory administered by the Oak Ridge Institute for Science and Education through an interagency agreement between the U.S. Department of Energy and EPA.

Executive Summary

The objective of this work was to engineer a robust, fieldable sensor for the detection of cannabinoids in real time. The chemically robust nature of this sensing platform must allow for the detection of any cannabinoid molecule (natural or synthetic) with a strong affinity for a cannabinoid receptor (ie. Effective against future SC drug designs). Implementing this technology into a fieldable device will provide the U.S. Armed Forces a tool to curb SC use in the military and ensure the combat readiness of U.S. military personnel. Our approach was multifaceted and combined computational modeling, experimental work, and the engineering of a detection device that would assay leaf extracts for the presence of cannabinoids. A number of experimental procedures were used during this project to make the most robust and usable sensor.

Synthetic Cannabinoid – Damiana Leaf Extracts

All of the detection schemes below require the use of extracted SC from the plant material. We worked to optimize a rapid and facile method to extract synthetic cannabinoids from leafy substrates in the field. The optimal extraction technique is the addition of 2% methanol or ethanol enhanced with 0.1M KCl to the plant material and shaking for 30 seconds by hand.

Detection Scheme 1:

BioNanoelectronics Platform

The first method built upon recent ARL efforts that yielded a unique BioNanoelectronics platform tailored towards highly selective molecular sensing [49-51]. The sensor, which is based upon energy transfer alterations in a nanoparticle-optical protein system, provides a real-time electrical output modulation upon target binding. In theory, a layer-by-layer approach is used to place a quantum dot (QD) onto bacteriorhodopsin (bR). The bR is able to convert the QD signal to an electrical output which can be converted to a simple “yes” or “no” output. Layered on the QD is a receptor molecule of interest, in this case a CB receptor. A lower affinity CB ligand is modified to carry a dark quencher molecule into close proximity of the QD through binding with the receptor. The DQ molecule captures the system output energy and sharply reduces the measured electrical output of the device. When a test sample enters the device, any molecule with a higher CB receptor binding affinity competitively displaces the relatively weakly bound ligand carrying the dark quencher, and the system energy returns to its original state; resulting in a sharp increase in the measured electrical signal signifying the presence of a cannabinoid molecule. However, due to the need for a highly pure receptor for this experimental setup, it was determined to move forward with the CB_2 receptor during this phase.

Component A.

Hand-held Sensor

A senior design team at Michigan Technological University successfully designed a sensor prototype for the BioNanoelectronic phase. This platform was designed to be handheld, need only

one operator, provide present/not present results in under two minutes, and require no more than five minutes of training time. These design objectives were achieved by creating an intuitive user interface, an integrated sample cross contamination prevention system, and a redundant verification process of the results.

Component B.

Modeling and Simulation

The purpose of the modeling component of the project was to define optimal characteristics for the SC-DQ conjugate. The simulations would provide how the conjugate entered the membrane, interacted with the receptor and if the DQ was within quenching distance of the QD for the BioNanoelectronics platform. CHARMM parameters for the simulation of synthetic cannabinoid compounds were developed. The solubility and diffusivity of synthetic cannabinoid compounds were computed to describe the behavior in the cell membrane. This information was used to determine the optimal cannabinoid for use in the BioNanoelectronics platform described above. The optimal dark quencher attachment location on the cannabinoid and linker length were also determined through modeling. The possible binding orientations of the cannabinoid**:**dark quencher complex to the CB_2 receptor were also modeled.

Component C.

SC-DQ Conjugates

For this BioNanoelectronics sensor platform, it is important to have purified SC-DQ conjugates that loosely bind to the CB receptor. Three SC-DQ conjugates were successfully synthesized, purified, and structurally verified by NMR. To our knowledge, these conjugates are the first successful attempt at linking a dye to a cannabinoid compound. The binding of all three conjugates were tested through the radioactivity assay. None of the conjugates activated the receptor, however the JWH-018:$(PEG)_4$:QSY 7 showed binding. The binding was in the micromolar range, but at that range it is too low to be useful for the BioNanoelectronic sensor detection. For this reason and the inability to get purified CB_2 receptor in a form that could be layered onto the QD, the effort was shifted to the optical G-Protein Activation Assay described below.

Detection Scheme 2:

Optical G-Protein Activation Assay Platform

The Optical G-Protein Activation Assay relies on the addition of a fluorescence molecule to GTP. The experiments were modeled on established GTP-exchange assays using radioactive GTP analogs. Briefly, after the CB_1 receptor is activated by a ligand, the molecule $G\alpha_{i1}$ releases bound GDP and binds with GTP. For this platform, the GTP has a fluorescent molecule attached to it.

Option A.

Europium-GTP

The Europium-GTP (Eu-GTP) platform theory is as described above. It is based on the Perkin Elmer assay that involves a filtration system. The GTP is bound to a fluorescent molecule of Europium. Rather than using a filtration system for this assay, a quencher molecule was added to the reaction. The quencher 1,1,3,3,3,3-Hexamethylindodicarbocyanine iodide (diCy) was used to quench unbound fluorescence from the Eu-GTP. When the CB_1 receptor is activated by a cannabinoid, it initiates the binding of Eu-GTP to $G\alpha_{i1}$. This protects the molecule from the quencher and leads to an increase in fluorescence. Unfortunately, the results were inconsistent. Through further studies, it was observed that the Eu-GTP may not actually be binding with the $G\alpha_{i1}$ subunit. It was determined that using the catalysis of GTP binding to $G\alpha_{i1}$ and the fluorescent guanine nucleotide analog Eu-GTP as a biosensor would not work for our purposes.

Option B.

BODIPY-GTP

The BODIPY-GTP molecule is also an available fluorescent GTP molecule. The detection mechanism is the same as that of the Eu-GTP approach, however, there is no requirement for a quencher. When unbound and in solution, the BODIPY fluorescence is quenched. The assay was tested on a high-throughput fluorescent plate reader with the following compounds, Δ9-tetrahydrocannabinol (THC), JWH307, Win55,212, and CP55,940. The tested cannabinoid agonists showed approximately a 30% increase in fluorescence under test conditions. In the current form, this assay is a high throughput lab based sensor that can test 92 samples in under ten minutes. Though additional work must be done to optimize the signal to noise ratio and create a handheld sensor, the proof of concept with the BODIPY-GTP plate reader method is promising for a rapid and simple testing of synthetic cannabinoid samples. This system allows for a receptor based detection system capable of detecting currently abused synthetic cannabinoids and those created in the future without additional modifications or development. It is desirable to develop BODIPY-GTP based handheld, lightweight, and fieldable sensor for high throughput detection with minimal manual efforts in sample manipulation.

Abstract

Synthetic cannabinoids (SCs), molecules that emulate the effects of the active ingredient of marijuana, have gained popularity over the last decade. The use of these SCs pose major legal and health concerns. There are countless different structures of synthetic cannabinoids available and these numbers are rising. The diversity of these structures presents a challenge in detection of SCs. Typically mass spectrophotometry is used for chemical identification of the compounds. We sought to develop a robust, fieldable, handheld sensor for use by the military and law enforcement personnel to aid in the detection of SCs. A receptor based sensor platform would allow for all current and future synthetic cannabinoids to be detected without the need for updating equipment or additional engineering. In order to develop such a universal SC detecting platform, a cannabinoid (CB) receptor based assay utilizing fluorescence resonance energy

transfer (FRET) coupling and dark quenchers was designed. Three dark quencher SC conjugates were successfully developed and characterized. Two of these conjugates showed weak, micromolar binding of the CB_1 receptor. However, the binding was insufficient for a reliable robust sensing platform. As a second approach, a fluorescence based CB_1 activation assay was developed in which fluorescent molecules tagged to guanine triphosphate (GTP) are bound to the G-protein after receptor binding with SCs. Two fluorescent reporters, Europium-guanine triphosphate (Eu-GTP) and boron-dipyrromethene- guanine triphosphate (BODIPY-GTP), were tested using a high throughput plate reader approach. The BODIPY-GTP assay was the most promising, as it was able to detect four cannabinoid compounds, namely Δ9-tetrahydrocannabinol, JWH307, Win55,212, and CP55,940 with a 30% increase in fluorescence under laboratory test conditions. In the current form, the BODIPY-GTP assay shows the most promise as a high throughput, laboratory- based sensor capable of testing 92 samples in under ten minutes.

Introduction and Background

Herbal mixtures, such as 'Spice' and 'K2', were exposed as hosts for synthetic molecules that imitate the effects of the psychoactive component of cannabis, delta-9-tetrahdyrocannabinol (THC).[1-5] Synthetic cannabinoid receptor agonists comprise a diverse group of chemically unrelated substances that have long evaded the U.S. legal system by being sprayed onto an inert dry plant substrate and subsequently merchandized as 'incense', 'plant food', and 'room odorizers' from as early as 2004.[1, 6-10] These herbal blends are also widely available on the internet and in retail outlets such as smoke and head shops with disclaimers that read "not for human consumption" with only natural ingredients listed on their packages.[11] When further tested, they have been found to contain neither tobacco nor cannabis, but still produce cannabimimetic effects. As a result, these herbal mixtures doped with synthetic cannabinoids have become widely abused as a supposed legal alternative to cannabis.[12-14]

Unfortunately, synthetic cannabinoids have also become a significant problem within the U.S. armed forces.[10, 15-17] 'Spice' and other related herbal products are readily abused by many military personnel as they can be purchased without age restrictions, are not detected in standard drug screens, and are commonly misinterpreted as safe since they are marketed as "herbal" and "natural" products.[18, 19] Consequently, these new and harmful cannabis substitutes pose major public health and legal predicaments. Scheduling these compounds presents a unique concern as there are so many cannabimimetic compounds available.[20, 21] Each time one synthetic cannabinoid is regulated, another derivative is made available that is not subject to regulation.[9, 17, 22] Thus, the DEA has moved towards scheduling the entire class of compounds. However, defining the class of compounds is problematic as the structures of these cannabimimetic compounds are very structurally diverse (**figure 1**).[23]

Synthetic cannabinoids (SCs) elicit physiological responses comparable to THC (tetrahydrocannabinol, the active ingredient in marijuana) by binding and activating the same cannabinoid receptors (CB) in the body, CB1 and CB2.[19, 24] CB1 is expressed in the central nervous system whereas CB2 is expressed in the peripheral nervous system.[25] CB1 is primarily responsible for the psychological and physiological effects generated by SC binding to the receptors.[26] SCs have been extensively studied and developed for over twenty years with the original intent to be used for pharmacotherapeutic purposes; however, companies and researchers were never able to circumvent the negative psychoactive side effects.[27] They also exhibit potencies from 10 to 100 times greater than that of THC, which raises many health concerns.[6, 18, 19, 28-32] Synthetic cannabinoid receptor agonists are categorized into seven major groups: naphthoylindoles (n=74), naphthylmethylindoles (n=9), naphthoylpyrroles (n=32), naphthylmethylindenes (n=3), phenlacetylindoles (i.e. benzoylindoles) (n=28), cyclohexylphenols (n=16), and classical cannabinoids (dibenzopyrans) (**figure 1**).[33] The numbers in brackets are indicative of the amount of members in each group that activate the CB1 receptor and are therefore cannabimimetic. The numbers of known SCs increase almost daily, with new analogs being synthesized to continue to skirt the legal system.

The spice products were banned in 2008 in many European countries after discovery of potent cannabinoid products, such as JWH-018 and CP-47,497 in them. The National Forensics Laboratory of the U.S. Drug Enforcement Agency (DEA) reported in 2011 that the number of synthetic cannabinoid samples submitted to forensic laboratories rose from 13 to a staggering 2,977 cases between 2009 and 2010. As the current primary means of detection is Gas Chromatography Coupled Mass Spectrometry (GC-MS) and Liquid Chromatography Coupled Mass Spectrometry (LC-MS) technologies, it is necessary to optimize the extraction method for isolating synthetic cannabinoids from the plant material in these various herbal mixtures.[34-48] Until recently, a fast, reliable, real-time sensing platform for SCs have been lacking.

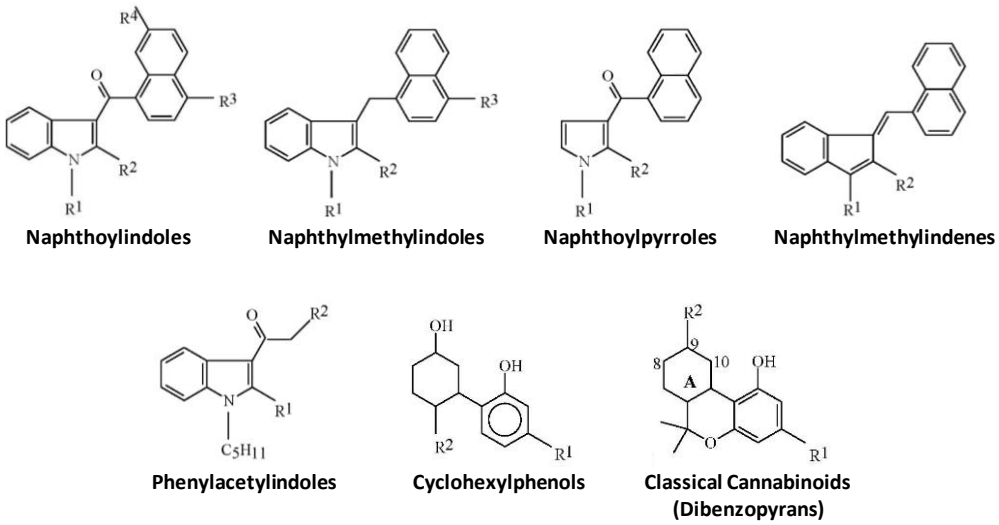

Fig. 1 Example subset of chemical structures of synthetic cannabinoids.

Recent ARL efforts have yielded a unique BioNanoelectronics platform that has proven capable of being tailored towards highly selective/ sensitive molecular sensing [49-51]. The sensor, which is based upon energy transfer alterations in a nanoparticle-optical protein system, provides a real-time electrical output modulation upon target binding. Being entirely electrical in nature allows for it to be developed into an automated handheld analytical device and its' generic architecture allows it to be tailored to a wide variety of target species. Utilizing the demonstrated generic platform, materials and methodologies need to be developed to transition the systems towards the detection of synthetic cannabinoids (SC). Nanoscale deposition techniques will be used to construct the base bionanoelectronics substrate and integrate a highly selective cannabinoid receptor (CB_1) on the surface. A lower affinity CB_1 ligand, such as NADA (K_i = 2501 nM), will be modified to carry a 'dark quencher' molecule into close proximity of the bionanoelectronics substrate. The dark quencher molecule captures the system output energy and sharply reduces the measured electrical output of the device. When a test sample enters the device, any molecule with a higher CB_1 receptor binding affinity will competitively displace the relatively weakly bound ligand carrying the dark quencher, and the system energy will return to its original state; resulting in a sharp increase in the measured electrical response and signify the presence of a cannabinoid-like molecule. Work will initially focus on demonstrating the energy transfer upon target binding in an aqueous QD sensor, with later steps integrating the sensing scheme onto the bioelectronics platform. Specific target molecules that will likely be encountered in the field include: 5F-AMB, UR-144, FDU-PB-22, AB-CHMINACA, AB-FUBINACA, AB-PINACA, and +MAB-CHMINACA. The detection of these molecules with the proposed system will be fully characterized.

While the SC molecule's interactions with CB_1 have been characterized both experimentally *in vitro* and computationally, little is known about the structure of CB_1 in the sensor's solution environment. Additionally, recent work has shown that the structure of the CB_1 receptor affects the binding affinity of the SCs, as well as the binding conformations of the specific cannabinoid. Computational studies of the solution based CB_1 and synthetic cannabinoid can provide information about these affected properties. In concert with experimental work, computational binding studies can provide quantitative values of binding energy for various SCs and aid in the characterization of CB_1 binding pocket residues for the development of a synthetic peptide receptor. Our system will be modeled with the ARL developed software *XPairIt*—an application interface connecting free and open-source molecular dynamics, molecular docking (binding), and quantum chemistry codes. Using *XPairIt*, equilibrium dynamics simulations of CB_1 and the analog CB_2 receptor, and the SCs can be completed, leading to an atomic level description of the molecular structure. Binding studies can then be used to isolate the particular orientations of the bound SCs and their locations on CB_1. First binding attempts will be focused on the trans-membrane (TM) helix 6 of CB_1, as previous modeling work of CB_1 in the lipid bilayer was conducted on this helix.

The objective of this project was to integrate a generic cannabinoid sensing scheme into a compact prototype detector amenable to scale-up to a fieldable device. The chemically robust nature of this sensing platform allows for the detection of any cannabinoid molecule (natural or synthetic) with a strong affinity for a cannabinoid receptor (ie. Effective against future SC drug designs). Implementing this technology into a fieldable device will provide the U.S. Armed Forces a tool to curb SC use in the military and ensure the combat readiness of U.S. military personnel.

The major components of the system are: (1) Highly fluorescent CdSe\ZnS quantum dots (QD) that are capped with a cannabinoid 2 (CB_2) G-Coupled Protein Receptors (GCPR) and (2) engineered cannabinoid ligands that are tagged with a non-fluorescent quenching (dark quencher) molecule. In the control-state of the sensor system, the tagged cannabinoid ligand will be bound to the CB_2 receptor on the QD. The absorption spectra of the dark quencher molecule will be tailored to strongly overlap the QD energy emission peak, facilitating a direct fluorescent resonance energy transfer (FRET) coupling relationship. This FRET coupling relationship will quench the QD emission when the engineered ligand-dark quencher conjugate is bound to the CB_2 receptor, as represented in **figure 2**. The ligand component of this system will be chosen so that it will be readily displaced from the CB_2 receptor when synthetic cannabinoids are present in the system; ultimately moving the dark quencher out of FRET-coupling range of the QD and restoring the QD's photonic energy emission and signaling target detection. Integration of the fluoroanalytical detection scheme onto an optoelectronic bacteriorhodopsin substrate to transduce alterations in the QD energy levels into measurable alterations in system electrical output is shown in **figure 3**.

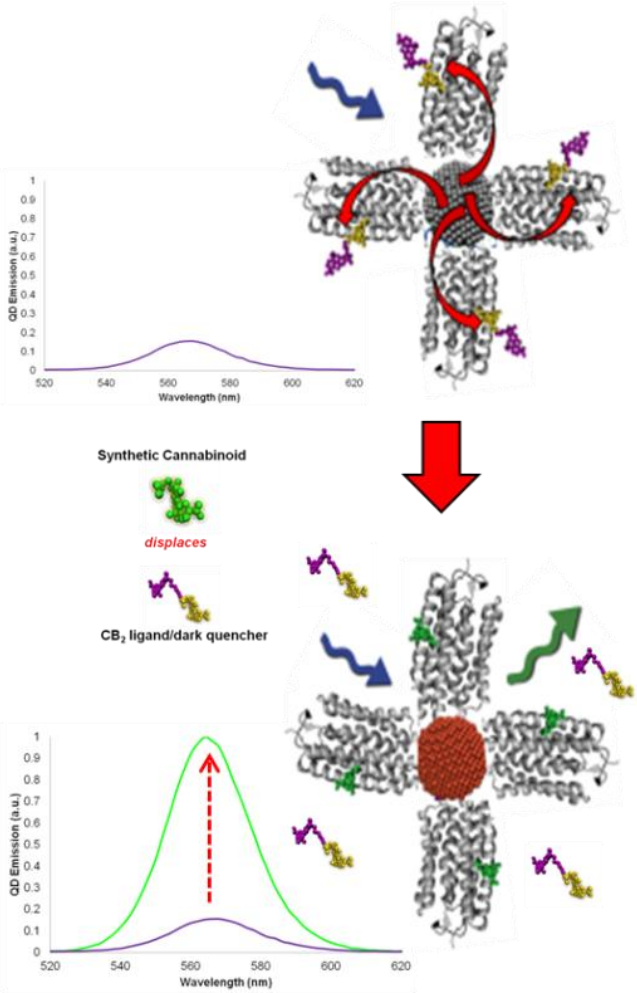

Fig. 2 Fluoroanalytical SC sensor concept

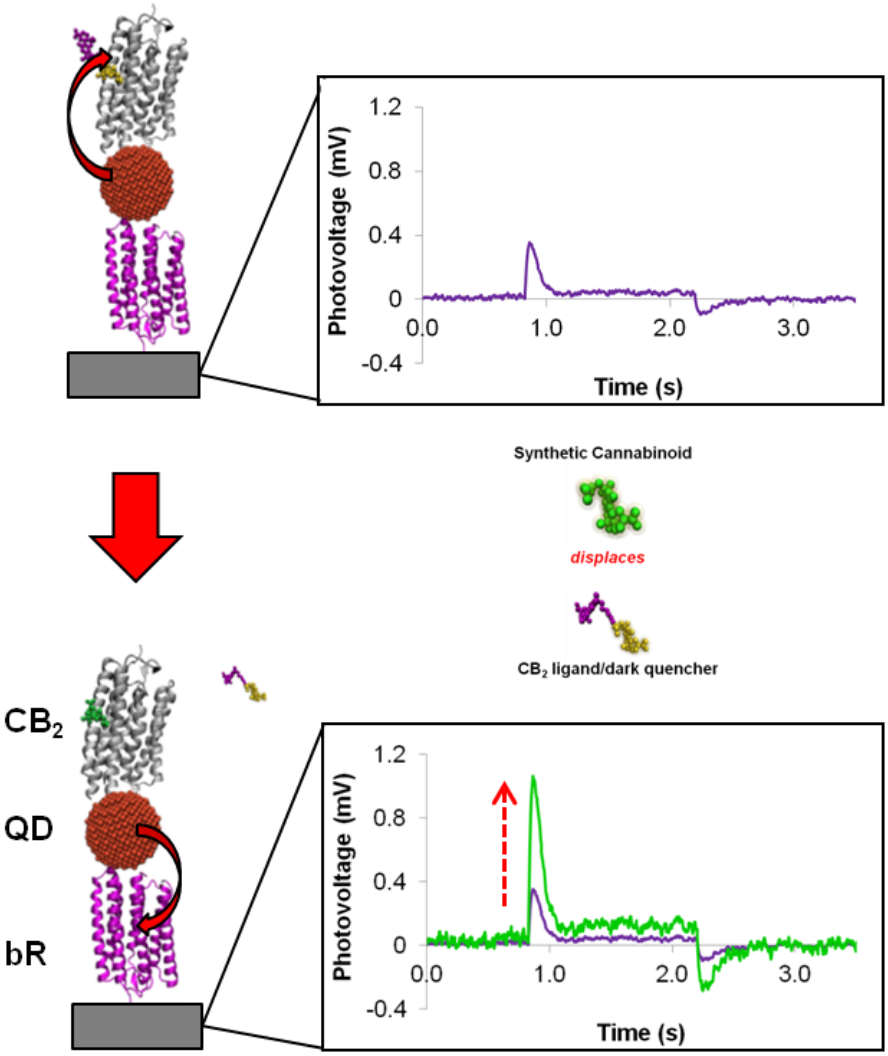

Fig. 3 SC bionanoelectronic sensing concept.

2. Modeling and Simulation

2.1 Overview

Computational support of this project was aimed to provide information about cannabinoid ligand binding to the CB_2 receptor through simulations to compute ligand properties and binding properties. Using the ARL developed software *XPairIt Simulation API* and other industry proven simulation codes [52-55], specific endocannabinoids, synthetic cannabinoids, the endocannabinoid-dye (dark quencher) complex, and the CB_2 receptor protein were modeled. Molecular dynamics and thermodynamic integration methods were used to compute ligand diffusivity in the lipid and ligand and ligand-dark quencher conjugate solubility. Simulations were also conducted on a specific ligand (or ligand-dark quencher complex) and its interactions with the CB_2 receptor to determine: (1) the effects of dark quencher attachment on the endocannabinoid ligand—CB_2 receptor binding process and (2) the specific CB_2 amino acids involved in binding the endocannabinoid and synthetic cannabinoid ligands. Optimal dark quencher attachment and linker length were also determined.

2.2 Cannabinoid Receptor 2 (CB_2) Homology Model and Simulation

To date, there is no NMR or crystallographically derived protein structure for the CB_1 or CB_2 receptors. Accordingly, the structure of CB_2 has been generated from sequence alignment to *squid rhodopsin*, identified as a top candidate starting structure for homology modeling and used in many simulations of the CB_2 receptor. [56-63] Details of the homology model are listed in the **Appendix**. The CB_2 receptor was equilibrated via molecular dynamics using nanoscale molecular dynamics (NAMD) at 300K and 1atm in a lipid bilayer with a physiological concentration of Na^+ and Cl^- ions. [55] This is shown in **figure 4**. Transmembrane helices 6 and 7 have been identified in a previous [57, 59] as the primary binding location for other cannabinoids on the CB_1/CB_2 receptors.

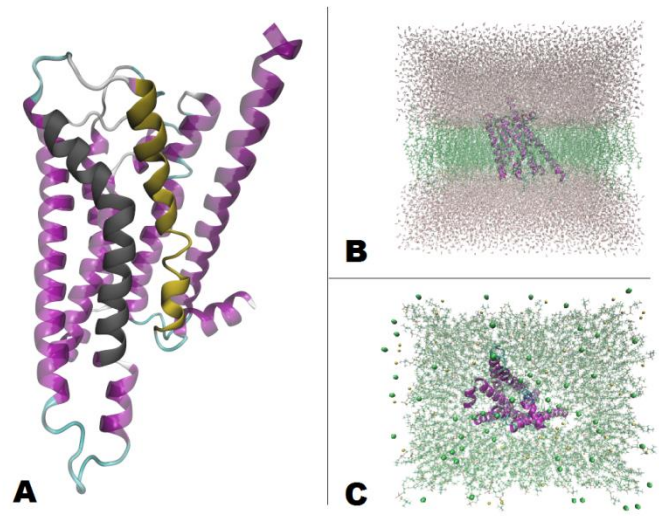

Fig. 4 [A] Homology model of CB_2, with transmembrane helix 6 (gray) and 7 (yellow) highlighted. [B] In-membrane simulation of CB_2, side-view. [C] In-membrane simulation of CB_2, top-view. [B,C] Simulation box contains water, counter-ions of Na^+ and Cl^-, a 1-Palmitoyl-2-oleoylphosphatidylcholine lipid bilayer, and the CB_2 receptor protein.

2.3 Cannabinoid Ligand Parameterization

Below is a common function used to represent the energy of atom-atom interactions in a biological system. [64, 65] Many types of simulation software use this function, known as "the CHARMM potential", and much work has been done in the parameterization of variables for proteins and other compounds to ensure this simulation software mimics natural behavior. Variables k, b_0, θ_0, δ, u_0, ω_0, and σ are adjustable parameters, and are specific to each atom pair for which E_{CHARMM} is being computed, where r and b are the atom-atom separation distance, θ is the angle between three atoms, and ϕ and u is the dihedral angle between four atoms. Typically, these parameters—those variables with a subscript—are tuned by developers of the program Chemistry at Harvard for Molecular Mechanics (CHARMM), but for new molecules, there are various avenues to determine these on your own. The most common is to use a quantum chemistry code to compute these values, and then fit the CHARMM potential parameters to match quantum results. This is the route we have taken in this project.

$$E_{CHARMM} = \sum_{bonds} k_b (b - b_0)^2 + \sum_{angles} k_\theta (\theta - \theta_0)^2 + \sum_{dihedrals} k_\phi [1 + \cos(n\phi - \delta)] +$$

$$\sum_{Urey-Bradley} k_b (u - u_0)^2 + \sum_{impropers} k_\theta (\omega - \omega_0)^2 + \sum_{\phi,\varphi} E_{CMAP} + \sum_{nonbonded} 4\varepsilon \left[\left(\frac{\sigma}{r}\right)^{12} - \left(\frac{\sigma}{r}\right)^{6} \right] + \frac{q_i q_j}{\varepsilon r_{ij}}$$

Listed in the **appendix** are computed values for computing the electrostatic term in the CHARMM potential—the last term shown in the above equation. Optimized values of q are shown and represent fitting with respect to the molecule's other atoms and interactions with H and O of water. All synthetic cannabinoids simulated were parameterized for the CHARMM forcefield using Visual Molecular Dynamic's (VMD) force field toolkit (FFTK) plugin and Gaussian to compute and optimize bond strengths, water-molecule interactions, dihedral angle strength, and atomic charges. [53, 66-68]. **Figure 5** is an example of multiple water-molecule calculations to determine interaction energies and atomic charges.

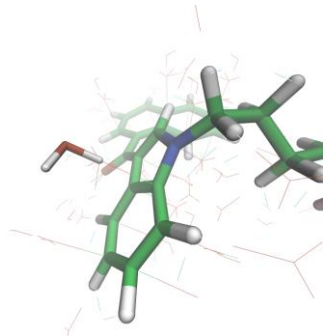

Fig. 5 Setup of AM2201-H_2O interaction for CHARMM parameterization using VMD's FFTK plugin and Gaussian. Lines in background of molecule represent various water positions around AM2201

2.4 Cannabinoid/Conjugate Solubility and Diffusivity

Studies of the solubility of each of the ligands involved in this work provide a standard for verification of our parameterization work and value to compare to experimental studies. For example, solubility values can be compared to high performance liquid chromatography (HPLC) experimental studies of cannabinoid ligands and their dark quencher conjugates. After reviewing several methods, solubility is determined by computing the logarithm of the 1-octanol/water partition coefficient, shown in the equation below. [69, 70]

$$\log P^{1-octanol/water} = \frac{\Delta G_{sol-water} - \Delta G_{sol-1-octanol}}{2.303RT}$$

The logarithm of the 1-octanol/water partition coefficient (logP)—a means to quantify the partitioning of molecule between phases—was computed for virodhamine and its conjugate with QSY-9 dark quencher and GLY_4 spacer **(figure 6**), as well as JWH-018-n-pentanoic and its conjugate with QSY7 dark quencher (**figure 7**) and other synthetic cannabinoids. This is a widely used method and the molecular dynamics software we are using in this work is particularly suited for it. [55] Using thermodynamic integration, several molecular dynamics simulations of a ligand in each solvent are run. The interactions of the ligand and solvent are scaled, from zero interaction

to full (natural) interaction to determine the Gibbs free energy difference (ΔG) between the ligand in a vacuum and the ligand in the solvent. This difference is computed for water and 1-octanol, to compute the partition coefficient (logP), where R is the ideal gas constant and T is temperature. Results are shown in **table 1**.

When comparing the endocannabinoid and the synthetic metabolite (when attached to QSY7, used to "load" the CB_2 receptor), the synthetic metabolite exhibits a lower logP, indicating reduced affinity towards non-polar solvents. This also denotes an increased aqueous solubility when compared to virodhamine. In a similar fashion, when the respective dark quenchers are added, the endocannabinoid virodhamine+QSY-9 exhibits a higher logP value than JWH-018-npentanoic+QSY7. Both show a reduction in non-polar affinity, however the addition of QSY7 alters the conjugate's affinity almost twice as much as the endocannabinoid conjugate.
This information is necessary to characterize the efficacy and mechanisms of experimental binding studies.

Longer simulations of JWH-018 synthetic cannabinoid and JWH-018-npentanoic metabolite were conducted to improve the error associated with free energy of solvation calculations for the respective molecules in water and octanol. With values for the synthetic cannabinoid and metabolite as a baseline, we are able to correlate and hypothesize on the effects of the hydrophobicity (and accordingly, the lipophilicity) of the conjugate molecules. For comparison, while it is known that JWH-018 binds readily to the CB_2 receptor, JWH-018-npentanoic metabolite has been shown to bind extremely weakly. With a higher logP, solubility results indicate that a conjugate with QSY7 may bind to the CB_2 receptor.

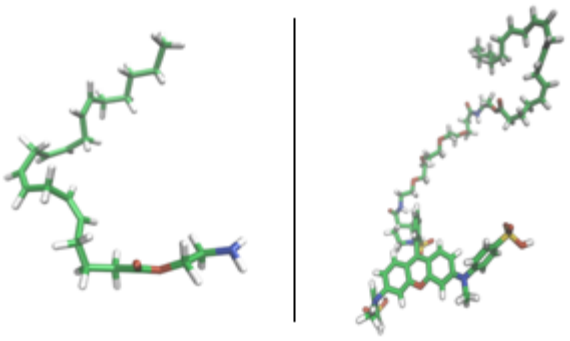

Fig. 6 Representation of virodhamine endocannabinoid (LEFT) and virodhamine + GLY_4 spacer + QSY-9 dark quencher (RIGHT).

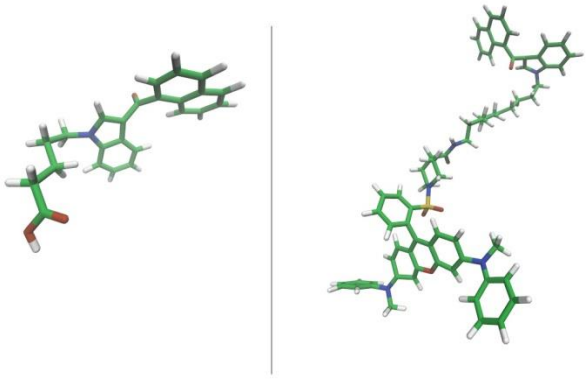

Fig. 7 Representation of metabolite JWH-018-npentanoic (LEFT) and metabolite JWH-018-npentanoic + QSY7 dark quencher (RIGHT).

Table 1. Free energies of solvation and computed logP$^{1\text{-octanol/water}}$ at 300K. ΔG error computed from the standard deviation of 5 simulations, propagated to give logP error.

	$\Delta G_{sol\text{-}water}$ (kcal/mol)	$\Delta G_{sol\text{-}1\text{-}octanol}$ (kcal/mol)	logP
Virodhamine *endocannabinoid*	-6.756 +/- 0.521	-14.322 +/- 0.802	5.514 +/- 0.697
JWH-018-npentanoic *metabolite*	-17.162 +/- 0.278	-22.226 +/- 0.495	3.691 +/- 0.414
JWH-018 *synthetic cannabinoid*	-9.802 +/- 0.134	-18.795 +/- 0.760	6.555 +/- 0.563
AM2201 *synthetic cannabinoid*	-11.546 +/- 0.215	-19.312 +/- 0.686	5.659 +/- 0.524
QSY7 *dark quencher*	-48.282 +/- 0.448	-62.684 +/- 1.540	10.497 +/- 1.169
Virodhamine-GLY_4-QSY-9	-51.733 +/- 4.860	-55.140 +/- 5.571	2.483 +/- 5.389
JWH-018-npentanoic-QSY7	-61.863 +/- 1.131	-67.906 +/- 2.146	4.405 +/- 1.768

The diffusivity of virodhamine and its QSY-9 conjugate in a lipid bilayer was calculated, and dynamics of the molecule were observed. **Table 2** lists values for the computed diffusivities, and relative to lipid self-diffusivity. For a majority of the simulation, QSY-9 remains at the water/lipid interface while virodhamine interacts with QSY-9 at the interface and then partitions into the lipid, as represented in the simulation snapshots in **figure 8**. Based on diffusivity calculations, we see increased virodhamine mobility in the lipid due to the attachment of the QSY-9 dark quencher.

Table 2. Diffusivity values for cannabinoid in lipid.

	D (10^{-9} cm^2/s)
Virodhamine	6.083
Virodhamine-GLY$_4$-QSY-9	901.58 +/- 65.88
Lipid (self-diffusivity)	~ 10

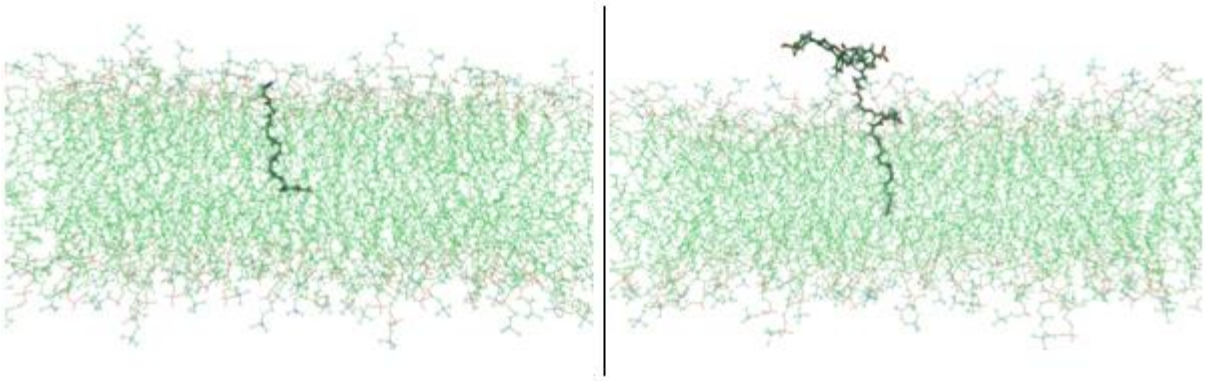

Fig. 8 Simulation snapshots of molecules in lipid bilayer with surrounding water. LEFT: Virodhamine endocannabinoid. RIGHT: Virodhamine + GLY$_4$ linker + QSY-9 dark quencher.

2.5 Synthetic Cannabinoid Binding Location and Energy

Following the molecular dynamics simulations of both *JWH-018 n-pentanoic* and *WIN55-212* in the CB_2 binding pocket, binding energies for each cannabinoid were computed and configurations of the protein's amino acids have been saved for further investigation, as shown in **figure 9** and their total interaction energies in **table 3**. In **table 4**, we report the specific interaction energies for the ten strongest interacting residues. For all residues within 16.0Å, a typical CHARMM potential cutoff, the binding energies are -78.5336 kcal/mol for *JWH-018 n-pentanoic*, and -87.5095 kcal/mol for *WIN55-212*. A lower (more negative) number indicates stronger binding, and these energies have been computed without water interactions.

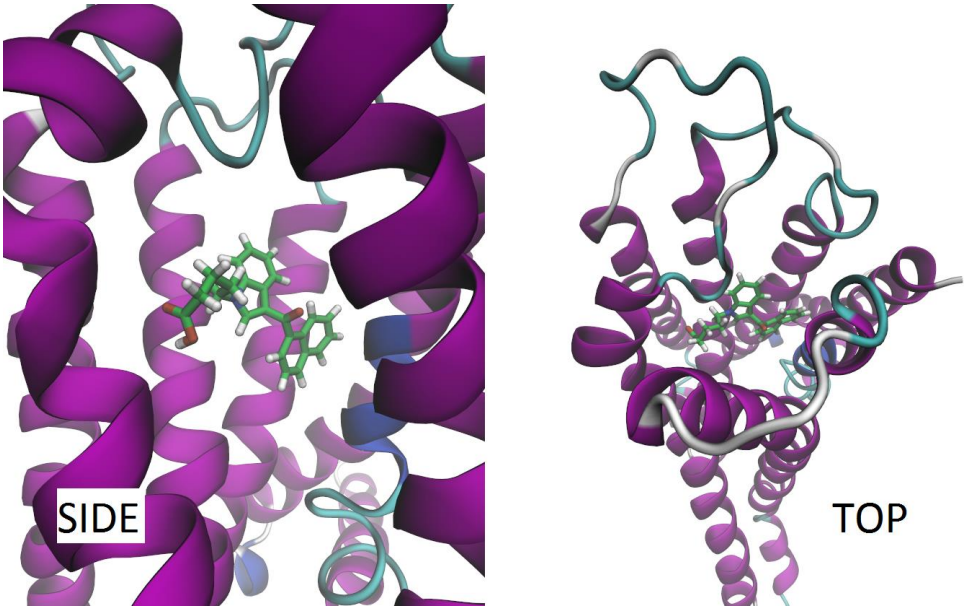

Fig. 9 Snapshot of JWH-018 n-pentanoic ligand in CB_2 receptor. *TOP* is extracellular view.

Table 3. Total interaction energy of select cannabinoids bound to CB_2 receptor. ($k_bT=0.593kcal/mol$)

	kcal/mol
JWH-018 n-pentanoic	-78.5336
WIN55-212	-87.5096

Table 4. Top 10 CB_2 receptor residues based on interaction energies for JH-018 n-pentanoic and WIN55-212 cannabinoids. Common residues are bold, 6 of 10.

JWH-018 n-pentanoic		WIN55-212	
CB_2 Residue	Energy (kcal/mol)	CB_2 Residue	Energy (kcal/mol)
113	-2.6117	87	-2.9444
114	-2.1063	120	-2.6087
281	-1.9720	288	-2.4832
87	-1.9719	113	-2.3806
117	-1.8661	290	-2.2568
258	-1.6451	291	-2.2259
121	-1.6254	258	-2.0514
84	-1.4880	117	-1.6907
288	-1.4261	281	-1.6866
289	-1.2407	80	-1.3274

2.6 Optimal Dark Quencher (DQ) Linkage

We can estimate the best locations for QSY7/9 attachment to the synthetic cannabinoid through analysis of several molecular simulations. Shown in **figure 10** is a snapshot of the JWH-018 synthetic cannabinoid diffusing in a lipid bilayer. The orientation shown—alkyl tail parallel to the lipid tails—is common to the ligand over the course of the simulation (~50 nanoseconds). [71] Attachment of the DQ to the cannabinoid should minimize deviation of the ligand from this orientation, as it is hypothesized that the cannabinoid enters the CB_2 receptor in this orientation.

Figure 11 shows the orientation of JWH-018 n-pentanoic and WIN55-212 within the CB_2 receptor, with a view through the hypothesized binding pathway of TM6 and 7. Based on ligand orientation in **figure 11** *and* the idea that the ligand does not significantly change orientation once in the binding pocket, the alkyl tail of JWH-018 and ether-end of WIN55-212 would proceed first through the opening between TM6 and TM7 during binding. This mechanism was cited previously for an endocannabinoid. [59] To have minimal impact on this binding process, the attachment location of a DQ linker would be on the indole or carbon ring ends of the synthetic cannabinoid, and the linker would follow out of the opening between TM6 and TM7 to the DQ.

Taking into account lipid and CB_2 bound orientation, but not experimental feasibility, **figure 12** outlines optimal areas of DQ attachment. The optimal attachment location is at one of the carbons in the non-indole ring structure, shown in *green*. Second, is a carbon on the indole in *yellow*. Third is attachment to the alkyl chain in *red.*

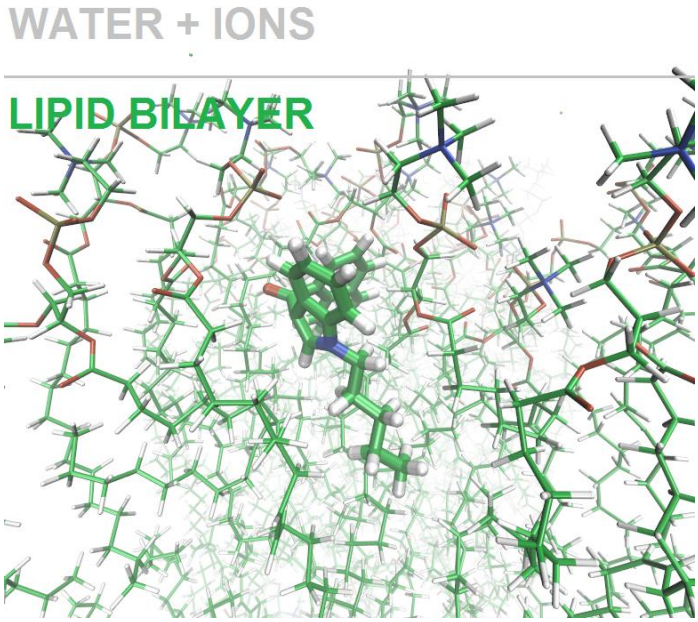

Fig. 10 JWH-018 (thick lines) diffusing in a lipid bilayer (thin lines).

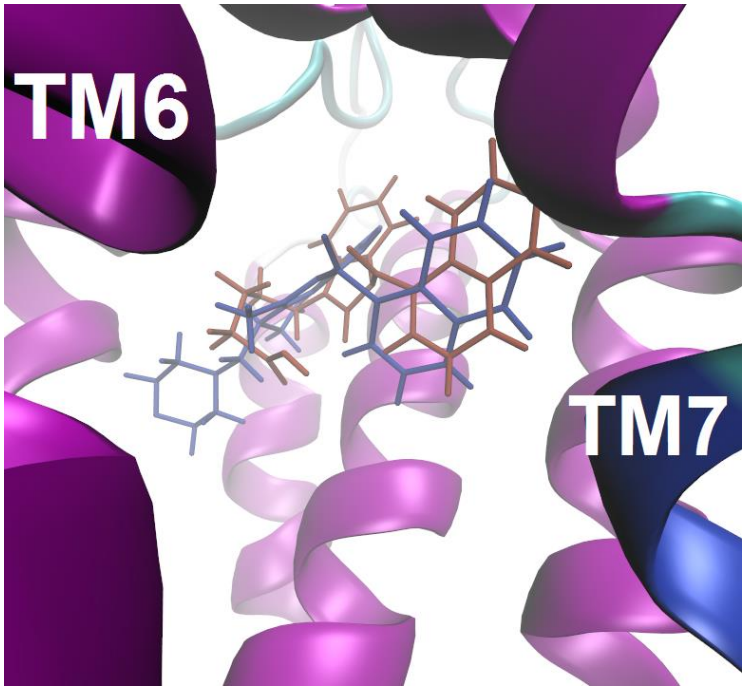

Fig. 11 JWH-018 *n-pentanoic* (red) and WIN55-212 (blue) in the CB2 receptor.

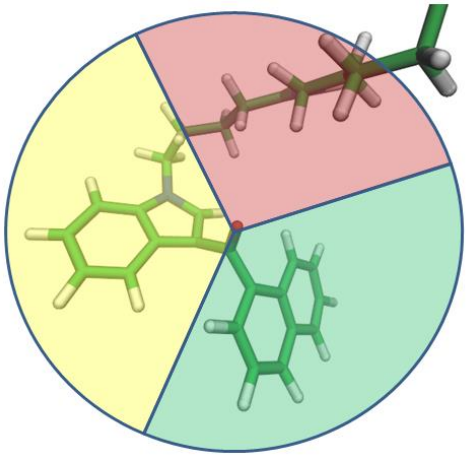

Fig. 12 Alkyl chain (red), indole (yellow), and carbon rings (green).

We have shown optimal location of several endo and synthetic cannabinoids in the lipid bilayer and within the CB_2 binding pocket. With the attachment of the dark quencher however, binding could be hindered due to DQ size, resulting in an inability of the conjugate to reach the binding

pocket. To maintain the desired orientations of the cannabinoid in the binding pocket after DQ attachment, we propose modifications to direct conjugate, JWH-018-*n-pentanoic*-QSY7. The addition of PEG (polyethylene glycol) spacers at the attachment point may provide both flexibility for the cannabinoid-end of the conjugate to bind to CB_2, and length for the DQ to exist at the lipid/solvent interface.

Conservatively accounting for fluctuations in temperature, a PEG multiplier of 10x or greater may achieve the desired flexibility and length. The estimated spacing distance is ~25 to 35Å from the cannabinoid attachment point to the lipid/solvent interface, following the surface of the CB_2. Linear length of one PEG unit (OCH2CH2), from O to C is ~3.37Å. As shown in **figure 13**, 10 PEG spacers allow for DQ position at the interface, while preserving the normal bound orientation of JWH-018. Here, PEG spacers span the distance from the CB_2 TM3 (trans-membrane helix 3) side of the binding pocket, between TM6/7, and finally up toward the lipid/solvent interface.

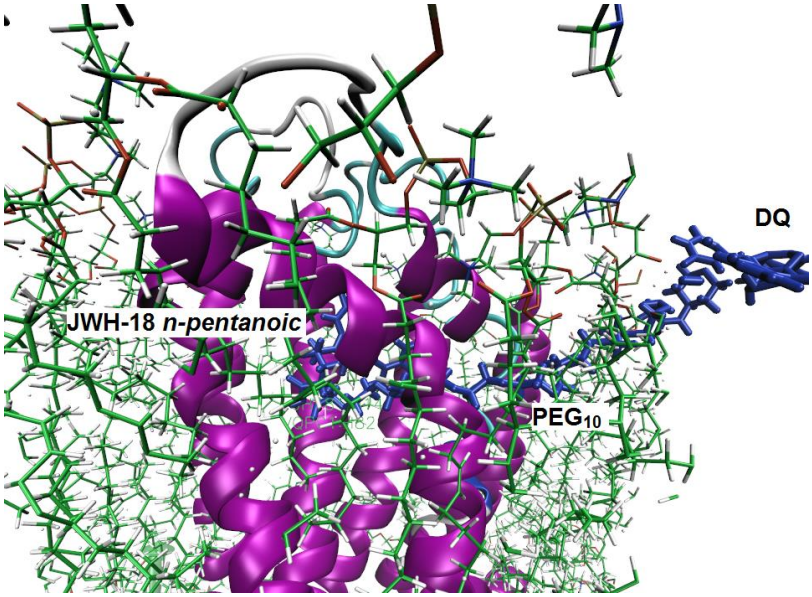

Fig. 13 Artificial configuration of JWH-018 *n-pentanoic/*QSY7 conjugate with 10x PEG spacer bound to CB_2 receptor. A lipid bilayer within 5Å of the CB_2 receptor is shown for perspective. Labels of conjugate components are shown on image.

2.7 Simulations of Conjugate Binders

Assuming a positive binding ability of the JWH-018-QSY7 conjugate we hypothesized that the ligand conjugate could be adopting alternate binding configurations within the receptor. These alternate configurations may not be optimal for efficient activation of the CB_2 when compared to single cannabinoid activation; however a small portion of CB_2 could see activation through

alternative binding. If CB_2 activation in an experimental study of a cannabinoid-DQ conjugate is observed, this could be due to the alternate binding orientation.

Accordingly, a long molecular dynamics simulation using an alternate binding orientation of the conjugate was conducted to test the validity of the above hypothesis. Starting from a CB_2 structure taken from a simulation where JWH-018 *n-pentanoic* metabolite was bound, the JWH-018-QSY7 conjugate was inserted in place of the original ligand. **Figure 14** shows the inserted conjugate. In contrast to JWH-018 *n-pentanoic*, an alternate orientation was created allowing the linked QSY7 to extent directly out of a known binding pathway between transmembrane (TM) helicies 6 and 7. **Figure 15** shows an extracellular view of the initial structure.

After several nanoseconds of simulation, the behavior of the ligand and surrounding CB_2 structure were analyzed. In **figure 16**, an overlay of TM6 and 7 are shown for a CB_2 containing the bound JWH-018 *n-pentanoic* metabolite ligand (green) and a CB_2 containing the conjugate in an alternate bound configuration (blue). The thicker band shows evidence of alpha-helix formation, while the thin strand shows structurally disrupted helix. The alternate binding orientation of the conjugate causes a greater disruption in the helical structure of TM7 in comparison to the single cannbinoid ligand metabolite. In **figure 17**, an overlay of the bound orientation of JWH-018 *n-pentanoic* and the JWH-018-QSY7 conjugate is shown. Similar atoms in both ligands are identified and it is estimated that the new orientation is close to a 90 degree rotation of the cannabinoid end. Of note is the location of the indole ends of the ligands. Both the single cannabinoid metabolite and conjugate share a similar location of their indole rings, although they are angled slightly differently. Overall, simulation of the alternate binding location demonstrates a probable bound structure of the conjugate. We have not, however, attempted to demonstrate CB_2 activation via this direction of binding.

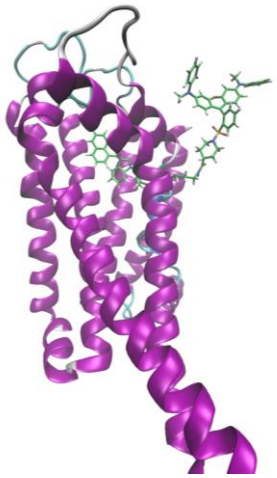

Fig. 14 JWH-018-QSY7 conjugate inserted into binding pocket of CB_2 receptor. QSY7 end extends out of the receptor through TM6/7.

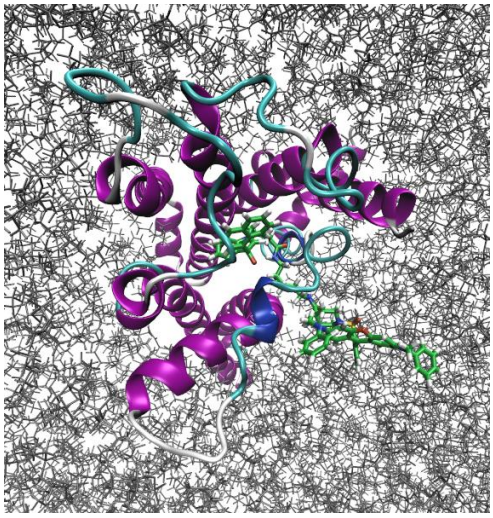

Fig. 15 Top view of JWH-018-QSY7 conjugate bound to CB_2 receptor. Water and ions have been removed for clarity, lipid bilayer shown in gray.

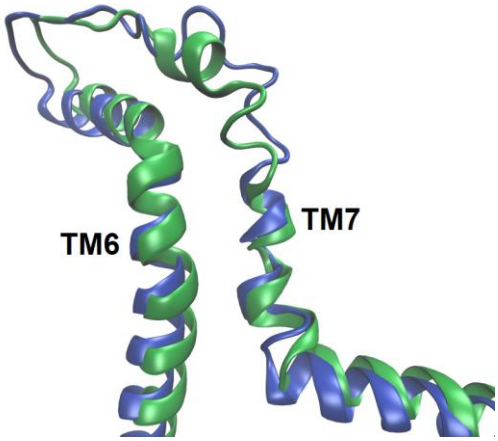

Fig. 16 Overlay of CB_2 TM6 and 7 for bound JWH-018 *n-pentatnoic* (green) and bound JWH-018-QSY7 conjugate (blue).

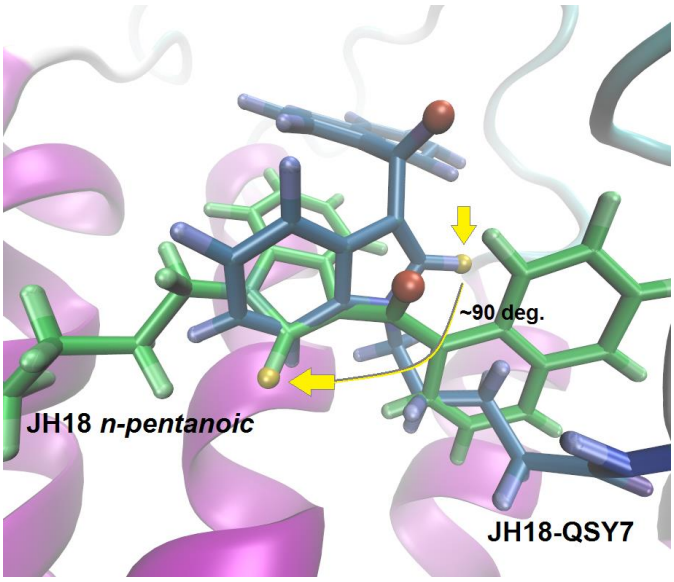

Fig. 17 Overlay of JWH-018 n-pentanoic (green) and JWH-018-QSY7 conjugate (blue) bound to the CB_2 receptor. Similar atoms on both ligands are highlighted with colored spheres. Estimated difference in binding orientation is ~90 degrees.

3. Synthesis of Materials

3.1 Synthesis of Cannabinoid Receptor 2 (CB_2)

A plasmid vector which expresses the human CB_2 protein was inserted into *E. coli* cells. *E. coli* cells were grown in medium containing ampicillin and glucose. Fermentation of cells continued for 42-45 hours, during which functional CB_2 protein was synthesized by the *E. coli*.[72] The cell walls of *E. coli* cells were removed, turning the cells into spheroplasts. After being resuspended in ice cold water, the spheroplasts underwent osmotic lysis, and remaining intact cells were sonicated and broken up. The extract was centrifuged and resuspended in Tris buffer. After the cell debris was sonicated and centrifuged out of the solution, it was filtered and purified through immobilized metal affinity chromatography.[72]

Nanodiscs have the advantage of containing one or very few proteins, allowing for greater access to and control over the proteins' physical parameters and can be incorporated into nanodevices.[73] The CB_2 receptor is pre-solubilized in a detergent, which is then removed by a column. It is then mixed with varying ratios of phospholipid and membrane scaffolding protein (MSP), and the CB_2 will self-assemble into Nanodiscs.[74, 75]

3.2 Characterization of CB_1 Infections

Four previously synthesized, independent infections of Sf_9 cells with baculovirus encoding human CB_1 receptor were analyzed for CB receptor activity. **Figure 18** and **figure 19** show the activity of two of the previously synthesized infections. Based on this data, a urea wash was performed on CB_1#4 to remove some of the endogenous G protein.

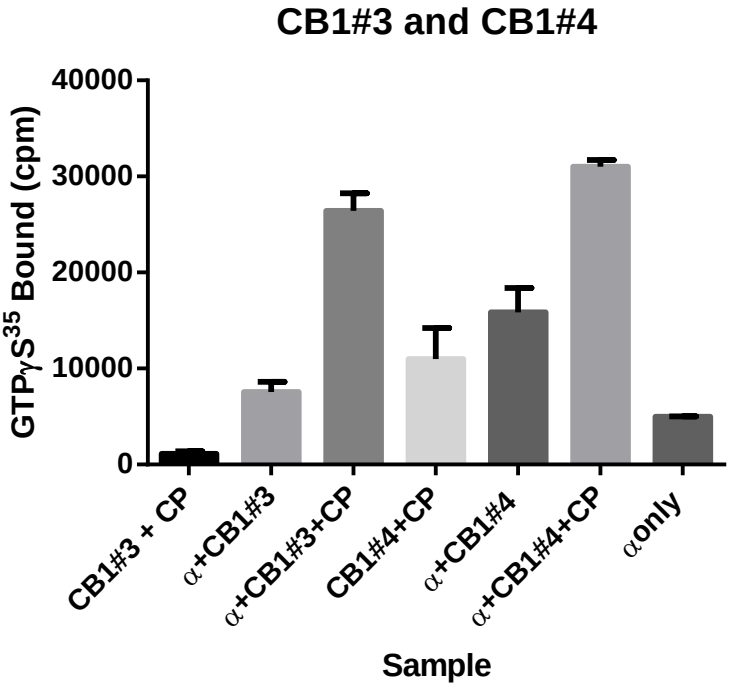

Fig. 18 Characterization of a urea extracted plasma membrane fraction (CB_1#3) and untreated plasma membrane fraction (CB_1#4). These data show the presence of CB activity based on activation by CP55,940 and also the extraction of endogenous G protein by urea treatment of CB_1#3.

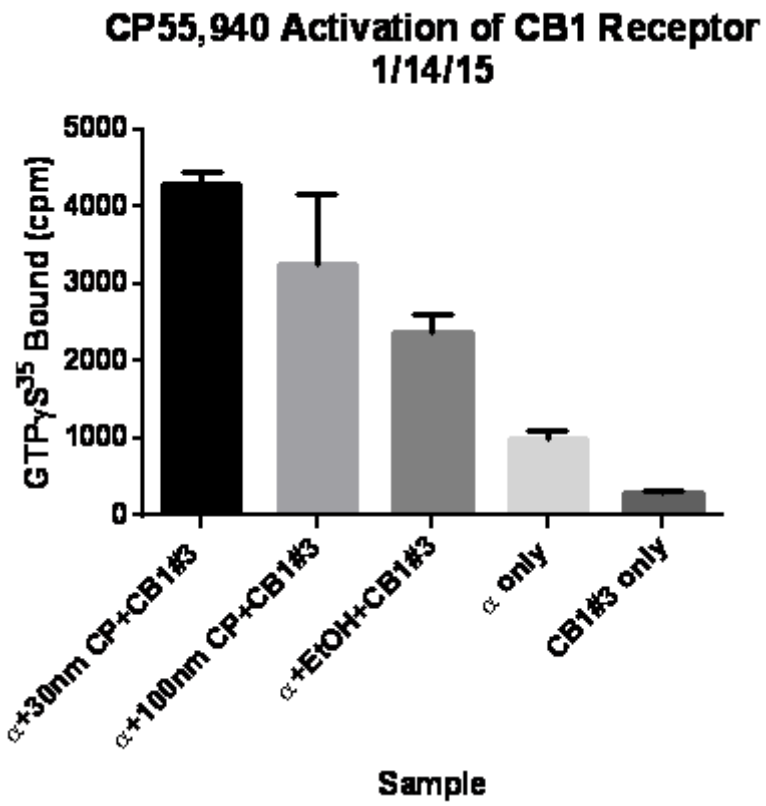

Fig. 19 Activation of CB_1 receptor with 30nM, and 100nM CP55,940.

3.3 $G\alpha_{i1}$ Production

E. coli cells expressing myr-$g\alpha_{i1}$ were grown to five liters in medium containing ampicillin and kanamycin. The cells were pelleted and lysed. The lysate was then purified (Modified from Mumby and Linder, Methods of Enzymology, vol. 237, pages 254-268, 1994) by DEAE-A25 Sephadex, DEAE Sphacel, and phenyl sepharose fast flow operated by an FPLC. After the phenyl sepharose column, the fractions were analyzed by GTPγS assay. The results of one purification can be seen in **figure 20** and **figure 21**. The fractions containing α_{i1} were pooled and concentrated using an Amicon PM 30. A Fast Q FPLC column was run to further purify and separate the α_{i1} sample. The sample was analyzed, concentrated, and then a desalting G-25 column was run to remove excess guanosine diphosphate (GDP).

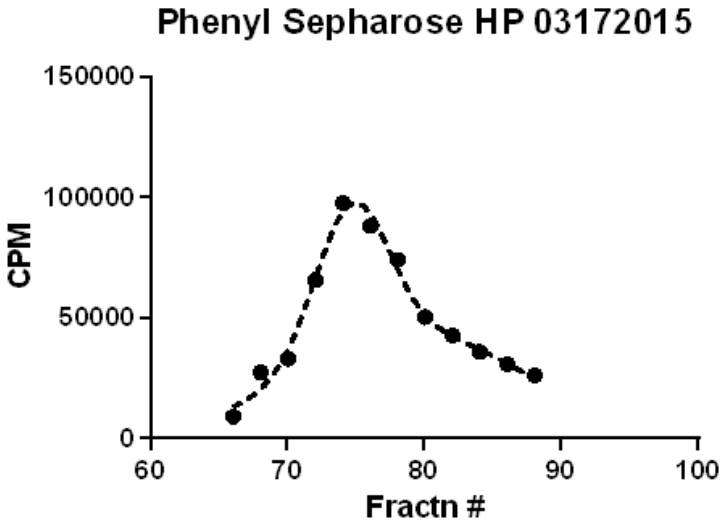

Fig. 20 GTPγS analysis of various fractions containing α_{i1} after FPLC phenyl sepharose column purification. The data best fits the sum of two gaussians, showing the presence of both myristolated and non-myristolated α_{i1}.

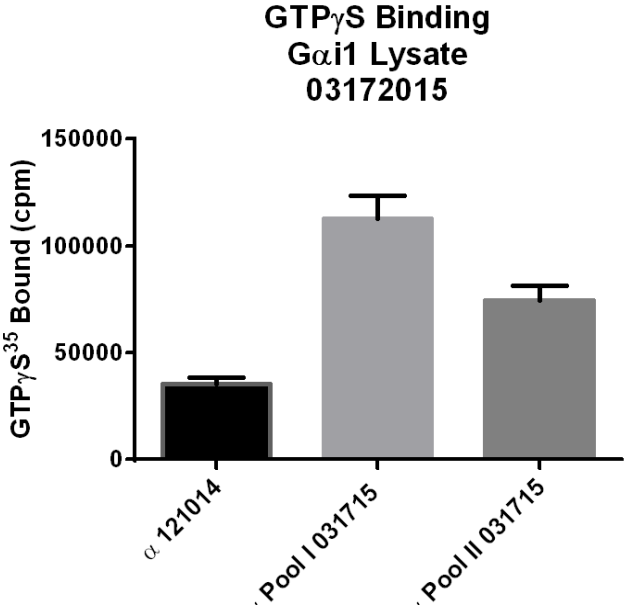

Fig. 21 GTPγS analysis of various pools containing α_{i1} after purification.

3.4 Ligand-Dark Quencher Conjugation

A properly designed ligand-dark quencher system that is highly robust and functional is critical to the development of both the fluoroanalytical and bionanoelectronic synthetic cannabinoid detection platforms. The primary design requirements of the ligand-dark quencher conjugate are two-fold:

1. A ligand whose affinity for the CB_2 receptor protein is in a range such that it is readily displaced by the majority of synthetic cannabinoids while not being competitively displaced by other molecules (non-cannabinoids) in the system.
2. Transport a dark quencher molecule within FRET-coupling range of the fluorescent quantum dot.

The first step in meeting the stated criteria is the selection of a CB agonist of relatively low binding affinity compared to synthetic cannabinoids that is also amenable to linkage chemistry. The endocannabinoid Virodhamine, structure shown in **figure 22**, is a potential candidate due to its CB_2 binding affinity of 381nM [76-78]. Although a binding affinity of 381nM is strong in biological terms, it is relatively low compared to the target synthetic cannabinoids of interest. Virodhamine will thus be readily displaced from the CB_2 binding pocket by the vast majority of cannabinoid molecules, as shown in **Table** 5**5**. Additionally the functional amine group on tail-end of the Virodhamine molecule allows it to be potentially amenable to simple linkage chemistry.

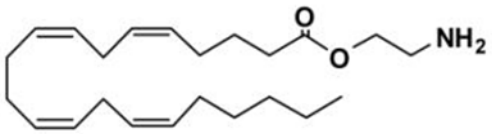

Fig. 22 Molecular structure of the endocannabinoid virodhamine.

Table 5. Relative CB_2 binding affinity of select cannabinoid molecules versus virodhamine

Compound	CB2 Ki (nM)	Relative Affinity (ref. Virodhamine)
Virhodamine	381	1.00
Noladin ether	3000	0.13
NADA	12001	0.03
Anandamide	279	1.37
2-Arachidonylglycerol	145	2.63
AM-2201	2.6	146.54
JWH-018	2.94	129.59
JWH-081	0.12	3175.00
JWH-122	1.2	317.50
JWH-203	7	54.43
JWH-210	0.69	552.17
JWH-250	33	11.55
MAM-2201	2.6	146.54
RCS-4 2-methoxy isomer	33	11.55
CP 55,940	0.68	560.29
HU 210	0.17	2241.18
O-2545	0.32	1190.63
WIN 55,212-2	3.13	121.73
Bay 59-3074	0.28	1360.71
9-THC	3.13	121.73

Utilizing virodhamine as the dark-quencher carrier, a conjugation scheme was designed to synthesize the ligand-dark quencher pair. The dark quencher used in this design was a succinimide ester functionalized QSY-9 molecule [79], as shown in **figure 23**. With its strong absorption maxima at 562nm (ε_{562} = 86,000$M^{-1}cm^{-1}$), its energy level is in the desired range to achieve the quantum dot FRET-coupling competition for the bacteriorhodopsin bioelectronics.

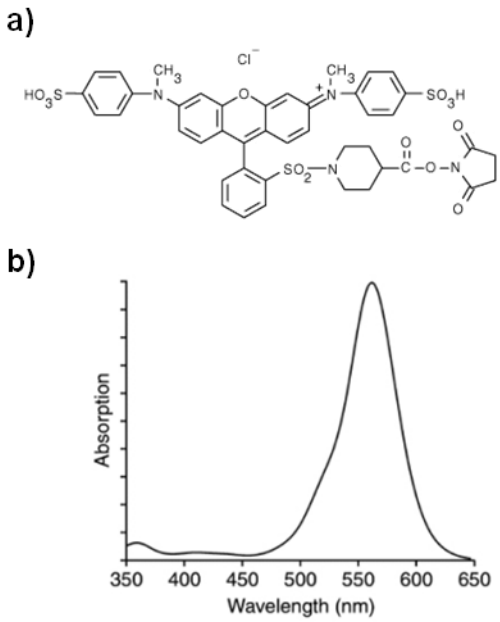

Fig. 23 (a.) Molecular structure of NHS-QSY-9 dark quencher and (b.) corresponding absorption spectra.

The QSY-9 molecule can be ordered pre-functionalized with 1-Ethyl-3-(3 dimethylaminopropyl) carbodimide (EDC) and N-hydroxysulfosuccinimide (sulfo-NHS) to be highly reactive to available amine groups (Invitrogen #Q20131). This will allow for a zero-length linkage of the Virodhamine amine group to the NHS functionality on the QSY-9 molecule, as shown in **Fig. 24** Direct linkage mechanisms forming Virodhamine-QSY-9 conjugate

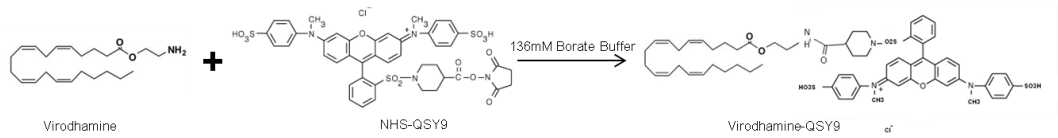

Fig. 24 Direct linkage mechanisms forming Virodhamine-QSY-9 conjugate

Peptide bond formation between the carboxylic acid of the QSY-9, and the primary amine of Virodhamine, will produce a stable linking of the two molecules. Using the commercially available succinimidyl ester functionalized QSY-9; the reaction proceeds well under basic conditions. The reaction was performed in borate buffered DMSO pH 8.5, with a 3:1 molar ratio of virodhamine to QSY-9, stirred at room temperature for 2.5 hours in dark conditions. Using cold ether, the product was precipitated and washed several times again with ether, leaving a dry purple solid. The products were dissolved and characterized by using a 6000 series Agilent ® LC/ MS, fitted with a Zorbax C-18 SB column and quadrupole electrospray ionization (ESI) mass spectrometry (MS).

The large QSY-9 molecule (MW 951.43 g/mol) could hinder access of the virodhamine molecule to the CB_2 binding pocket or the degree of binding affinity of the CB_2 to the tagged virodhamine. In anticipation that such hindrances could occur, additional ligand-dark quencher systems were synthesized by integrating a polyethylene glycol spacer, as shown in **figure 25**, between the virodhamine and QSY-9 molecules to allow greater mobility of the virodhamine. Spacer lengths of 1.81nm (Thermo #26120), 3.36nm (Thermo #26122), and 4.68nm (Thermo #26124) were achieved utilizing engineered PEG molecules with integrated carboxyl and amine functional groups, as shown in **figure 11**. A multi-reaction process is required to create the Virodhamine-(PEG)x-QSY-9 conjugate and is outlined in **figure 26**.

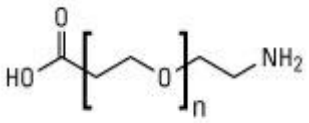

Fig. 25 Carboxyl and amine functional PEG spacers.

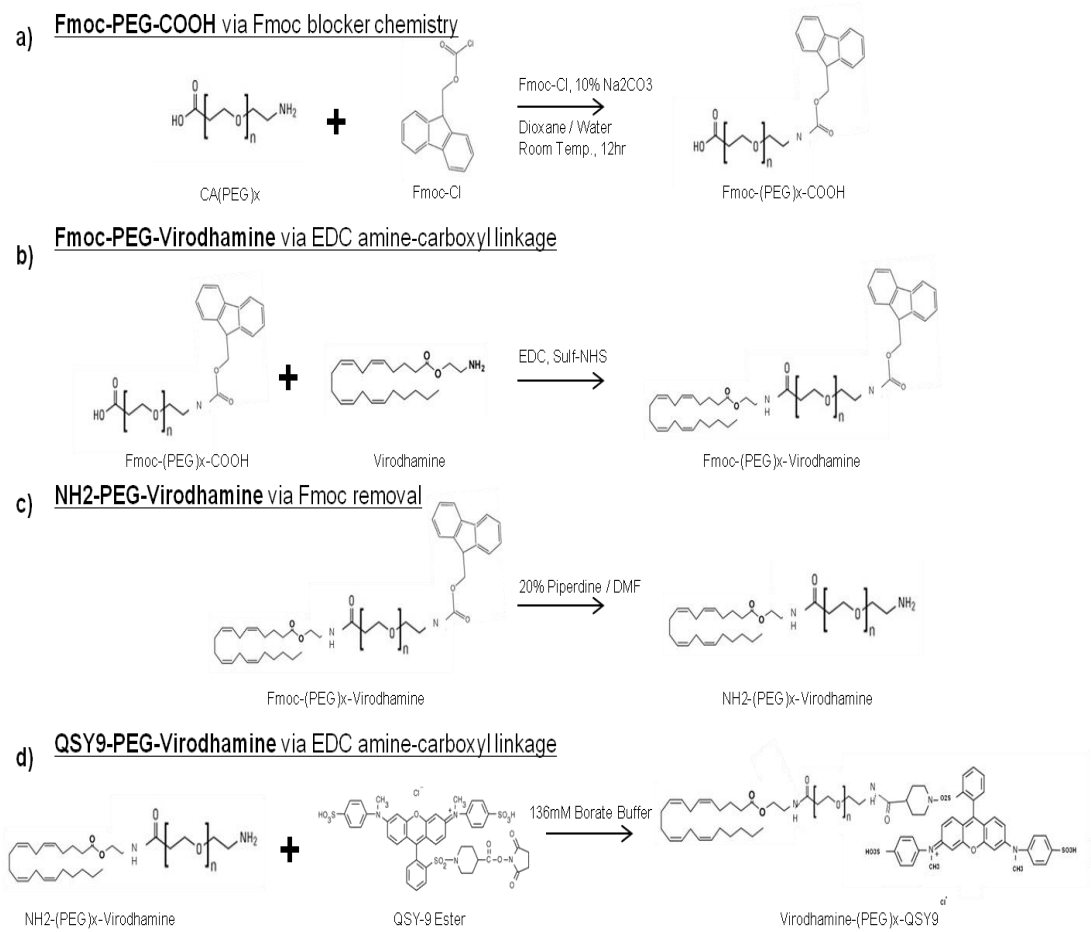

Fig. 26 Synthesis route to form ligand-dark quencher conjugate with varying PEG spacer lengths of 1.81nm, 3.36nm, and 4.68nm. Steps involve: (a) Blocking the amine group on the COOH-(PEG)x-NH2 material, (b) linking the functional carboxyl group on the (PEG)x to the Virodhamine amine group through a zer-length

heterofunctional linker, (c) removal of the amine blocker on the (PEG)x, and (d) linking the NH2-(PEG)x-Virodhamine conjugate to the NHS-QSY-9 dark quencher.

3.4.1 Virodhamine - QSY-9 Conjugates

Figure 27 shows the mass fragment of the virodhamine to QSY-9 conjugation product in a positive ion scan. **Figure 28** shows the LC chromatogram in which multiple peaks are present, identifying impurities in the product. ^{1}H nuclear magnetic resonance (NMR) was carried out, however the over saturation from dimethyl sulfoxide (DMSO) signal decreased the products signal, with more scans and removal of excess DMSO chemical structure can be determined. The virodhamine ligand was dissolved in ethanol before use; the presence of this alcohol may have reacted with the succinimidyl ester of the QSY-9. To avoid this side reaction a solvent exchange of virodhamine from ethanol to DMSO was carried out prior to the reaction.

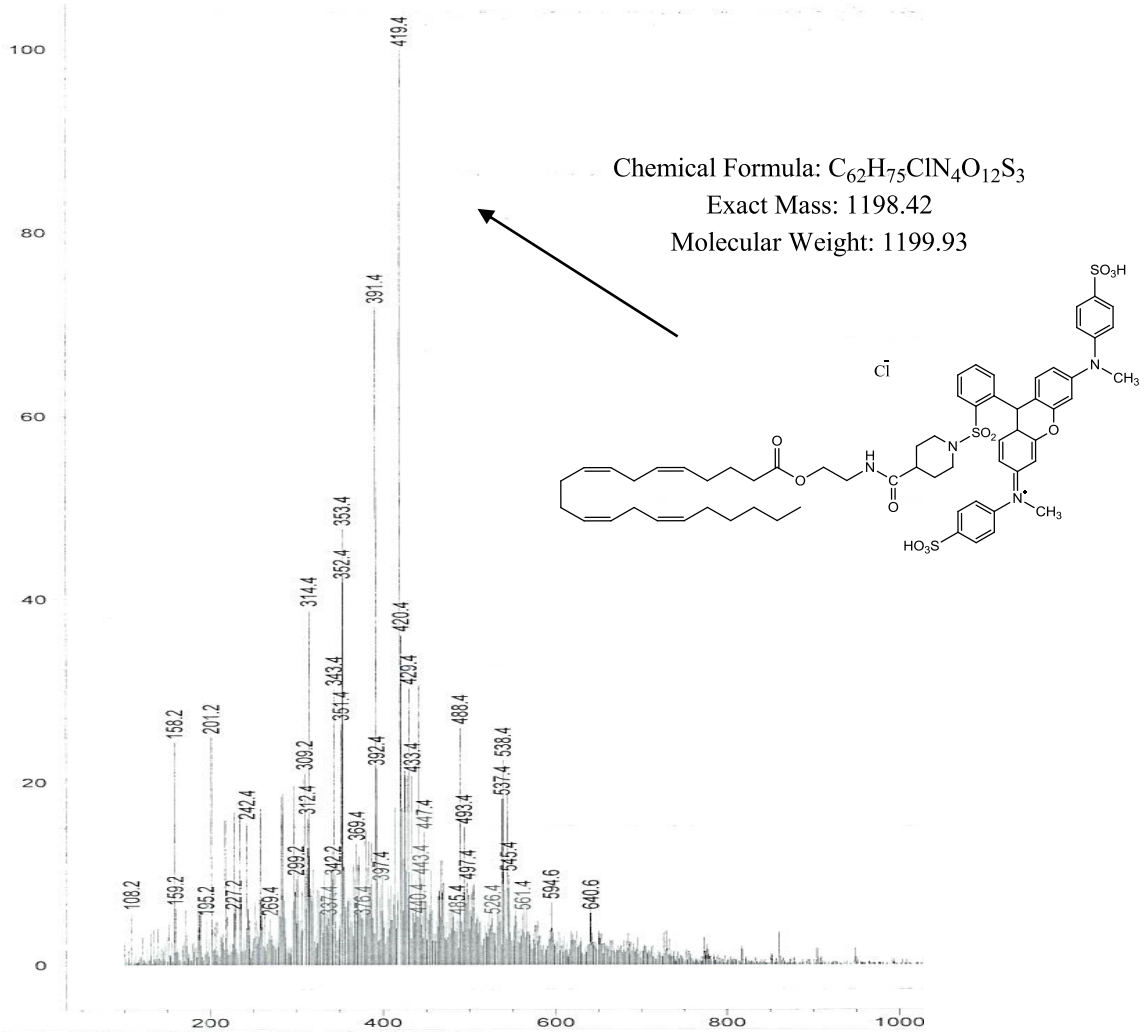

Fig. 27 MS of Virodhamine-QSY-9 conjugate with fragment main peak of 419.4 with added H_2O (1198 + H^+ /3).

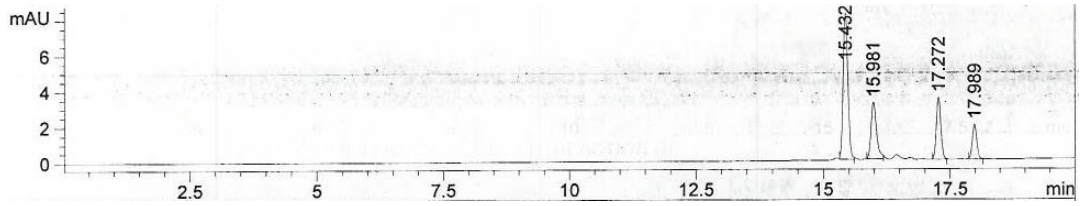

Fig. 28 LC chromatogram using gradient method 0-100%B in from 0-20 min, with 5mM ammonium formate H_2O as solvent A, and MEOH as solvent B.

Results from the initial linking protocol showed a large quantity of impurities in the final sample. To clarify the impurities, further analysis of the virodhamine molecule was performed on a gas chromatography – mass spectrometer (GC/MS) instrument. The virodhamine sample was extracted directly from the stock container, and inserted into the GC/MS for analysis. The resultant eluted compounds versus run time are shown in **figure 29**.

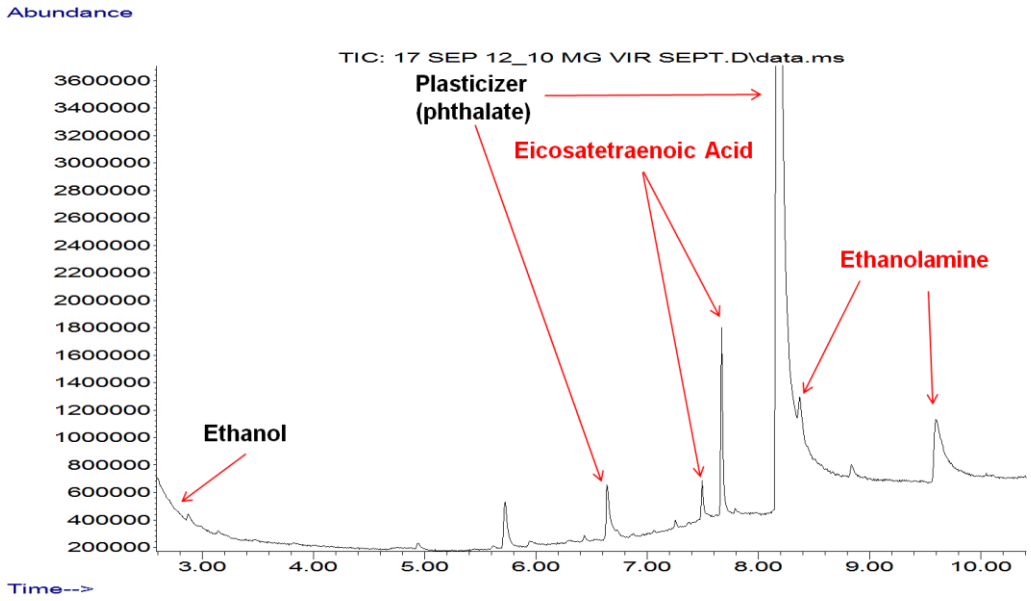

Fig. 29 GC/MS chromatogram of virodhamine stock solution.

It can be seen in **figure 29** that a multitude of compounds are present in the sample, with most of the major peaks being associated with plasticizers from the product packaging. It is known from previous research that virodhamine, which is derived by forming an ester linkage between arachidonic acid and ethanolamine, will ionize and the ethanolamine compound with a 62m/z ratio is the primary marker. From the chromatogram, the ethanolamine mass/charge ratio was found at

two different time points, as shown in **figure 30**. Isolating those elution points, as shown in **figure 31**, reveals a large array of compounds present.

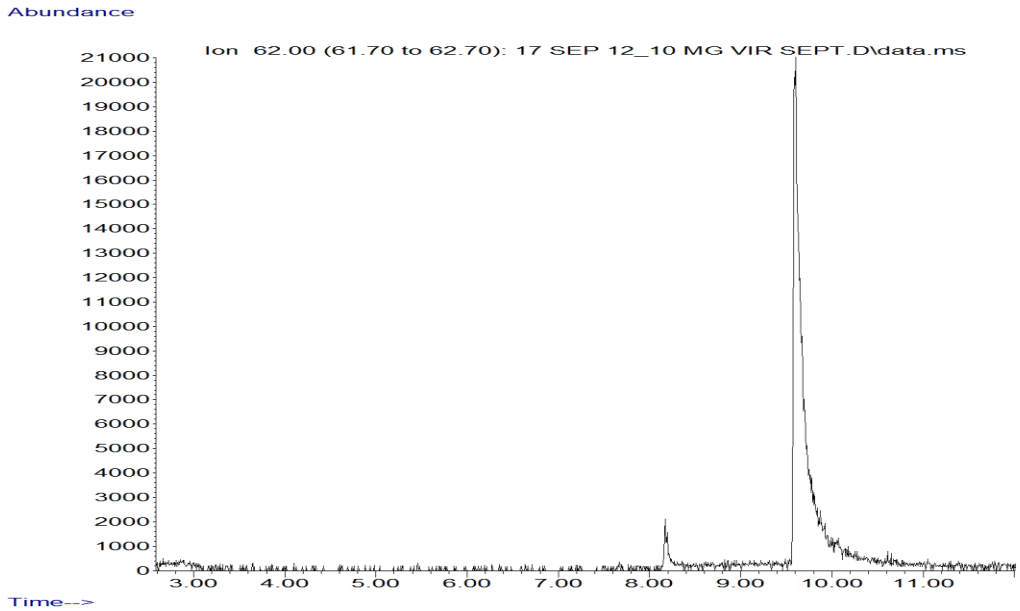

Fig. 30 GC/MS chromatogram isolating a 62m/z ion, which possibly relates to ethanolamine.

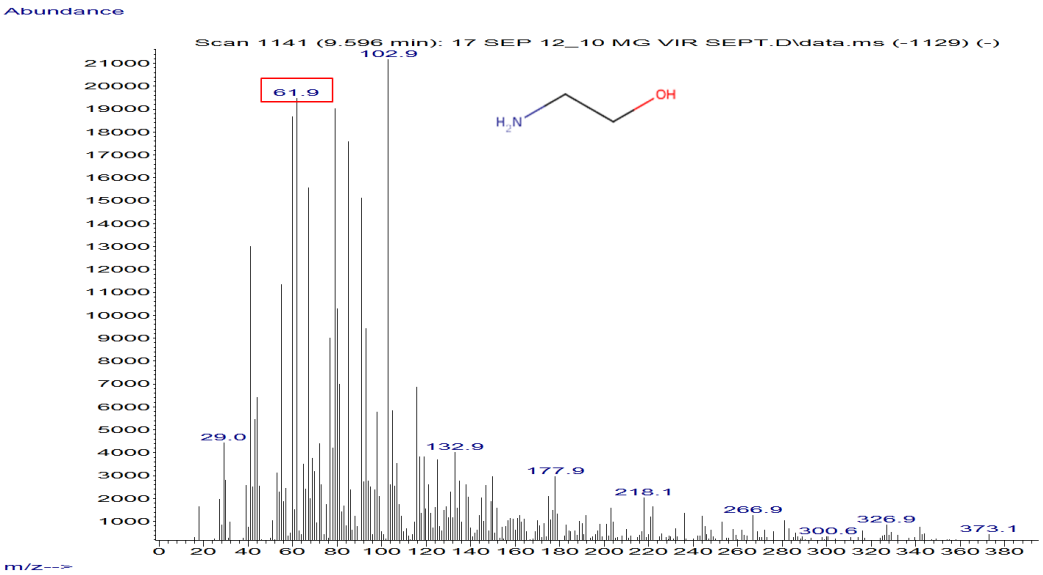

Fig. 31 Mass spectra of elution points yielding potential ethanolamine ions.

Additionally, apart from the ethanolamine component, the arachidonic acid ionized compound could also be located. As shown in **figure 32**, a spectra is revealed that matches that of arachidonic acid, although the GC/MS library labels the molecule as Eicosatetraenoic acid; which is a similar long-carbon chain molecule.

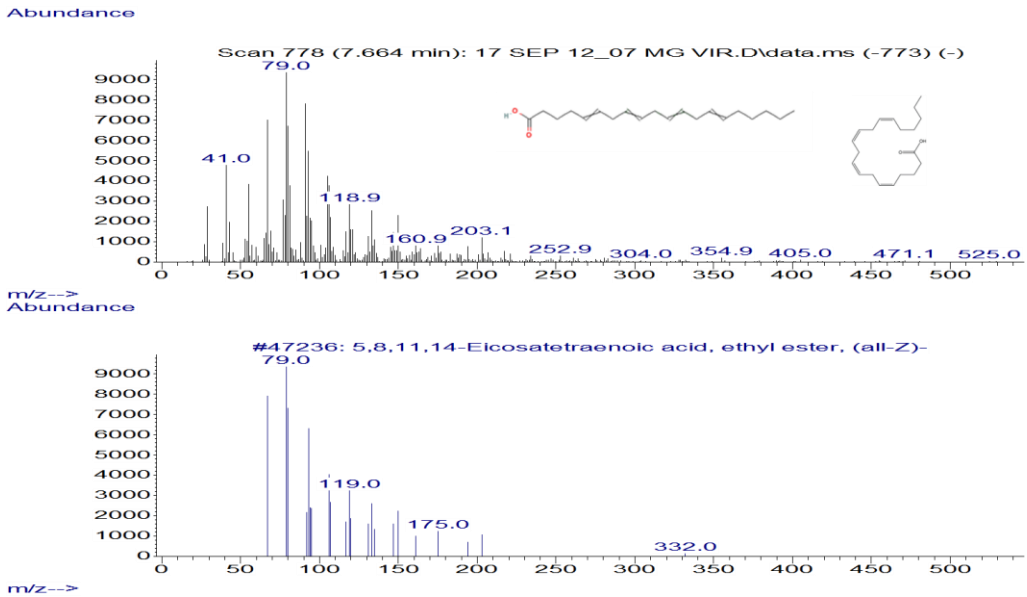

Fig. 32 Mass spectra from Virodhamine conjugate (top) in comparison to Eicosatetraenoic acid (bottom), a compound similar to arachidonic acid.

No ionization spectra was found correlating to the intact virodhamine structure. This, in correlation with the varying elution times of the virodhamine related compounds, suggest that potentially the stock virodhamine had hydrolyzed.

The strong presence of plasticizers and potentially hydrolyzed material implies that the purchased virodhamine stock might not be of optimal quality. A new order was placed from a different supplier for virodhamine. A new, unopened sample of virhodamine that was stored under dessicant at -20℃ was analyzed on the GC-MS. This sample looks identical to the previous GC-MS data for the opened virodhamine vial. Therefore, one may conclude that the method of analysis is less than ideal and the sample itself is intact (e.g. the hard ionization method coupled with the high heat >300℃ destroys the endocannabinoid).

Results from the initial linking protocol showed a large quantity of impurities in the final sample. These high levels of impurities found after the linkage reaction are resultant of improper product purification subsequent to the linkage reaction. Cold ether precipitation generally removes most impurities, however impurities with similar solubilities still persist. To further purify the virodhamine-QSY-9 conjugate, silica short column chromatography were used with n-hexane/ethyl acetate as the eluent.

Liquid chromatography coupled mass spectrometry (LC-MS) is an attractive alternative to GC-MS. LC-MS differs from GC-MS in both the column phase and the ionization method. The column is run in liquid phase at room temperature in contrast to the high temperature gas phase found in GC-MS. In addition, the ionization method for LC-MS uses a much gentler technique than that

found in GC-MS and will allow for detection of the full length compound as opposed to the fragmentation pattern observed in GC-MS. The liquid chromatography aspect of the LC-MS utilizes HPLC to separate the compounds. The ability to separate a variety of cannabinoids via HPLC has been widely described in the literature and should prove much more useful in the separation and characterization of the cannabinoid and the cannabinoid/dark quencher conjugate.[38] The use of LC-MS to confirm the presence of cannabinoids in solution has also been widely published.[34, 35, 41, 80]

3.4.2 JWH-073 – QSY-9 Conjugates

Alternative approaches for cannabinoid to dark quencher linkages were pursued. In this alternative approach the enhanced stability and storage properties of synthetic cannabinoids are harnessed. Synthetic cannabinoids tend to be more stable than their endogenous counterparts because they are designed as possible therapeutic agents. WIN 55, 212-2 (**figure 33a**) and nabilone (**figure 33b**) were used as additional SC-DQ linkage options. The dark quencher QSY-7, amine (**figure 33c**) was also acquired. The additional dark quencher was necessary as the linkage chemistry between WIN 55, 212-2 or nabilone and the dark quencher required reductive amination of a ketone,[81] while the virodhamine linkage chemistry involved coupling between the NHS ester of QSY-9 and the terminal amine of virodhamine. QSY-7 is very similar in overall structure to QSY-9 and has almost identical quenching properties. Therefore, the energy minimization and diffusion calculations are easily adapted to accommodate QSY-7, amine. Nabilone is of interest as the ketone location is different than that of WIN 55, 212-2 (**figure 33**). **Figure 34** illustrates the different structures of the two alternative cannabinoid-dark quencher conjugates.

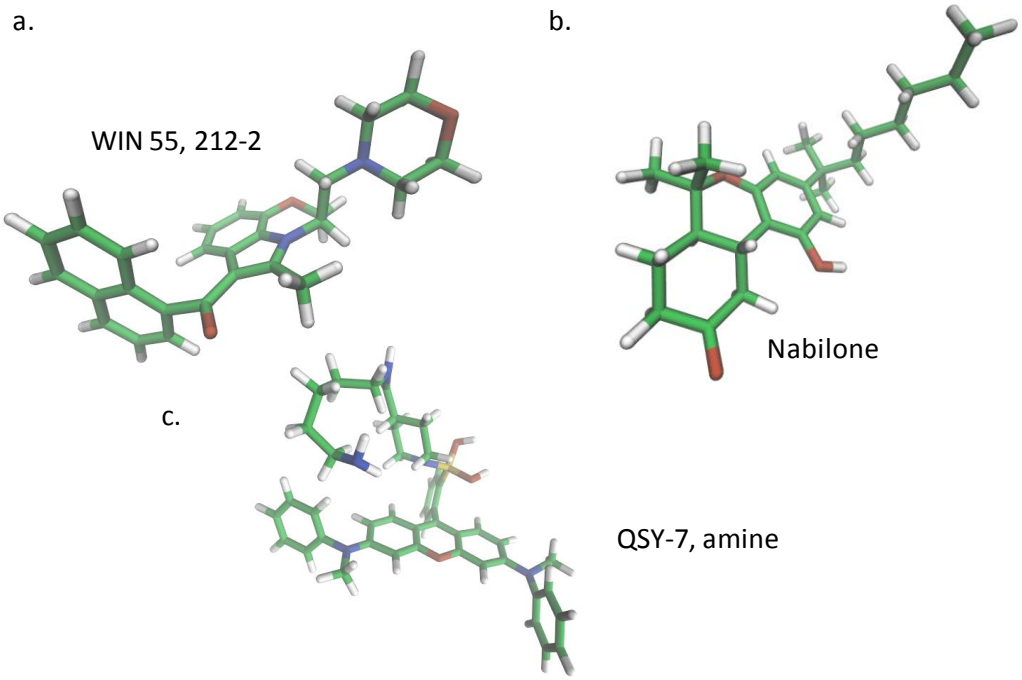

Fig. 33 Structures of the synthetic cannabinoids (a) WIN 55, 212-2, and (b) Nabilone and the dark quencher (c) QSY-7, amine.

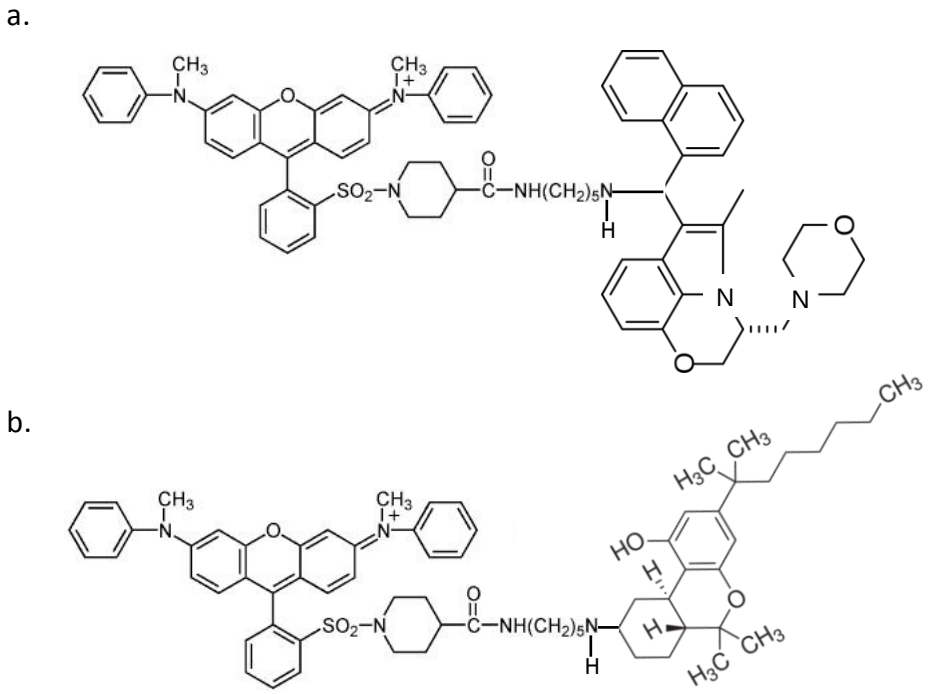

Fig. 34 Conjugation products of (a) WIN 55, 212-2 to QSY-7 and (b) Nabilone to QSY-7. (c) Practice reaction between hexylamine and benzophenone.

Upon further characterization of the products from the practice reactions involving benzophenone (WIN 55, 212-2) or cyclohexanone (Nabilone) and a primary amine hexylamine (QSY-7 amine), the reaction of cyclohexanone was successful while the reaction involving benzophenone was not (**figure 35a and 35b**). In this case the ketone of benzophenone was reduced to the corresponding alcohol as seen by proton NMR. It is hypothesized that harsher reducing agents will be necessary to overcome the steric hindrance caused by the two benzene rings which would then require a two step reaction process. In order to overcome this obstacle, a metabolite of the SC JWH–018 (**figure 36a**) which contains the full structure of the parent compound in addition to a carboxylic acid added at the end of the alkyl chain (**figure 36b**) was used. The standard reaction of direct peptide coupling between the amine of QSY-7 and the carboxylic acid of the JWH–018 metabolite are used for linkage. As the only difference between the parent compound and the metabolite is the addition of a carboxylic acid at the site of DQ conjugation we would hypothesize that utilizing the metabolite in the linkage reaction would be feasible; i.e. the final conjugation product should not affect CB_2 receptor binding any more than the original conjugation products proposed. A model peptide linkage reaction between two compounds, hexylamine and 1-pyrenebutyric acid (**figure 37**), that resemble QSY-7, amine dark quencher and JWH-018 n-pentanoic acid synthetic cannabinoid metabolite (**figure 38**) was created.

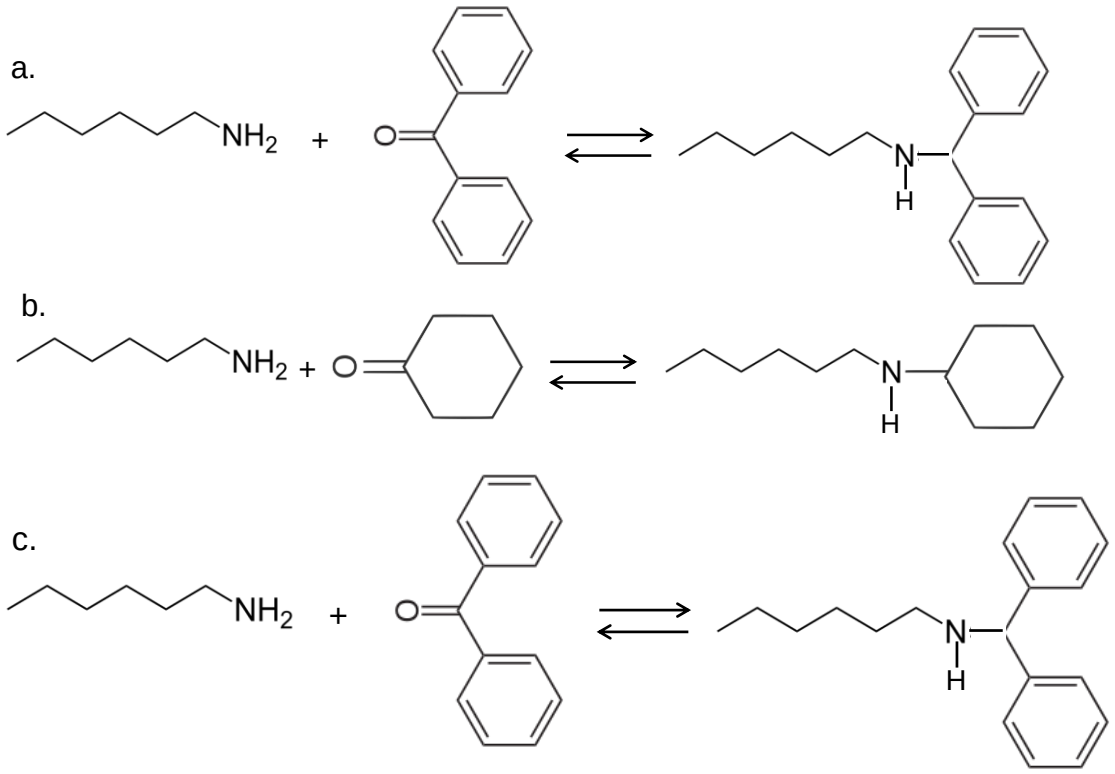

Fig. 35 Conjugation products of practice reaction between (a) hexylamine and benzophenone, and (b) hexylamine and cyclohexanone.

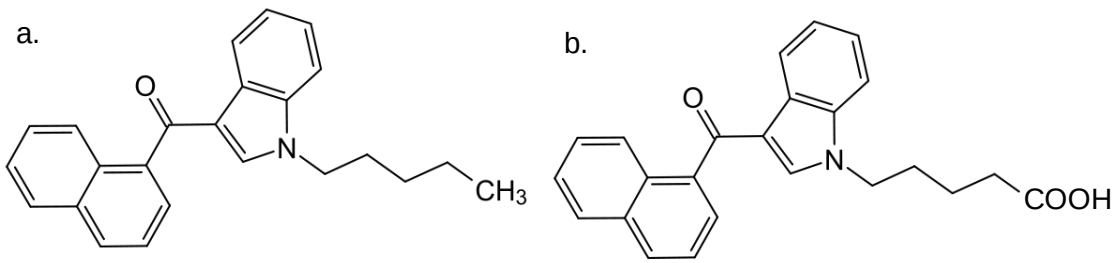

Fig. 36 (a) JWH–018 parent compound and (b) JWH–018 N-pentanoic acid metabolite.

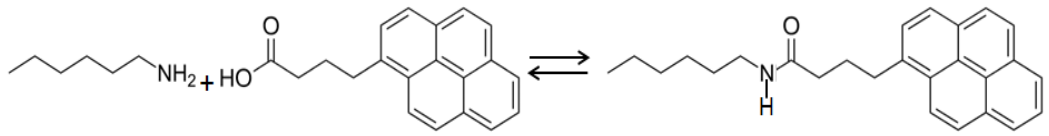

Fig. 37 Conjugation product of practice reaction between hexylamine and 1-pyrenebutryic acid.

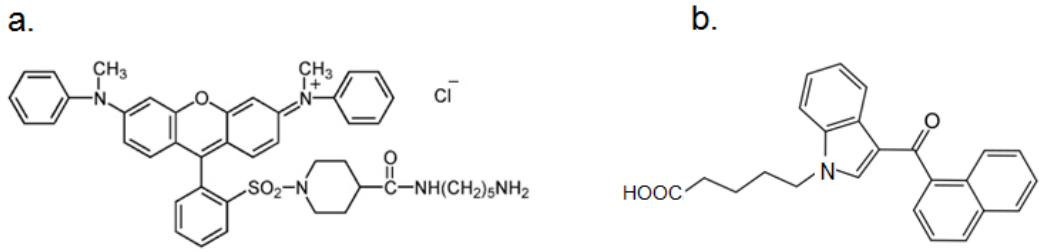

Fig. 38 Molecular structures of (a) QSY-7, amine and (b) JWH- 018 n-pentanoic acid.

The conjugate of QSY-7, amine to JWH-018 pentanoic acid (**figure 39**) was constructed and characterized via Liquid Chromatography Mass Spectrometry. A mass peak at 38.068 minutes of 1096.8 g (**figure 40**) was observed. The expected mass of the QSY-7:JWH-018 conjugate is 1097 g/mol. As shown in **figure 41**, the product peak on the LC chromatogram was relatively small and broad compared to the excess QSY-7 peak that follows at 41.6 minutes. As a result, the ratios between JWH-018 pentanoic acid and QSY-7 should be optimized in the future to obtain as much product as possible and remove the low molecular weight contaminants observed in the mass spectra.

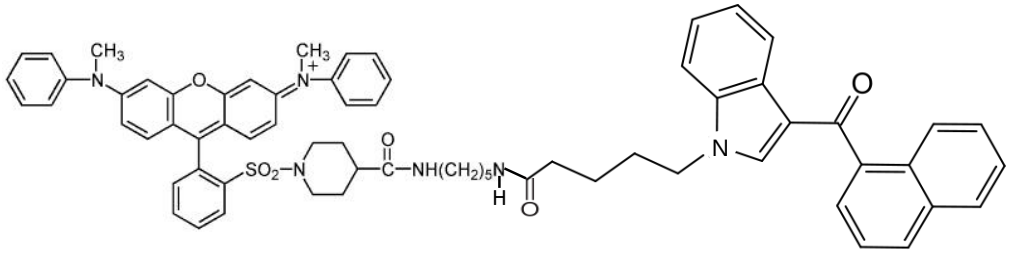

Fig. 39 Conjugation product of QSY-7, amine to JWH-018 pentanoic acid.

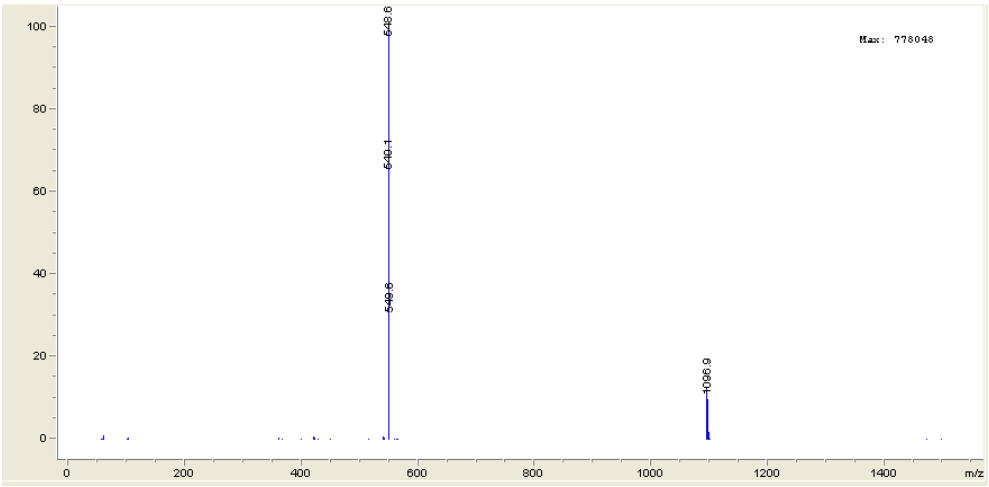

Fig. 40 Mass spectra highlighting the expected mass peak of 1097 g/mol for the conjugate of QSY-7, amine to JWH-018 pentanoic acid.

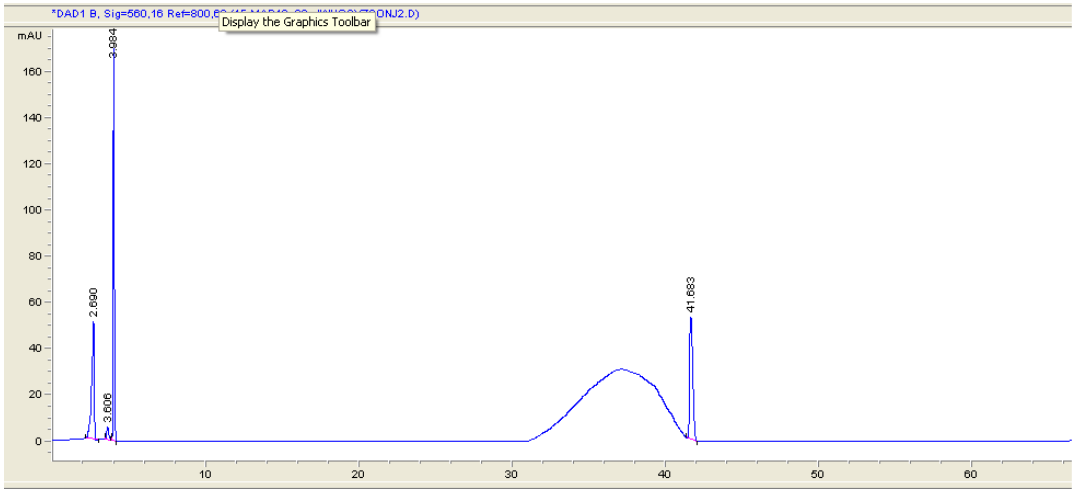

Fig. 41 Liquid chromatograph highlighting the conjugate peak centered at 38 minutes, followed by the excess QSY-7 peak at 41 minutes.

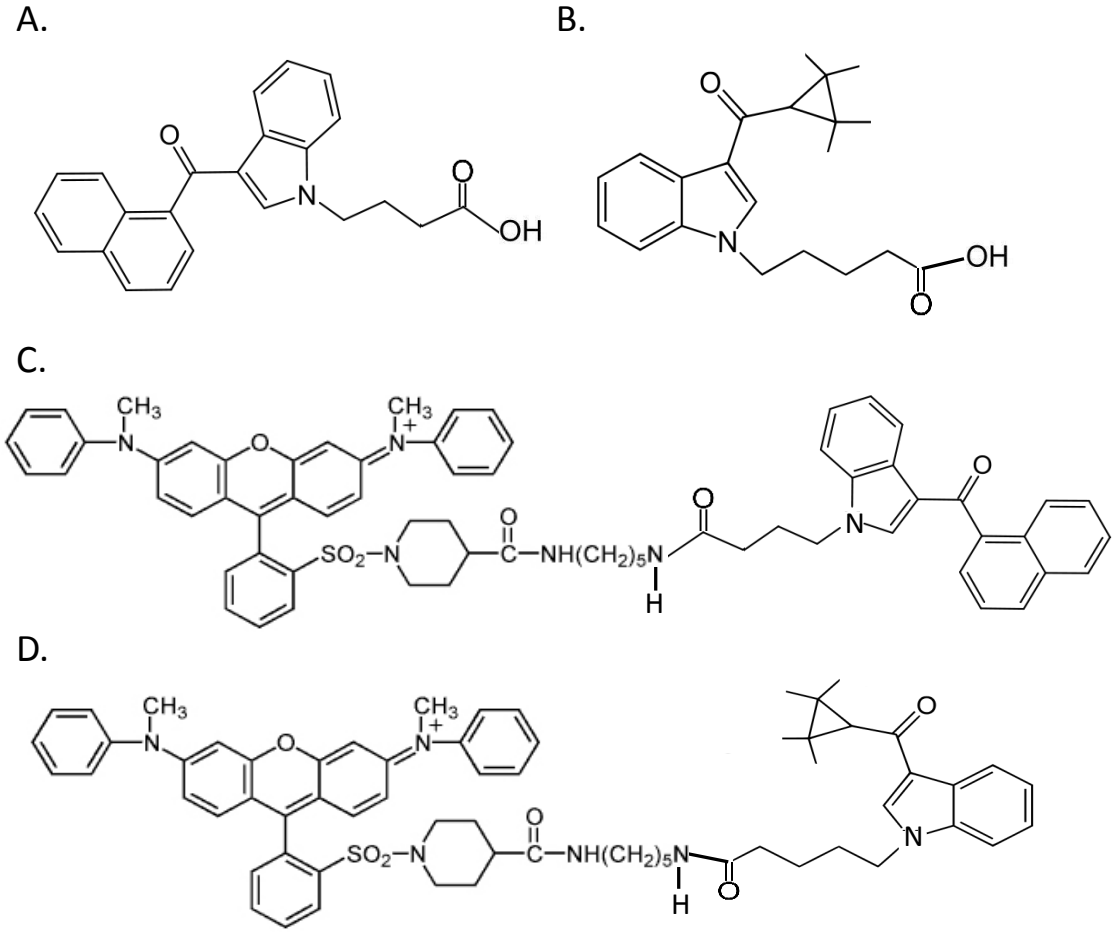

Fig. 42 Alternate SC-DQ linkage options. A. JWH-073 butanoic acid metabolite. B. UR-144 pentanoic acid metabolite. Conjugates of JWH-073 butanoic acid (C) and UR-144 pentanoic acid (D) to QSY-7 amine.

We have successfully synthesized and characterized two new synthetic cannabinoid to dark quencher conjugates: (i) UR-144 pentanoic acid metabolite:QSY-7 amine and (ii) JWH-073 butanoic acid metabolite:QSY-7 amine, as represented in **figure 42**. Both compounds contain a carboxylic acid moiety for conjugation to QSY-7 amine using the same method previously employed with the JWH-018-QSY-7 conjugation. These two metabolites have their conjugation points (carboxylic acid groups) in different spots on the compound when compared to JWH-018 pentanoic acid metabolite and to each other (**figure 43**).

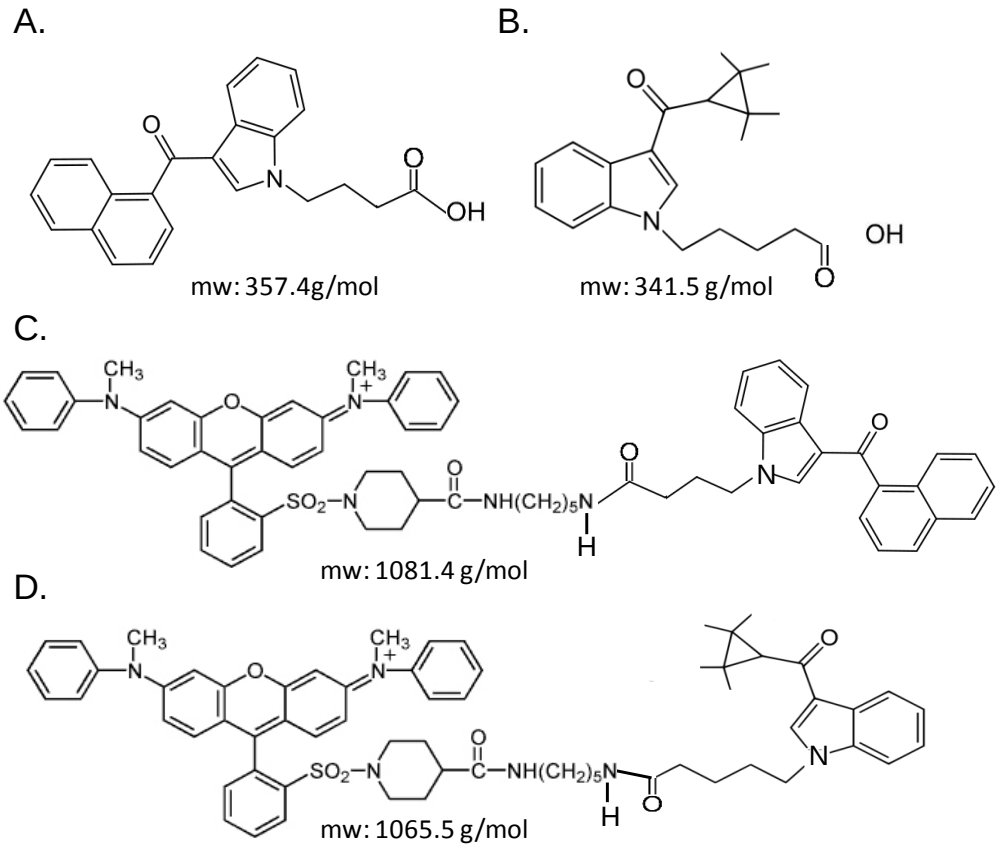

Fig. 43 Structures and molecular mass of (a) JWH-073 butanoic acid, (b) UR-144 pentanoic acid, (c) JWH-073 conjugated to QSY-7, and (d) UR-144 conjugated to QSY-7.

The starting materials and synthesis products were analyzed via LC-MS. JWH-073 butanoic acid elutes at 34.9 minutes with an observed mass of 358.2 which corresponds to the positively ionized form of the SC (**figure 44**). UR-144 pentanoic acid elutes at 40.7 minutes with an observed mass of 342.2, also corresponding to the positively ionized form (**figure 44**). The positively ionized form of QSY-7 amine elutes at 39 minutes with an observed mass of 784.4. The conjugation products for JWH-073 butanoic acid and UR-144 pentanoic acid eluted at 51.0 and 43.7 minutes, respectively. The JWH-073 butanoic acid conjugate had an observed mass of 1081.5 compared to an expected mass of 1081.4 g/mol whereas the UR-144 pentanoic acid conjugate had an observed mass of 1065.5 compared to an expected mass of 1065.5 g/mol.

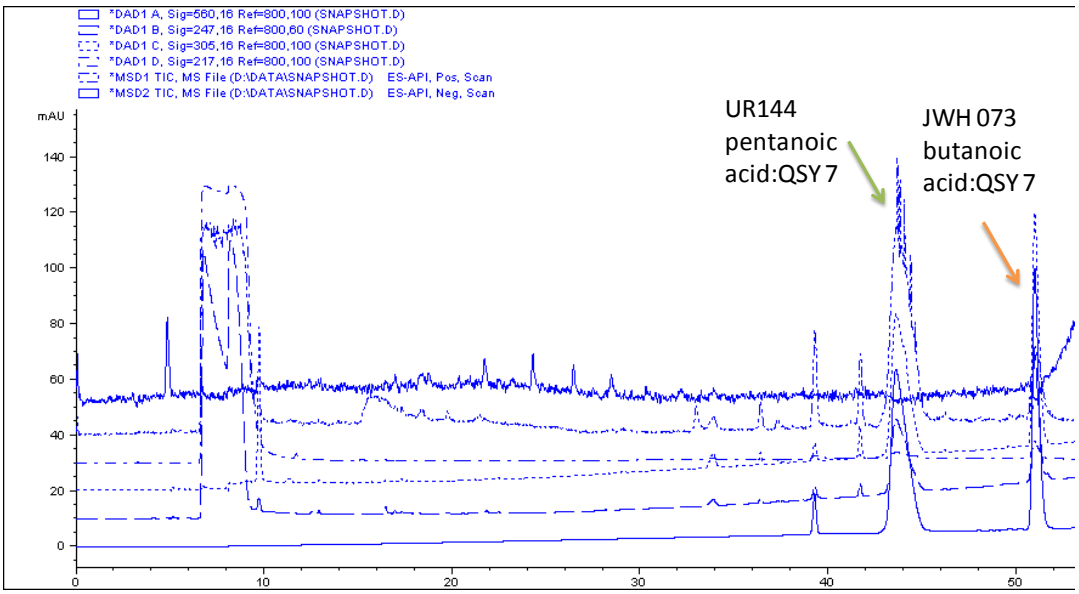

Fig. 44 Mass spectral analysis of JWH-073 and UR-144 conjugates.

3.4.3 PEG Spacers

After analysis of the computational data that describes both cannabinoid entry and equilibration within the membrane and the dark quencher behavior with membrane association, we decided that adding a linker molecule between the synthetic cannabinoid (SC) and the dark quencher (DQ) may be necessary to allow for strong binding between the conjugate and receptor. Specifically, the computational data demonstrated that the QSY-7 or-9 would prefer to "float" on the surface of the membrane as opposed to diffusing into it. As the cannabinoid will need to penetrate the membrane for receptor binding, it could be necessary to increase the distance between the DQ and the SC. We have a PEG linker that is functionalized on one end with an amine and the other end with a carboxylic acid group (**figure 45**). These functional groups allow us to use the current peptide bond linking chemistry that we have previously used for the parent conjugates (**figure 45**). Although the computational data indicated that a PEG spacer length of 10x would allow the dark quencher to exist outside of the receptor upon binding, this longer PEG linker might allow for the conjugate to fold on itself. Initial experiments with the PEG linker was done with a shorter length of 4x, as represented in **figure 46.**

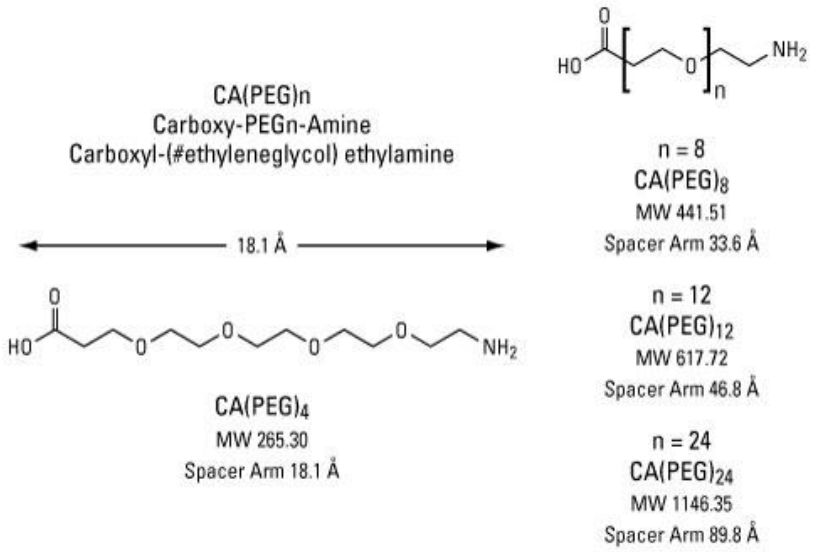

Fig. 45 Structures of PEG spacers Source: *http://www.piercenet.com/product/carboxy-peg-amine-compounds*.

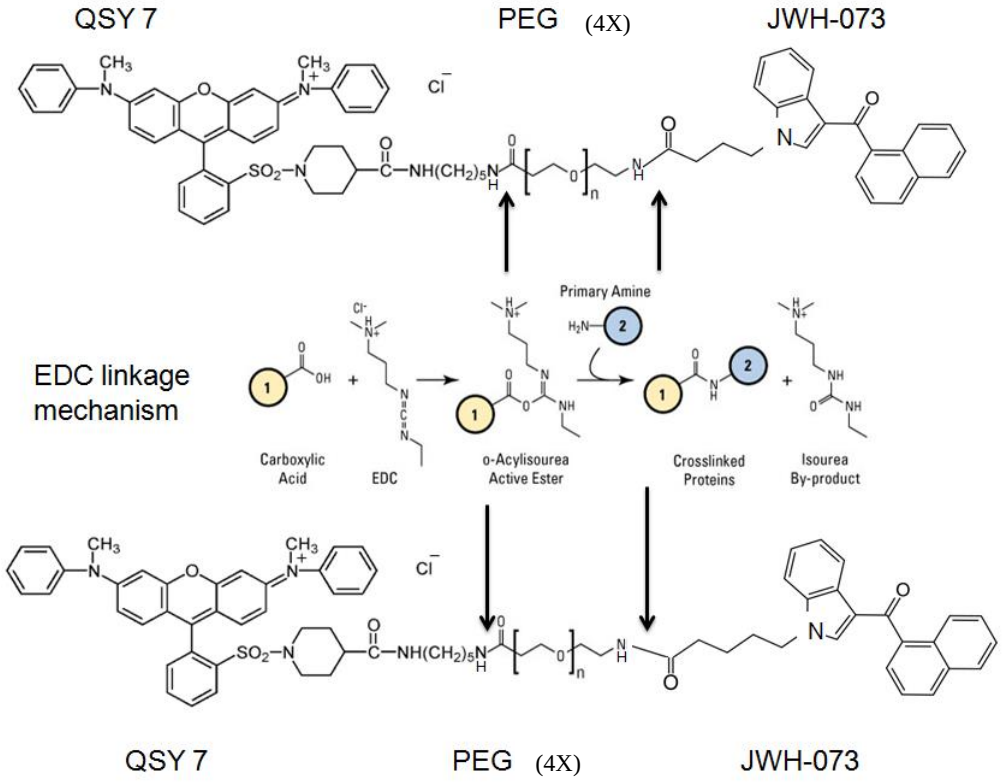

Fig. 46 Structures of SC-DQ conjugates with PEG(4x) linker.

Three different synthetic cannabinoid-dark quencher compounds were synthesized, purified, and delivered to NIH to determine their binding efficiency towards the CB_2 receptor protein. Synthetic cannabinoid-dark quencher conjugates are necessary for the use in fluorescence based cannabinoid

detection platforms. The carboxylic acid reactive QSY-7 amine was reacted with the carboxylated metabolites of JWH-018 and JWH-073 via a simple peptide conjugation reaction with the catalyst HBTU to yield three new dark quencher conjugates.

Molar equivalents and quantities of reagents used in the synthesis protocol are highlighted in **table 6**. QSY-7 amine and JWH-018 or JWH-073 were each resuspended in 500 mL of DMF and added to a 5 mL vial. HBTU was added to the vial, the mixture stirred vigorously for 5 minutes, followed by addition of TEA. After stirring for 4 hours, the reactant to product conversion was monitored via thin layer chromatography (TLC) in 100% ethyl acetate.

For product purification the reaction was diluted 3X with ethyl acetate and filtered through celite. The excess solvent was removed under reduced pressure followed and dried under high vacuum.

TABLE 6. MOLAR EQUIVALENTS AND QUANTITIES OF REAGENTS USED IN THE SYNTHESIS PROTOCOL.

Compound	Molar Equivalents	mmol used	Molecular Weight	Amount added (mg)
JWH-018 pentanoic acid	1	0.013	371.4	5
JWH-073 butanoic acid	1	0.013	357.4	5
QSY-7, amine	1.2	0.0156	814.86	10
TEA	3	0.039	101.19	4

Thin Layer Chromatography and Liquid Chromatography coupled Mass Spectrometry show full conversion of the SC starting material to product with observed and expected masses of 1097 g/mol for JWH-018 pentanoic acid- QSY-7 amine and 1081.4 g/mol for JWH-073 butanoic acid-QSY-7 amine. Final purification of: (1) JWH-018 pentanoic acid to QSY-7 amine, (2) JWH-073 butanoic acid to QSY-7 amine, and (3) UR-144 pentanoic acid to QSY-7 amine were delivered to Dr. Gawrisch's team at the NIH along with the parent synthetic cannabinoid compound for reference. NMR analysis revealed the 1H and 13C spectra of the compound QSY-7-amine-and-JWH-073-butanoic-acid. Two intense proton/carbon resonances corresponding to a fragment –O-CH2-CH3 were also shown. The chemical shifts are somewhat different from ethanol suggesting that it is not a trace of solvent, potentially showing contamination from ethyl acetate. Also the integrals for those ethyl resonances seem to disagree with expectations for one homogeneous

compound. Furthermore, there are series of weaker resonances suggestive for the presence of contaminants at concentrations on the order of 10% compared to the major resonances. The latter is quite typical for ligand spectra. It may take several crystallization cycles to lower content of contaminants to non-detectable levels, so work toward radioactive binding assay analysis is proceeding forward with current sample.

Binding affinity of the synthetic cannabinoid dark quencher conjugates to the cannabinoid receptor (CB_2) must be determined. The conjugates must bind the receptor in order for the sensor to work. The conjugates should have a lower affinity than the synthetic cannabinoid compounds to be tested by the sensor. To determine the binding affinity of the synthesized ligand-dark quencher conjugates, a [S^{35}]GTP-γ-S G protein-activation assay with bacterial membranes containing recombinant MBP-CB_2 fusion proteins was utilized. For comparison, the strongly binding agonist CP-55,940 was also tested; which has a known binding affinity of ~1nM. It is important to note that this experiment measures **agonistic** activity of the ligand upon binding to the CB_2 protein, thus if the ligand binds but is a weak agonist or an antagonist it will not register due to low agonistic activity. The comparative results of the CP-55,940, JWH-018-dark quencher, and JWH-073-dark quencher are shown in **figure 47**.

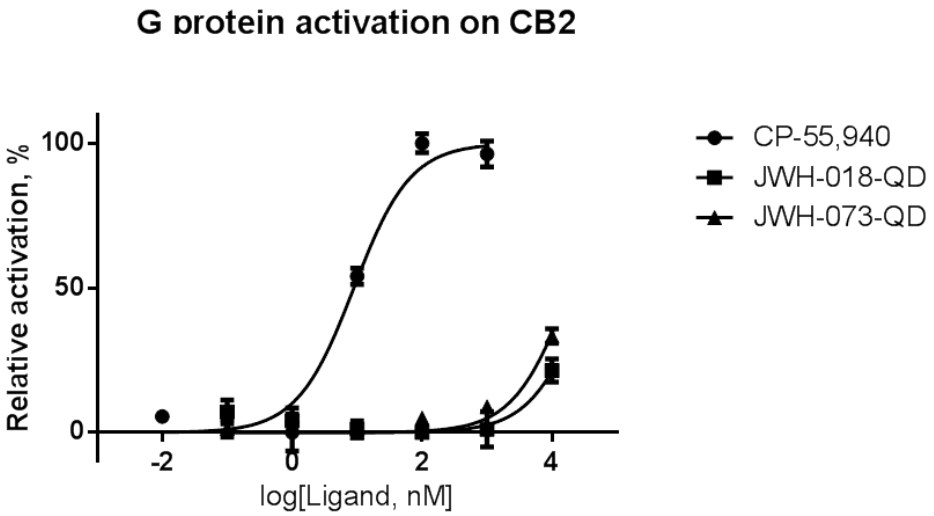

	CP-55,940	JWH-018-QD	JWH-073-QD
log(agonist) vs. normalized response			
Best-fit values			
LogEC50	0.9513	4.569	4.283
EC50	8.938	37099	19182
Std. Error			
LogEC50	0.08266	0.08241	0.05326
95% Confidence Intervals			
LogEC50	0.7643 to 1.138	4.388 to 4.751	4.166 to 4.400
EC50	5.811 to 13.75	24433 to 56329	14644 to 25126
Goodness of Fit			
Degrees of Freedom	9	11	11
R square	0.9730	0.6927	0.8860
Absolute Sum of Squares	495.8	226.8	175.3
Sy.x	7.422	4.540	3.992
Number of points			
Analyzed	10	12	12

Fig. 47 G-protein activation of select ligands and estimated EC_{50} values.

The CP-55,940 ligand represents a strongly binding agonist for comparison, which has similar binding affinities as synthetic cannabinoids seen in SPICE-like products, such as HU-210 and JWH-081. The important value in the current study is the EC50 value, which represents the concentration of ligand that is required to for 50% activation of the G-protein. For the strongly binding agonist CP-55,940 the EC50 value was found to be around 9nM. The prepared ligand-DQ conjugates were required at much higher concentrations to induce G-protein activations, with an EC50 of approximately 20uM and 35uM for the JWH-073 and JWH-018 based dark quencher conjugates, respectively. It should be noted that these high concentrations, any residual/unreacted JWH-073 and JWH-018 parent compounds could play a role in the activation.

To look closer specifically towards the binding affinity of the prepared conjugates to the CB_2 molecule a modified G-protein activation study was performed. In this study the G-protein activation from CP-55,940 was monitored at select concentrations, with the prepared conjugates being introduced at varying comparative concentrations from the nM to uM range. The comparison of G-protein activation with competitive displacement of the CP-55,940 with the prepared conjugates is shown in **figure 48**.

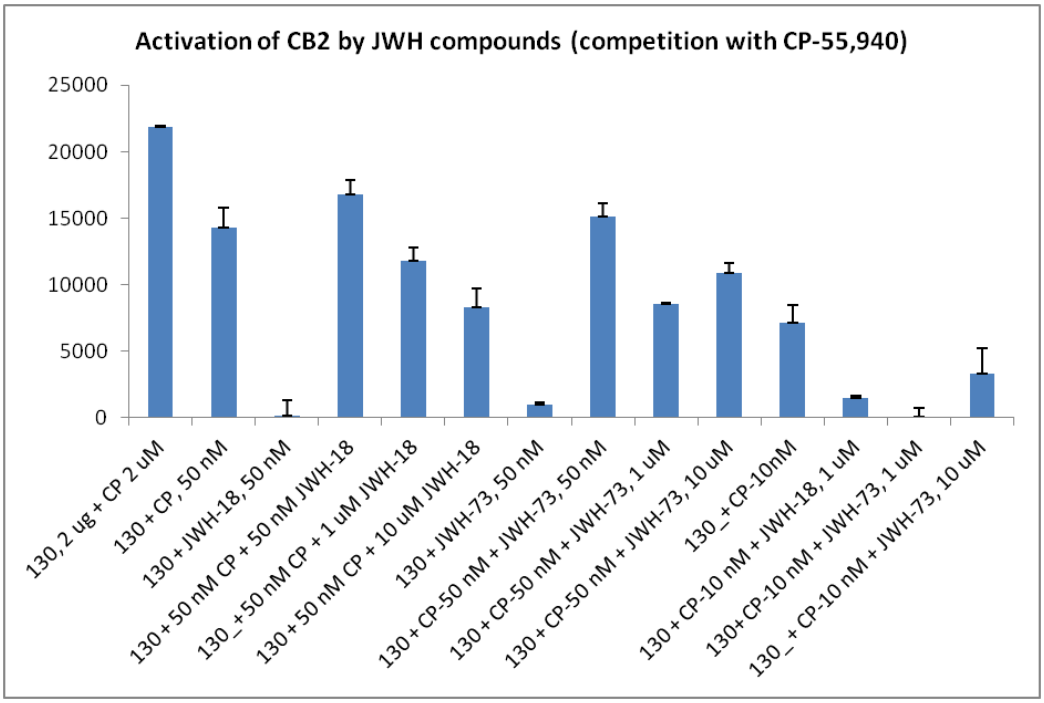

Fig. 48 linker G-protein activation of mixed CP55,940/dark quencher conjugate materials.

The concentration of the CP55,940 utilized in this experiment was set at 50nM and 10nM; which puts it at a G-protein activations of around 70% and 50%, respectively. With the 50nM CP-55,940 concentrations, only slight reductions in the activation was seen by the addition of the JWH-018 dark quencher conjugate, with an approximate 30% reduction in activation measured with the conjugate concentration 200-times that of the CP ligand. Similar results were seen with the JHW-073 conjugate, but with an increase in G-protein activation seen at high conjugate concentrations; signaling the JHW-73 conjugate is binding and activating at that concentration. A more interesting picture is seen when working around the CP EC50 of 10nM concentrations. At a CP concentration of 10nM, the prepared conjugates were able to effectively compete off the strongly binding CP ligand when applied at a 2-orders of magnitude higher concentration (1uM). The addition of the dark quencher conjugates results in a 78% and 99% reduction in CP activity (implying it was displaced) for the JWH-018 and JWH-073 conjugates, respectively. Further studies need to be performed to determine the precise binding affinity of the prepared conjugates, but estimates for

the **Kd are in the 1um-5um range**, with the JWH-073 conjugate having a higher binding affinity than the JWH-018.

In terms of the envisioned synthetic cannabinoid sensor designs, a dark quencher conjugate with binding affinities in this range would be applicable and allow it to be easily displaced by SC's with binding affinities to the CB_2 greater than 1uM. All of these test were performed using the CB_2 receptor.

After this analysis was performed, NMR characterization was attempted on these samples. During the NMR characterization, it was determined that the samples were not sufficiently pure. There is a risk that the samples contained parent compounds unreacted with the dark quencher. This could greatly impact the binding studies. Further purification was performed.

3.4.4 Ligand-Dark Quencher Purification

The JWH-018:$(PEG)_4$:QSY-7 amine, JWH-368:$(PEG)_4$:QSY-7 amine, and JWH-073:QSY-7 amine conjugates were purified using high performance liquid chromatography (HPLC). It is important that the conjugates be pure and free from any remaining parent compounds in order to appropriately interpret the binding study data. The parent compound may bind with much greater affinity than the conjugate. The LC column was an Agilent Eclipse XDB C18 column (250 x 9.4 mm i.d., 5 μm particle size), maintained at 25˚C with a mobile phase flow rate of 2.00 ml/minute. Gradient elution mobile phases consisted of A (5mM ammonium formate in water) and B (acetonitrile). The gradients used for the purification of each conjugate are shown in **tables 7-9**. The detection wavelengths used in this study were 218, 316, and 560 nm. The expected mass of each compound can be seen in **table 10**.

Table 7. Gradients of solvents used in this study for the HPLC purification of JWH-368:(PEG)4:QSY-7 amine and JWH-368:QSY-7 amine..

Time (minutes)	%B
5	10
10	45
15	50
20	55
27	58
30	100

Table 8. Gradients of solvents used in this study for the HPLC purification of JWH-018:(PEG)4:QSY-7 amine and JWH-018:QSY-7 amine.

Time (minutes	%B
5	10
10	50
15	65
20	70
25	75
30	80
35	85
40	90
45	100

Table 9. Gradients of solvents used in this study for the HPLC purification of JWH-073:QSY-7 amine.

Time (minutes)	%B
5	15
10	30
15	50
20	70
30	80
40	90
50	100

Table 10. Expected masses of compounds used in this study.

Compound	Expected Mass (g/mol)
JWH-018 pentanoic acid	371.4
JWH-368	385.5
QSY-7, amine	814.86
JWH-018 pentanoic acid:(PEG)4: QSY-7, amine	1095.42
JWH-073 butanoic acid: QSY-7, amine	1081.42

The overall purity of the JWH-018, JWH-073, and JWH-368 conjugates was analyzed via LC-MS. A single quadrupole Agilent 6130 mass spectrometer was used in conjunction with an Agilent 1200 series LC system (Agilent Technologies, Santa Clara California). The LC column was an Agilent Eclipse XDB C18 column (150 x 4.6 mm i.d., 5 µm particle size), maintained at 25˚C with a mobile phase flow rate of 0.6 ml/min. Gradient elution mobile phases consisted of A (5mM ammonium formate in water) and B (acetonitrile). The same elution gradients shown previously in Tables 7-9 were used. Quantification of the analytes was undertaken using positive scan mode with a molecular mass scan from 100 to 1200 g/mol. The elution peaks from the LCMS can be seen in **figures 49-51**.

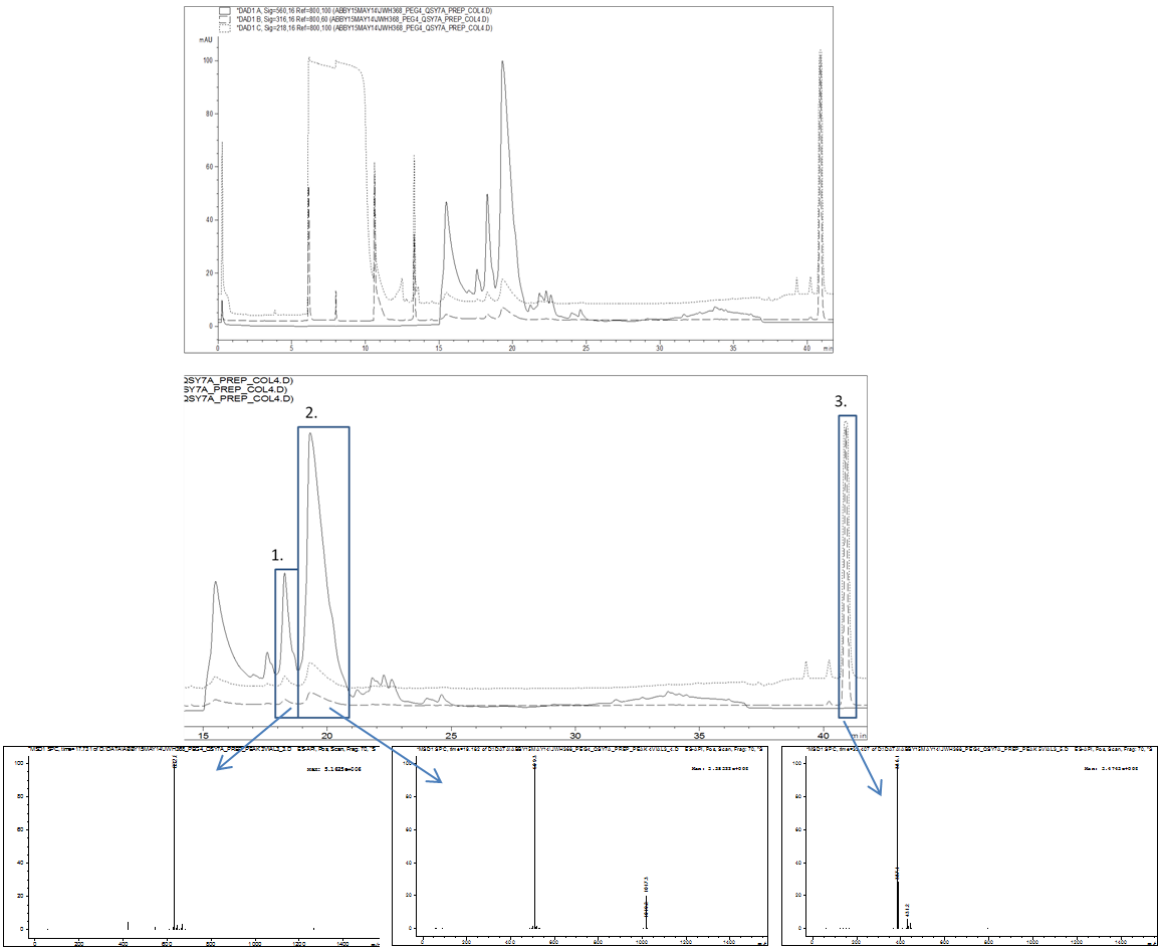

Fig. 49 The peaks observed during the purification of JWH-368:(PEG)4:QSY-7 amine using the optimized gradient (top). A zoomed in view of the top figure showing the peaks collected during that run (middle). The peak indicated with a number 1 represents the JWH-368:(PEG)4:QSY-7 amine conjugate. The peak indicated with a number 2 represents the JWH-368:QSY-7 amine conjugate. The peak indicated with a number 3 represents the JWH-368 compound. The mass spectra of each of the three peaks collected (bottom).

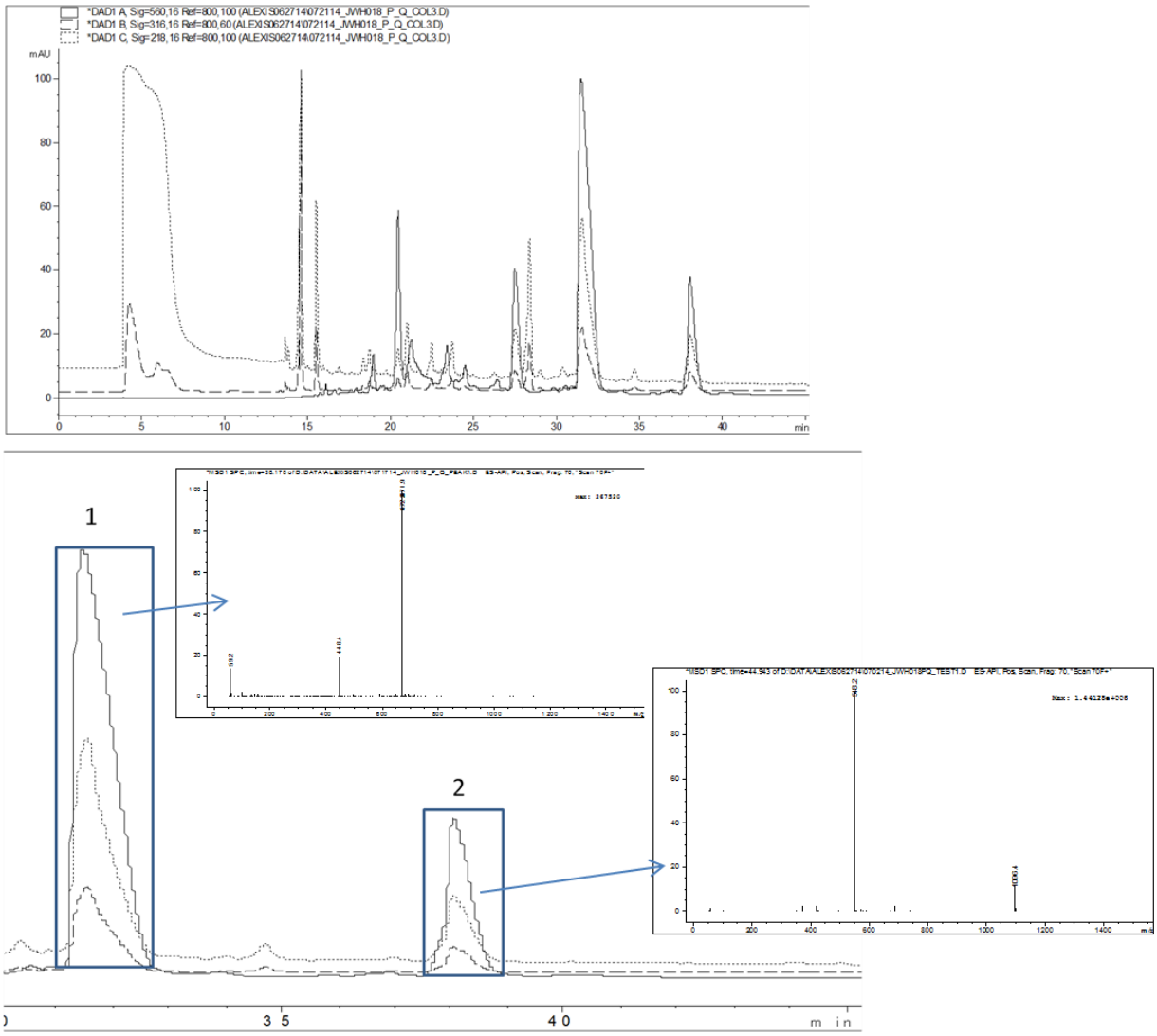

Fig. 50 The peaks observed during the purification of JWH-018:(PEG)4:QSY-7 amine using the optimized gradient (top). A zoomed in view of the top figure showing the peaks collected during that run and the associated mass spec data (bottom). The peak indicated with a number 1 represents the JWH-018:(PEG)4:QSY-7 amine conjugate. The peak indicated with a number 2 represents the JWH-018:QSY-7 amine conjugate.

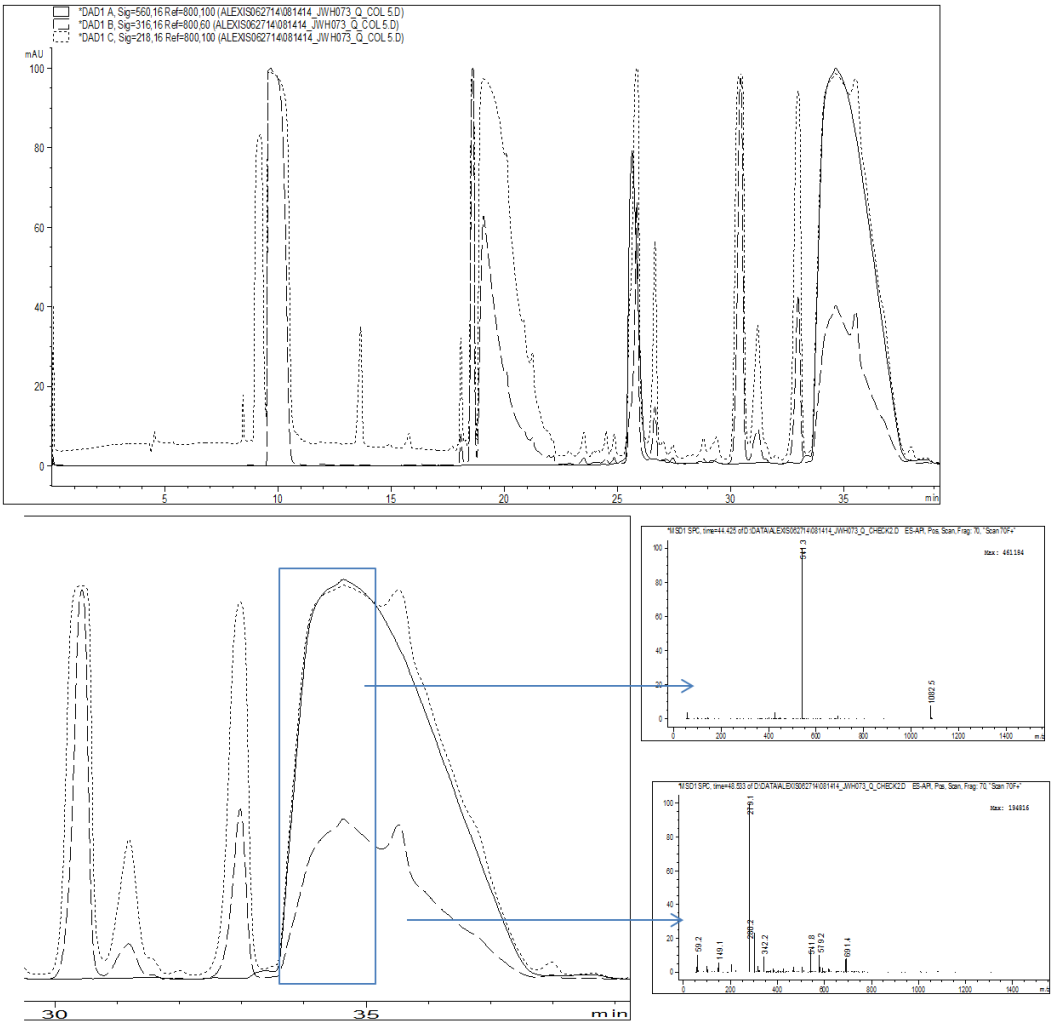

Fig. 51 The peaks observed during the purification of JWH-073:QSY-7 amine using the optimized gradient (top). A zoomed in view of the top figure showing the peaks collected during that run (bottom) and the associated mass spec data. The peak indicated with a box represents the JWH-073:QSY-7 amine conjugate.

During the separation of these conjugates, it was discovered that during synthesis of JWH-368:(PEG)4:QSY-7 amine and JWH-018:(PEG)4:QSY-7 amine, two part conjugates of the JWH compound and the dark quencher without the PEG linker were also formed (JWH-368:QSY-7 amine and JWH-018:QSY-7 amine). These conjugates were verified with mass spectrometry. The PEG spacer and JWH compound were added first and allowed to react, the reaction must have been inefficient and some JWH compound remained. This allowed for the JWH compound to react with the dark quencher when it was added to the reaction. Many additional peaks can be seen in the top portion of each figure above. These other peaks are impurities and unreacted compounds that can interfere with future binding affinity studies. It is therefore necessary to separate all of the synthesized conjugates for downstream testing. All of the peaks identified in **figures 49-51** were collected, lyophilized, and the purity was verified through mass spectrometry.

The structures of the synthetic cannabinoid metabolites JWH-073 n-butanoic acid and JWH-018 n-pentanoic acid are very similar and differ only by one carbon. Due to the similarity in structure, it would be expected that the conjugates of these structures with the dark quencher, QSY-7 amine, would elute from the HPLC column at similar times. JWH-073:QSY-7 amine elutes at 33.5 minutes at approximately 83.5% Solvent B. JWH-018:QSY-7 amine elutes at 37.5 minutes at approximately 87.5% Solvent B. These are similar elution times given that the JWH-368:QSY-7 amine conjugate elutes at around 19 minutes at approximately 54% Solvent B.

After HPLC separation had been completed with the conjugates, the separated products were subjected to LCMS and analyzed for purity. The LC chromatograms and corresponding mass analysis for each respective ligand-dark quencher conjugate are shown in **figures 52-56**.

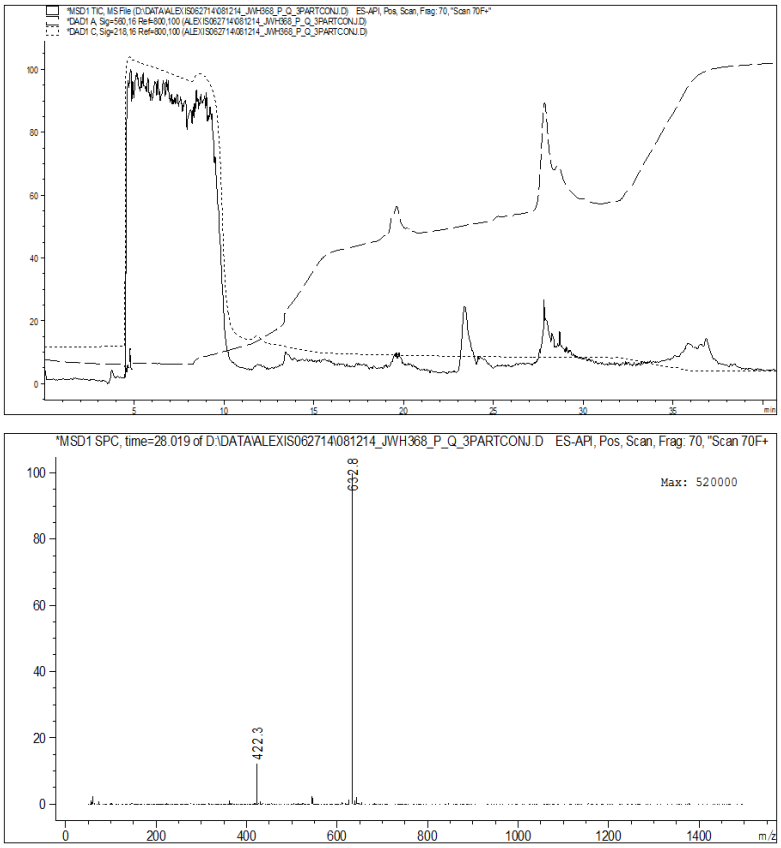

Fig. 52 LC chromatogram (top) and mass (bottom) of purified the three part conjugate, JWH-368:(PEG)4:QSY-7 amine. The conjugate has a retention time of 28.019 minutes and an observed half mass^{+} of 632.8 g/mol (expected: 1337 g/mol non-ionized).

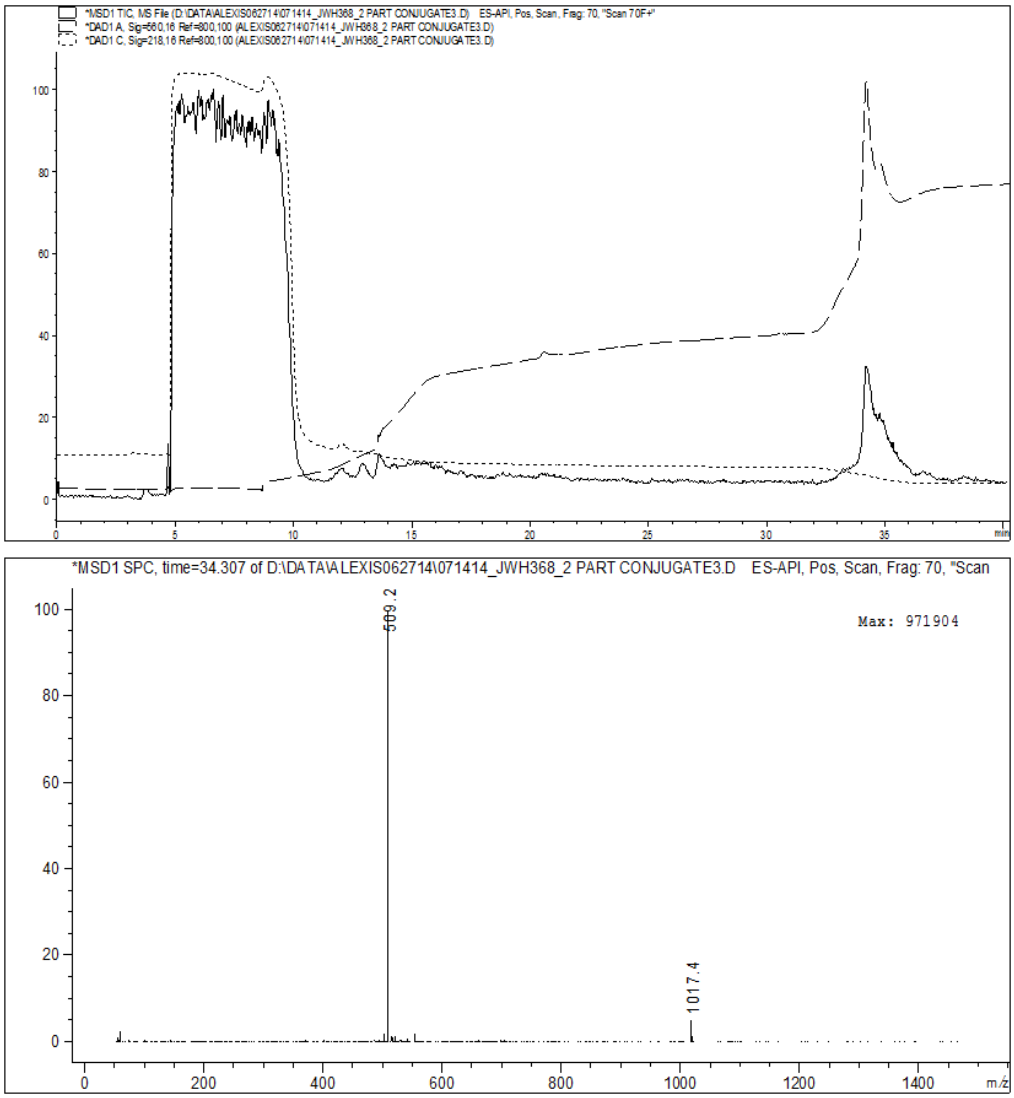

Fig. 53 LC chromatogram (top) and mass (bottom) of the purified two part conjugate, JWH-368:QSY-7 amine. JWH-368:QSY-7 amine has a retention time of 34.3 minutes and an observed mass$^+$ of 1017.4 g/mol (expected: 1017.8 g/mol non-ionized).

The LCMS analysis of the JWH-368:(PEG)4:QSY-7 amine conjugate showed a 94% pure product that elutes at 27.5 minutes. The observed half mass of the conjugate was 632.8 g/mol. The expected mass was 1337 g/mol (half mass of 668.5 g/mol). The observed mass was in slight discordance with the expected mass. The NMR data in the characterization section will help to explain this discrepancy. There is also an additional mass of 422.3 g/mol observed. This mass is inconsistent with any compounds added to the reaction. It is likely due to degradation of the conjugate. Analysis of the JWH-368:QSY-7 amine conjugate with LCMS showed a 98% pure product that elutes at 34 minutes. The observed mass of the conjugate was 1017.4 g/mol which is in very good agreement to the expected mass of 1017.8 g/mol.

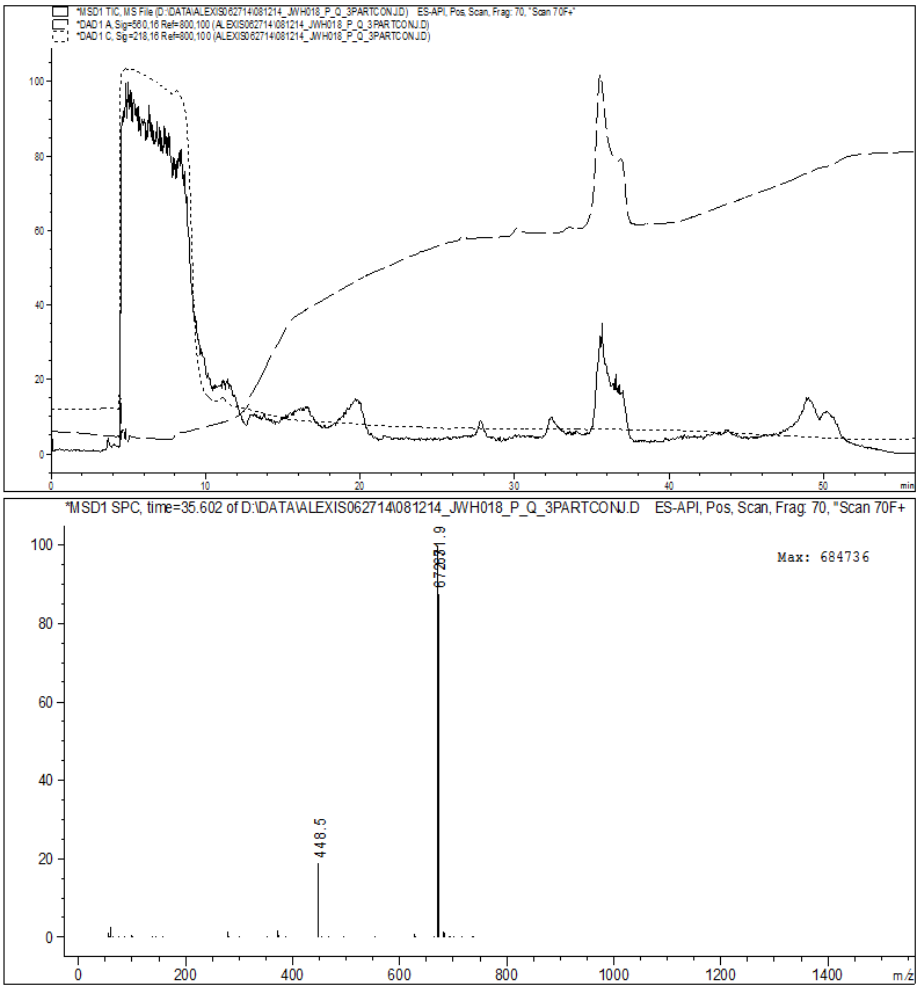

Fig. 54 LC chromatogram (top) and mass (bottom) of the purified three part conjugate JWH-018:(PEG)4:QSY-7 amine. JWH-018:(PEG)4:QSY-7 amine has a retention time of 35.602 minutes and an observed half mass$^+$ of 672.0 g/mol (expected: 1344.3 g/mol non-ionized).

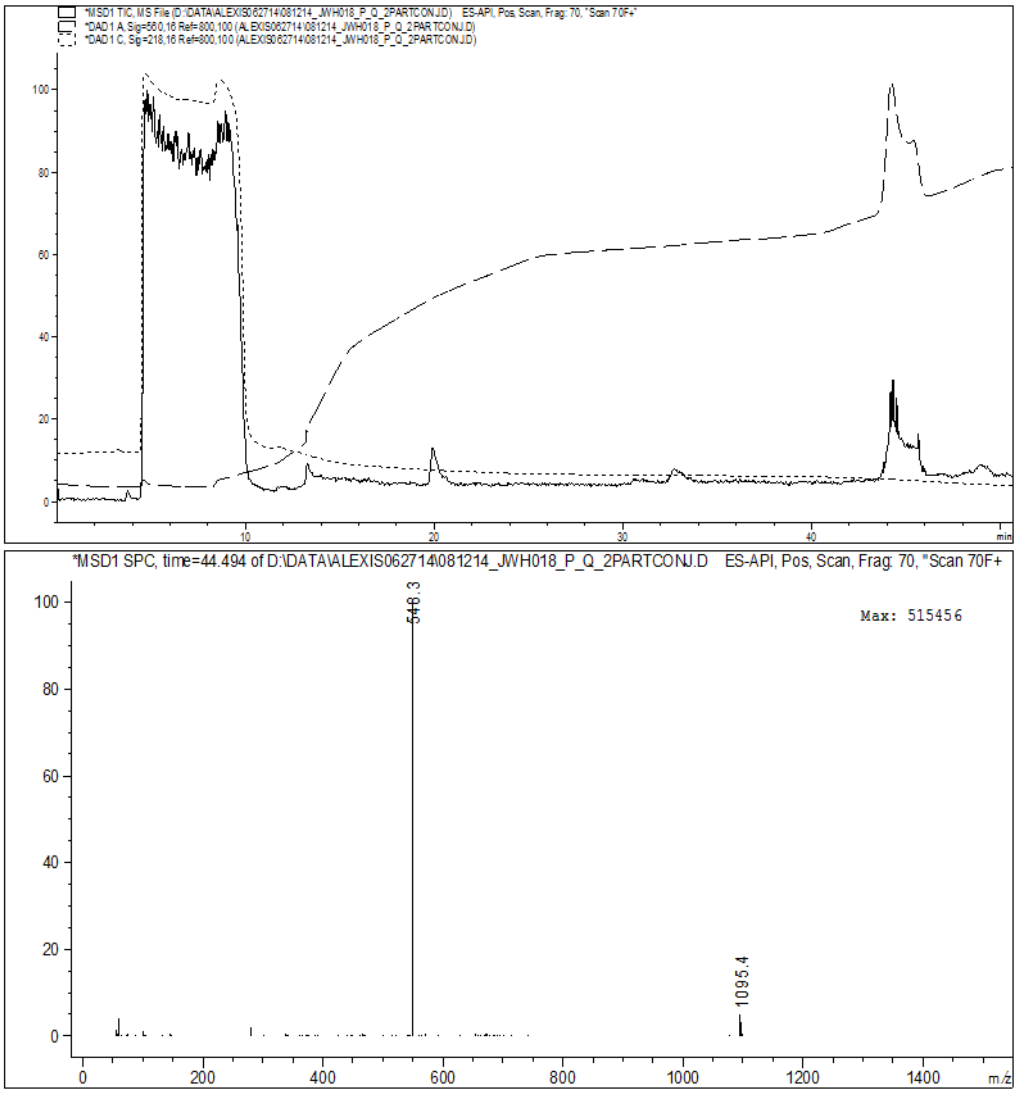

Fig. 55 LC chromatogram (top) and mass (bottom) of the purified two part conjugate JWH-018:QSY-7 amine. JWH-018:QSY-7 amine has a retention time of 44.494 minutes and an observed mass$^+$ of 1095.4 g/mol (expected: 1095.4 g/mol non-ionized).

The LCMS analysis of the JWH-018 n-pentanoic acid:(PEG)4:QSY-7 amine conjugate showed a 94% pure product that elutes at 34.5 minutes. The observed half mass of the conjugate was 672.0 g/mol which is in very good agreement to the expected mass of 1344.3 g/mol (half mass of 672.0 g/mol). There is an additional mass of 448.5 g/mol. This mass is inconsistent with any compounds added to the reaction. It is likely due to degradation of the conjugate. Analysis of the JWH-018 n-pentanoic acid:QSY-7 amine conjugate with LCMS showed a 96% product that elutes at 44 minutes. The observed mass of the conjugate was 1095.4 g/mol which is in very good agreement to the expected mass of 1095.42 g/mol.

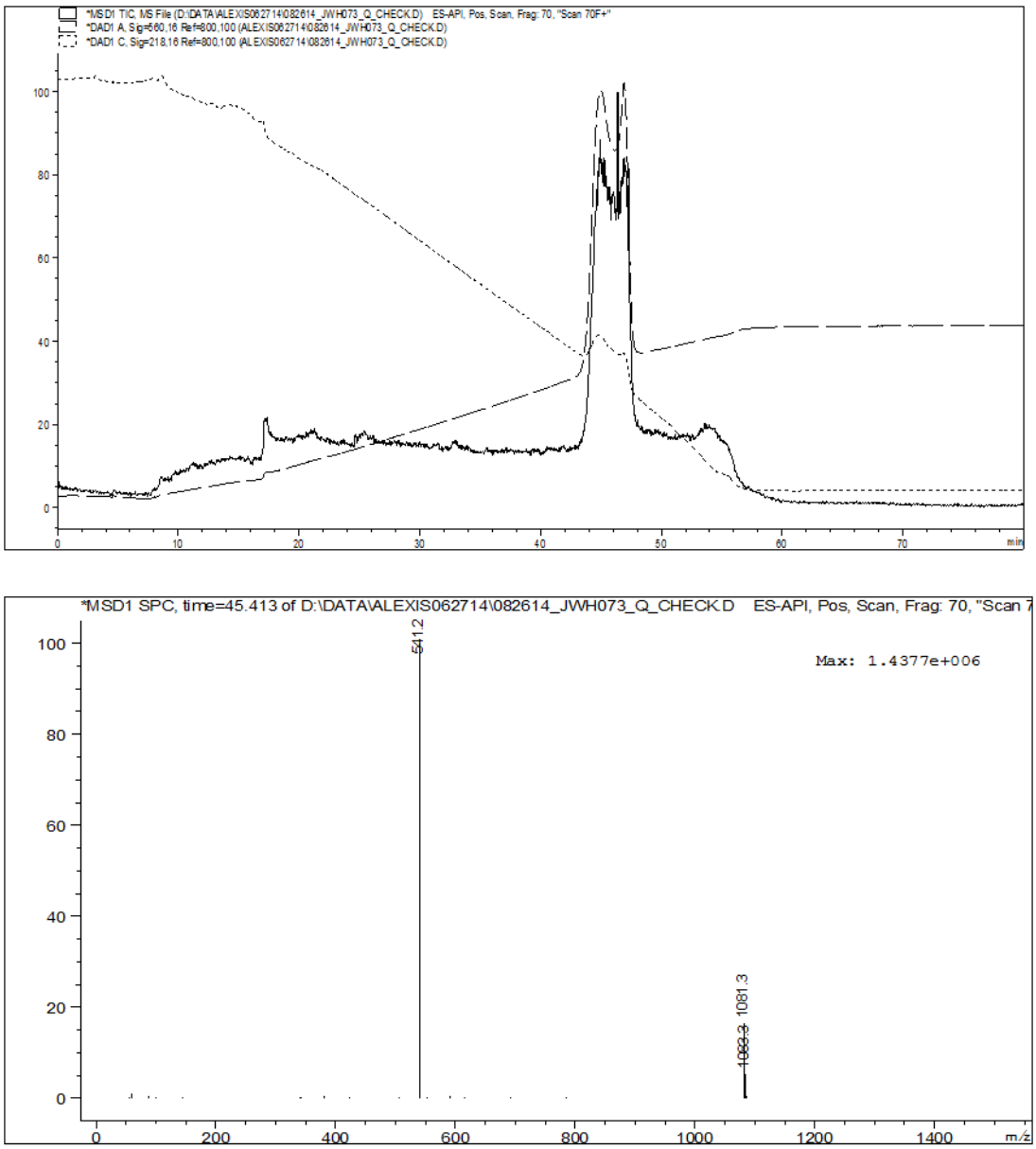

Fig. 56 Chromatogram (top) and mass (bottom) of the purified JWH-073 n-butanoic acid: QSY-7 amine conjugate. JWH-073:QSY-7 amine has a retention time of 44 minutes and an observed mass$^+$ of 1081.3 g/mol (expected: 1081.42 g/mol non-ionized).

Finally, the LCMS analysis of the JWH-073 butanoic acid:QSY-7 amine conjugate showed a 98% pure product that elutes at 43 minutes. The observed mass of the conjugate was 1081.3 g/mol which is in good agreement to the expected mass of 1081.42 g/mol.

3.4.5 Ligand-Dark Quencher Conjugate Characterization

NMR analysis was done to characterize the synthesized ligand-dark quencher conjugates, JWH-073:QSY-7 amine, JWH-368:(PEG)$_4$:QSY-7 amine, JWH-368:QSY-7 amine, JWH-018:QSY-7

amine, and JWH-018:$(PEG)_4$:QSY-7 amine. The NMR structure of each conjugate was consistent with the expected structure, except in the case of JWH-368:QSY-7 amine and JWH-368:$(PEG)_4$:QSY-7 amine. Both JWH-368 conjugates were missing the hydrophobic tail resonance during NMR. The molecular weight is also off from the expected. JWH-073:QSY-7 amine was found to have a concentration of 68.5 uM. JWH-018:QSY-7 amine was found to have a concentration of 19.3uM. JWH-018:$(PEG)_4$:QSY-7 amine was determined to have a concentration of 84.5uM. The purity of all conjugates was >98% and enough to proceed with GTPγS binding studies. Details of the NMR study can be found in **figures 57-61** below.

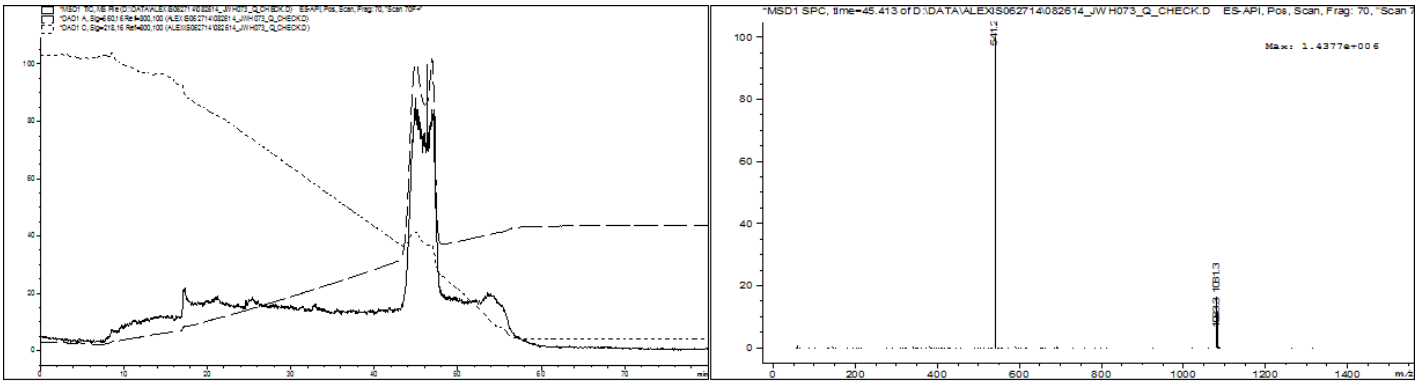

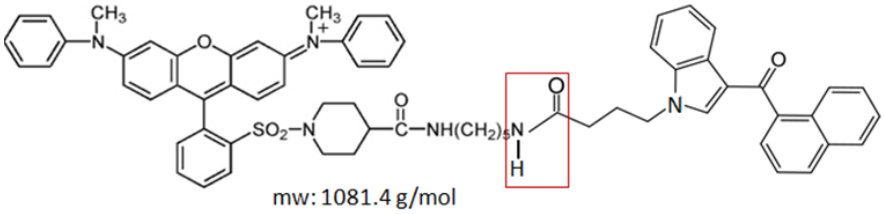

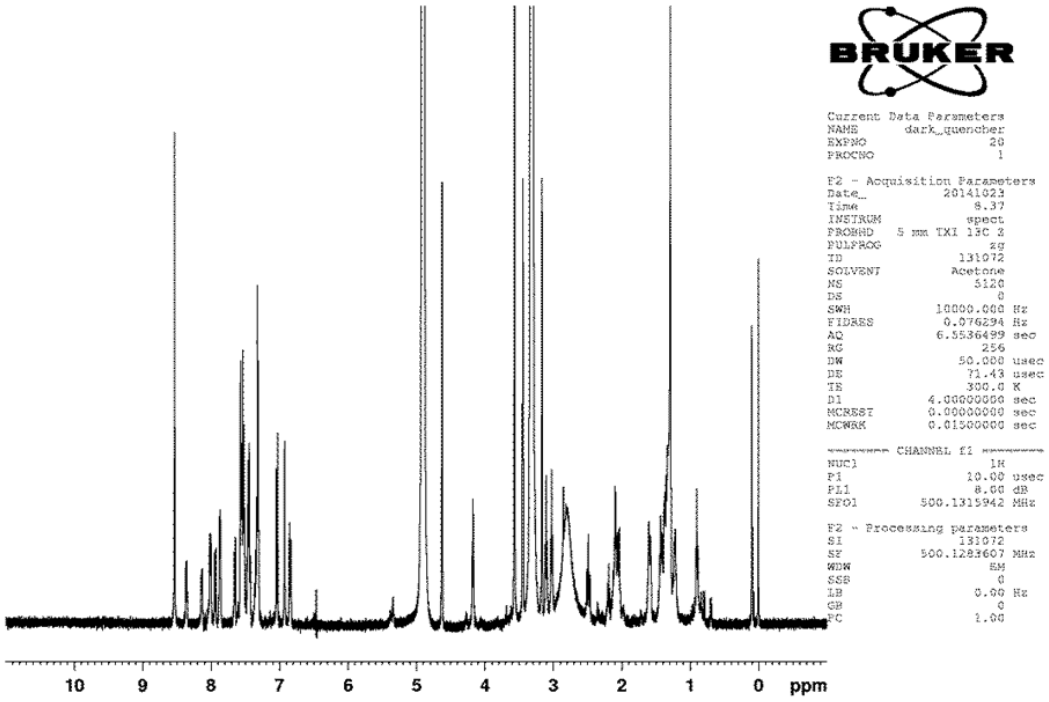

Fig. 57 JWH-073:QSY7 amine mass spec data, structure, and NMR analysis, shows >99% purity.

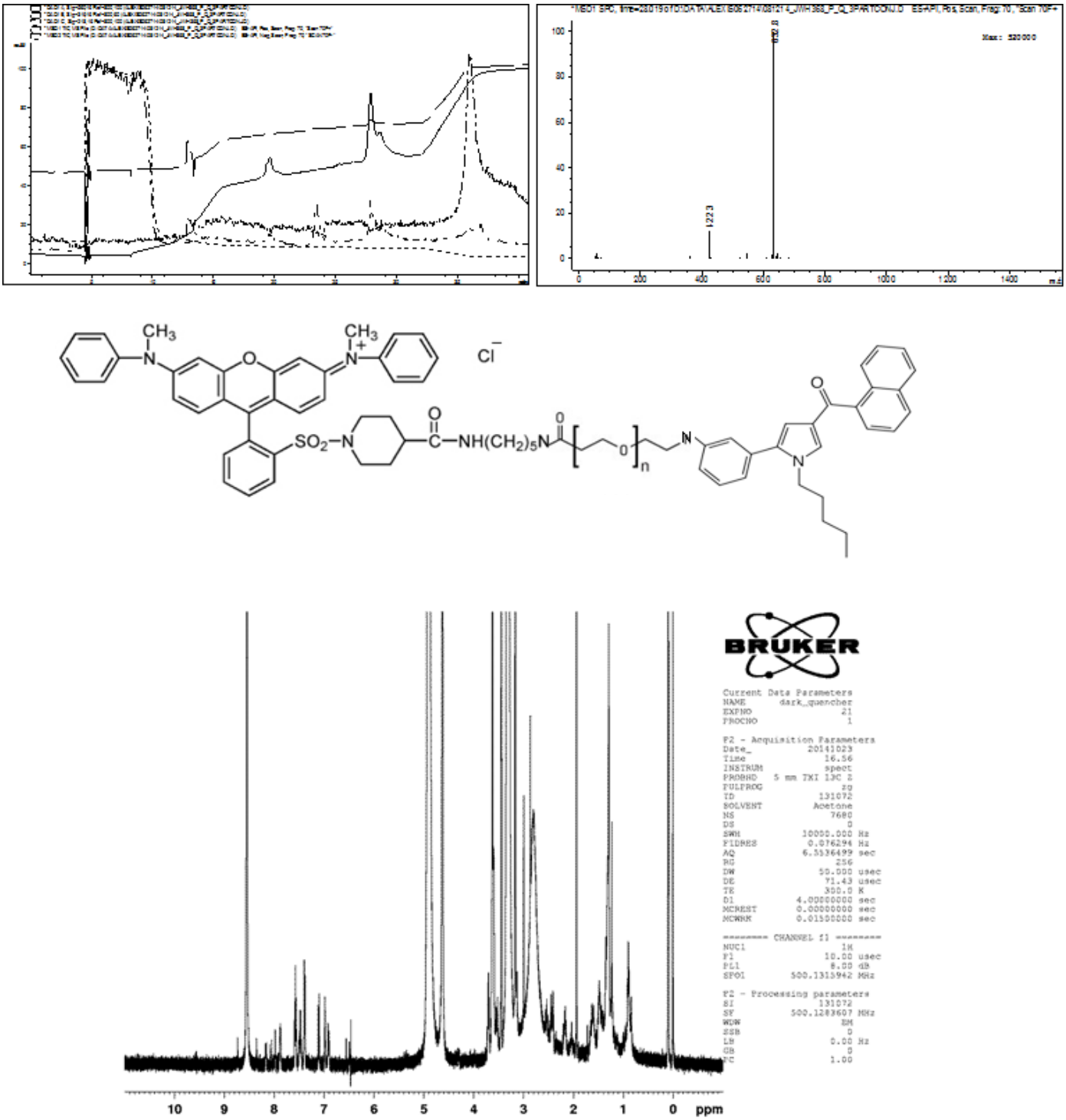

Fig. 58 JWH-368:(PEG)$_4$:QSY7 amine mass spec data, structure, and NMR analysis, shows an unexpected molecular weight as well as incorrect structure resonances during NMR analysis.

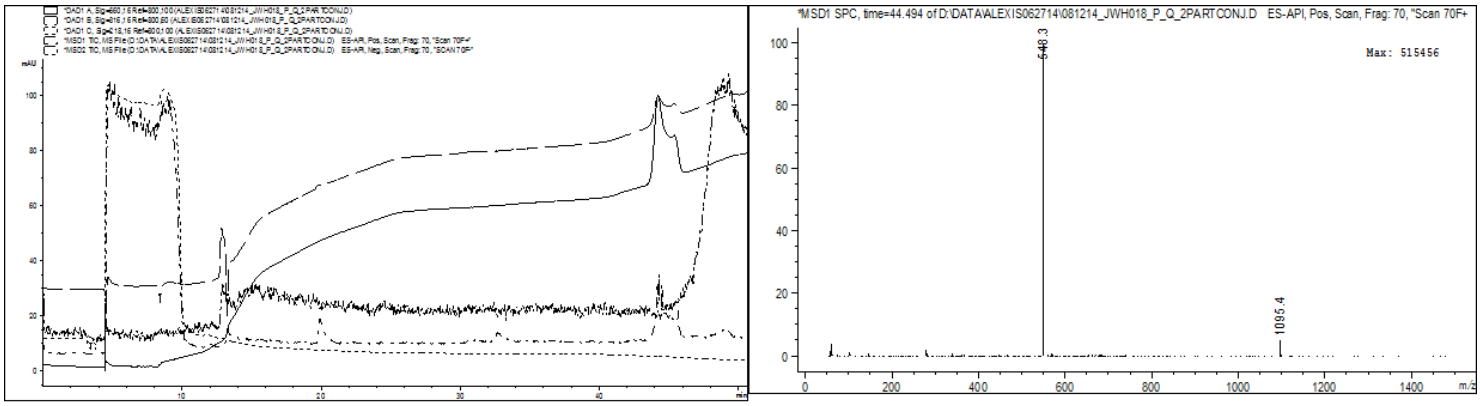

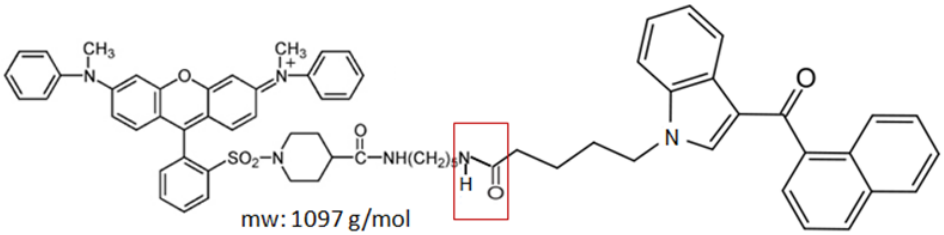

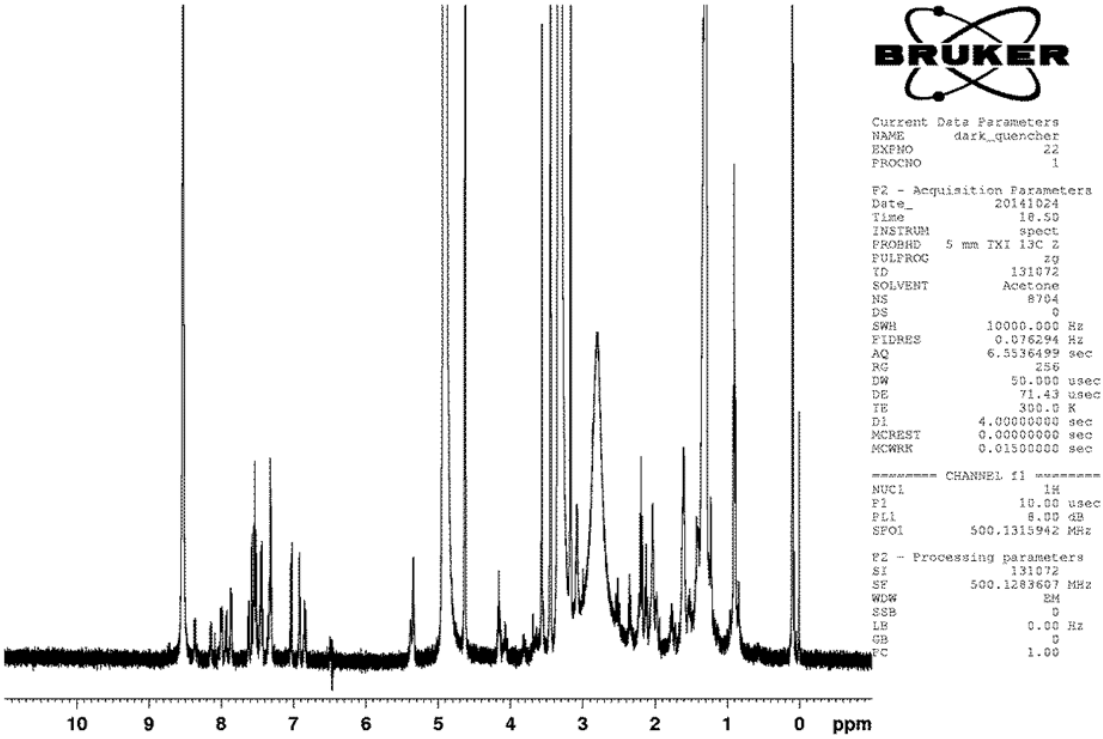

Fig. 59 JWH-018:QSY7 amine mass spec data, structure, and NMR analysis, shows the expected molecular weight, a purity >99%,and structure resonances during NMR analysis consistent with the expected structure.

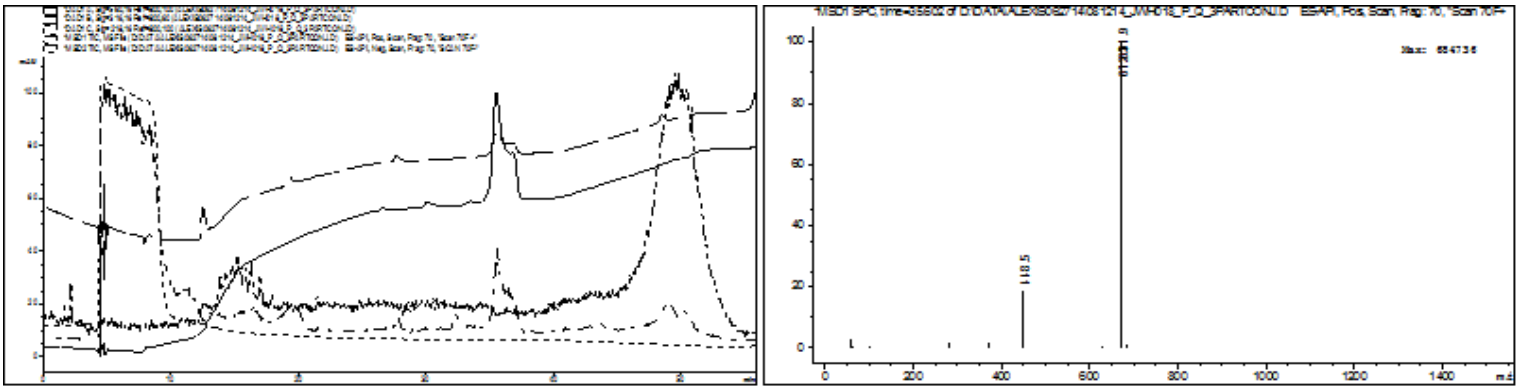

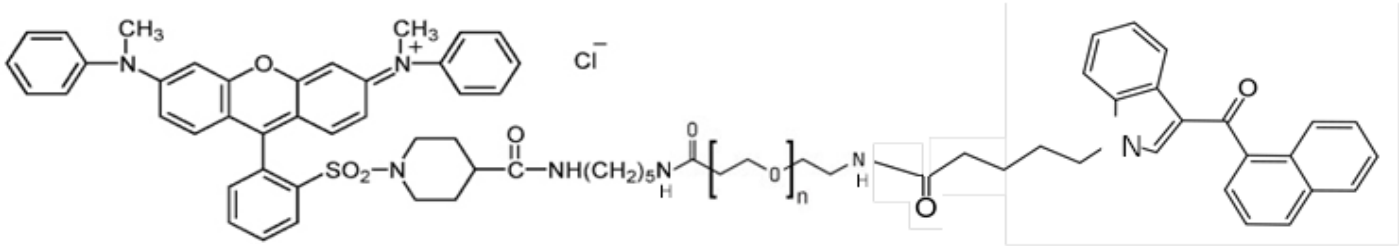

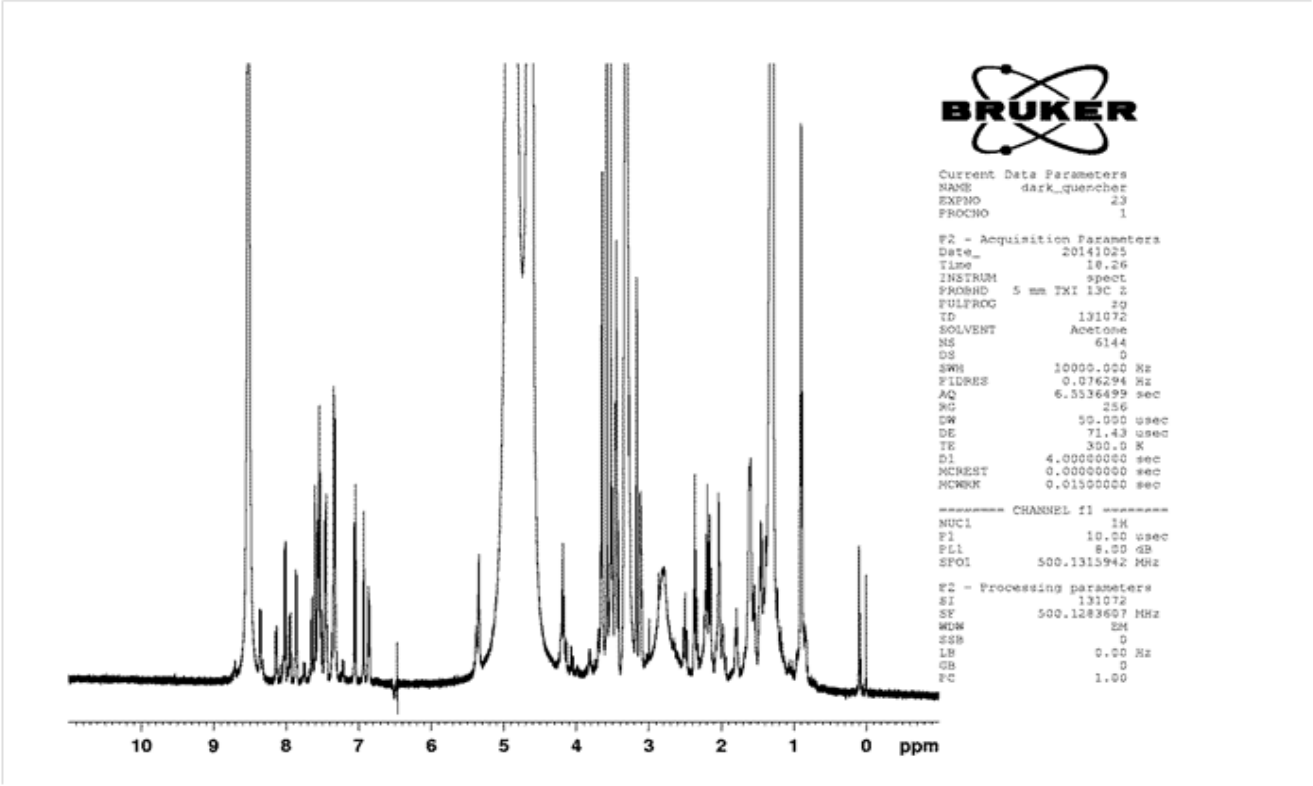

Fig. 60 JWH-018:(PEG)$_4$:QSY7 amine mass spec data, structure, and NMR analysis, shows the expected molecular weight, a purity >99%,and structure resonances during NMR analysis consistent with the expected structure.

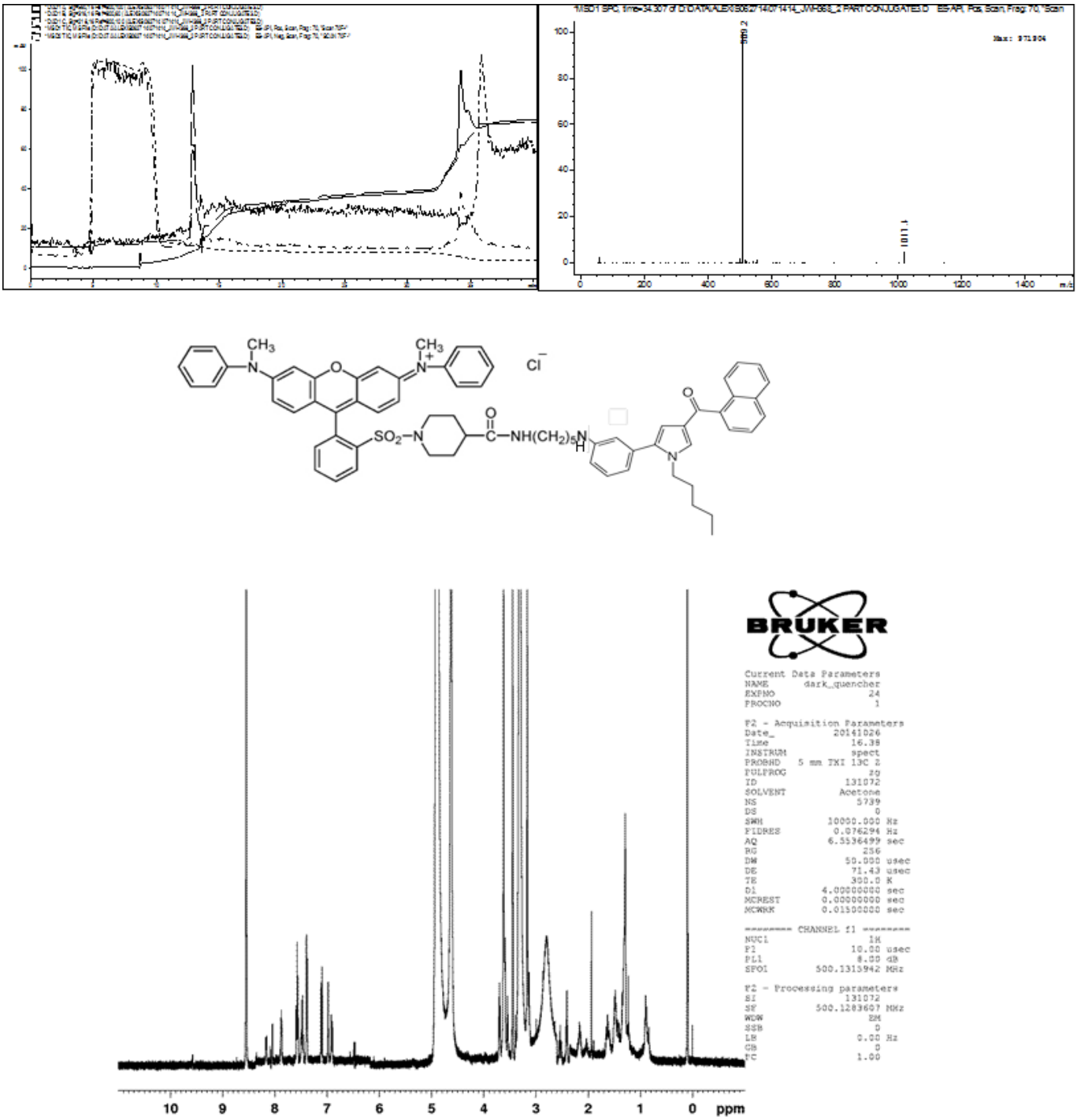

Fig. 61 JWH-368:QSY7 amine mass spec data, structure, and NMR analysis, shows an unexpected molecular weight as well as incorrect structure resonances during NMR analysis.

The three dark quencher conjugate samples identified as sufficiently pure and containing the correct chemical structures, DQ1 (JWH-073:QSY-7 amine), DQ3 (JWH-018:QSY-7 amine), and DQ4 (JWH-018:$(PEG)_4$:QSY-7 amine) were analyzed for CB_1 receptor interaction, as shown in **figure 62**. It is important to note that in this phase of the project, the receptor of focus switched from CB_2 to CB_1 because the latter receptor is more directly applicable to forensic needs. Additionally, the highly purified monomeric form of a receptor was no longer required due to the move from the QD/bR based sensor.

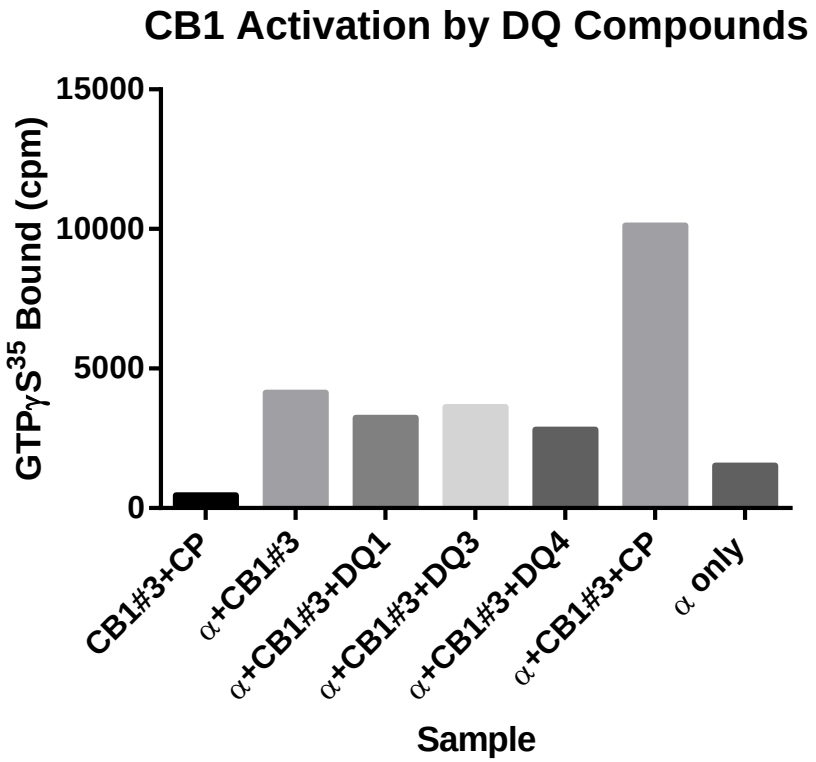

Fig. 62 Dark Quencher compounds were tested at 1ul volume addition to limit methanol in the activation to 2% in comparison to CP55,940 at 1uM also added as 1ul in methanol. No activation of CB_1 receptor was detected. Concentration of DQ compounds were 1.35uM of DQ1, 0.312uM of DQ3, and 1.374uM of DQ4.

No activation was observed for any of the candidate DQ compounds. To confirm this, the candidate DQ compounds were evaporated to dryness and dissolved in ethanol at 10-fold the initial concentrations and tests were repeated, also revealing no stimulation of CB_1 receptor. These data limit the affinity of the DQ compounds to K_d values >> 10 uM if they have agonist activity. As an alternative, the DQ compounds were tested as antagonists for CP55,940 activation of CB_1 receptor.

For antagonist studies, the EC_{50} of CP55,940 for activation of CB_1 under these assay conditions was determined by analysis of concentration-saturation of the catalyzed binding of GTPγS to Gαi1 as shown in **figure 63**.

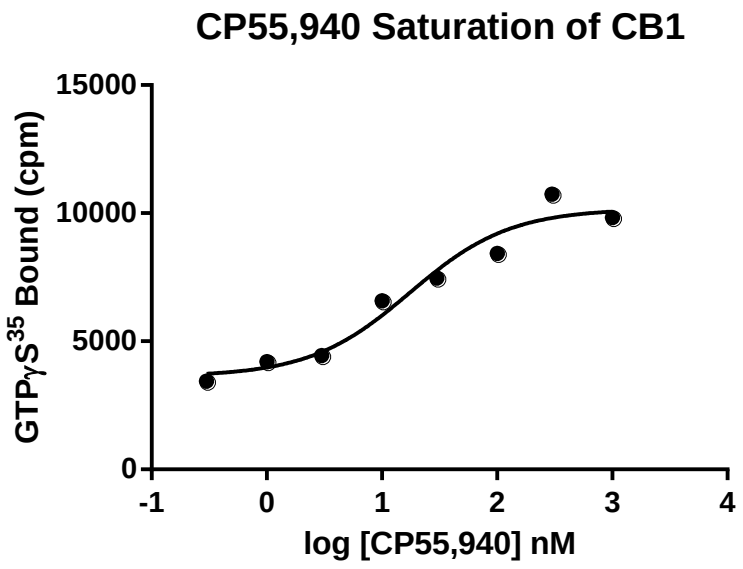

Fig. 63 Saturation of CB_1 receptor by CP55,940 was determined by addition of 1 uL volumes of CP55,940 providing the final concentrations indicated. These data were fitted to a single-site binding model to calculate an EC_{50} of 30nM.

For antagonism studies, the EC_{50} concentration of CP55,940 (30 nM) was used to activate CB_1 and candidate DQ compounds were tested as inhibitors at the maximum volume of methanol or ethanol that can be added to the CB_1 receptor (2%), as shown in **figure 64**. These experiments gave widely discrepant results using the samples in methanol, with somewhat more consistency for ethanol-dissolved samples. Only the DQ4 (JWH-018:$(PEG)_4$:QSY-7 amine) showed inhibition, albeit only partial, for CP55,940 activation of CB_1. Since it was tested at 13.7 µM, the apparent K_d for CB_1 receptor must be >7 uM. DQ1 K_d >> 7 µM, while DQ3 K_d >>4 µM.

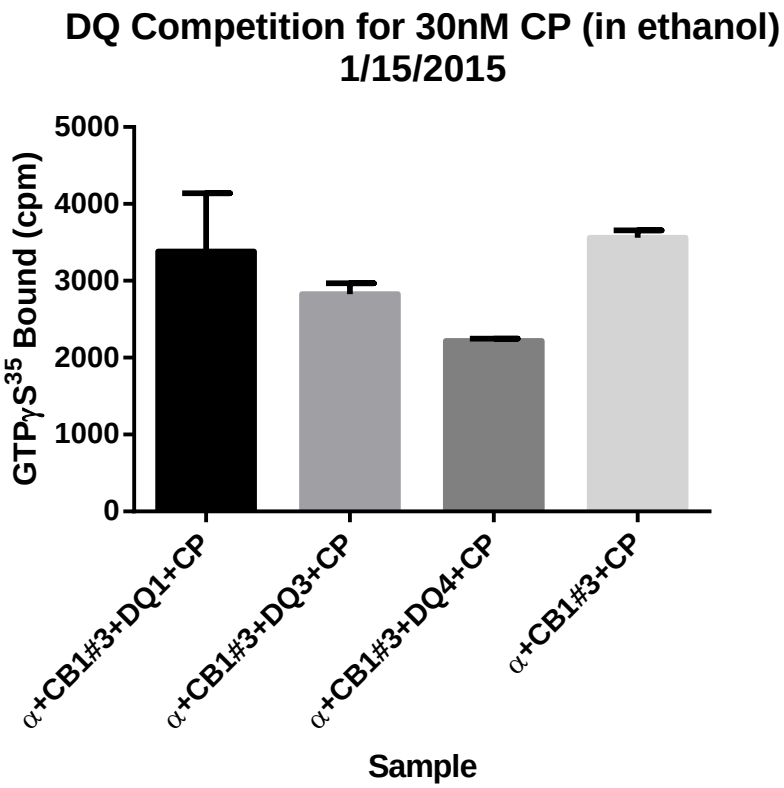

Fig. 64 Dark Quencher competition for 30 nM CP55,940 dissolved in ethanol. DQ1 was added at 13.5 uM, DQ3 at 3.1 uM and DQ4 at 13.7 uM. Only DQ4 (JWH-018:$(PEG)_4$:QSY-7 amine) shows partial inhibition for CP55,940 activation of CB_1.

These investigations would suggest that the currently available DQ candidates have too low an affinity for CB_1 to be utilized for a cannabinoid biosensor.

4.0 Theoretical QD-Dark Quencher FRET Coupling

The primary mechanism of this designed sensor platform is based upon the principles of Förster resonance energy transfer (FRET)[82], a non-radiative energy transfer process. The use of inorganic QDs and fluorescent biomolecules in FRET systems has been demonstrated [83, 84]. When inorganic QDs and biomolecules are suitably conjugated such that their spatial separation is less than 10nm and the fluorescence emission from the QD overlaps with the absorption spectrum of the biomolecules [84, 85], the QD donor can non-radiatively transfer energy to the biomolecule acceptor. QD-biomolecule FRET has been successfully used to develop and demonstrate QD-based biomolecular detection systems [84, 86, 87]. As described in the introduction, the synthetic cannabinoid sensing platform is based on competitive FRET coupling

between the energy donating QD and two different acceptor molecules, the ligand-coupled QSY-9 dark quencher and the opto-electronic protein bacteriorhodopsin. A comparison of the energy spectra of these materials is shown in **figure 65**.

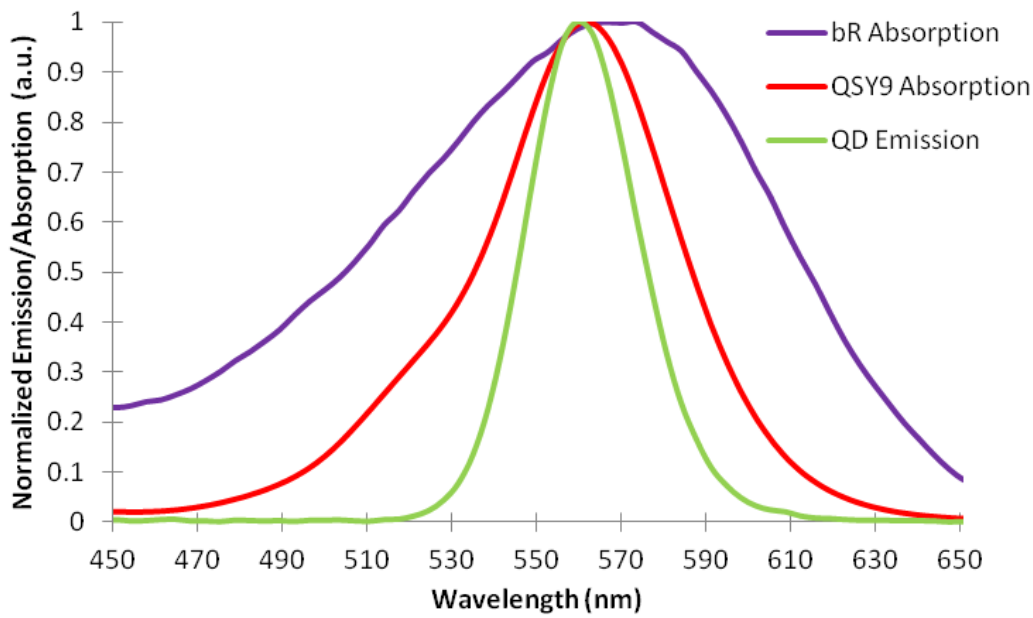

Fig. 65 Comparison of the QD emission spectrau (green) with the QSY-9 (red) and bR (purple) absorption spectrums.

For the year 1 efforts, the primary FRET relationship of interest is between the QD and the QSY-9 dark quencher, as the fluoranalytical sensor signal is based upon fluctuations in the QD fluorescent output resulting from changes in the QD-QSY-9 FRET coupling relationship. In order to calculate the theoretical FRET efficiency of a QD-QSY-9 coupled system, the Förster radius was first determined. The Förster radius (R_o) is the separation between the QD core and the QSY-9 molecule where 50% of the QD's energy is transferred to the QSY-9 via non-photonic energy transfer, defined as:

$$R_o^{\,6} = \left(8.8\times10^{23} mol\right)\left(\kappa^2\right)\left(\eta_D^{\,4}\right)\left(\Phi_D\right)\left(J(\lambda)\right) \qquad (1)$$

Where κ is the dipole orientation factor (0.66 for random dipole orientation), η_D is the refractive index of the medium (1.33 for water), Φ_D is the quantum yield of the donor (0.62), and J is the normalized overlap integral between the donor and acceptor at each specific wavelength (λ). The J-integral is calculated using the equation (2), where f_D is the peak normalized fluorescence spectrum of the donor, ε_A is the molar absorption coefficient of the acceptor (88,000 $M^{-1}cm^{-1}$ at 562nm), and λ is the wavelength.

$$J = \int f_D(\lambda)\varepsilon_A(\lambda)\lambda^4 \partial\lambda \qquad (2)$$

Using these equations R_o is calculated to be 8.13nm when coupling the QSY-9 molecule to a 565nm emission CdSe/ZnS quantum dot. With the Förster radius values determined, the theoretical FRET efficiency (E) at varying QD-QSY-9 separation distances can be determined using equation (3) and is plotted in **figure 66**.

$$E = \frac{R_o^{\ 6}}{R_o^{\ 6} + R^6} \qquad (3)$$

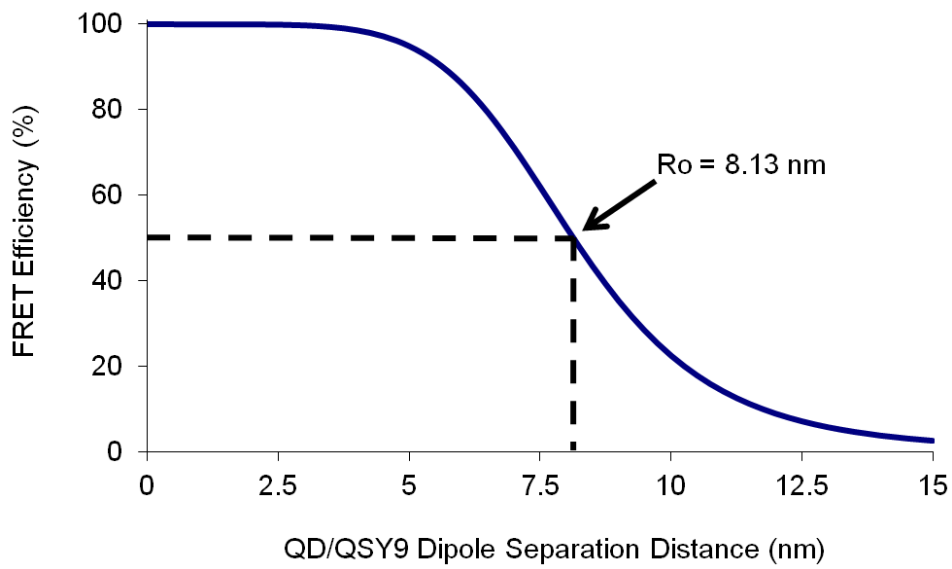

Fig. 66 QD-QSY-9 FRET efficiency versus dipole separation.

To put this into perspective with, the bR FRET efficiency plot with the identical energy level QD is compared to the QD-QSY-9 FRET efficiency in **figure 67**. It can be seen that when coupled to a 565nm emission QD, the QSY-9 dark quencher molecule has a larger Förster radius than the bR molecule, with Förster radii of 8.13nm and 7.82nm respectively. This is expected due to the increased degree of spectral overlap between the QD emission and QSY-9 absorption, as shown in **figure 66**, and that the QSY-9 molecule has a substantially greater molar extinction coefficient relative to bR, as outline in **table 11**. The larger Forster radius of the QSY-9 dark quencher implies a stronger FRET coupling relationship with the QD than that of the QD-bR coupled pair.

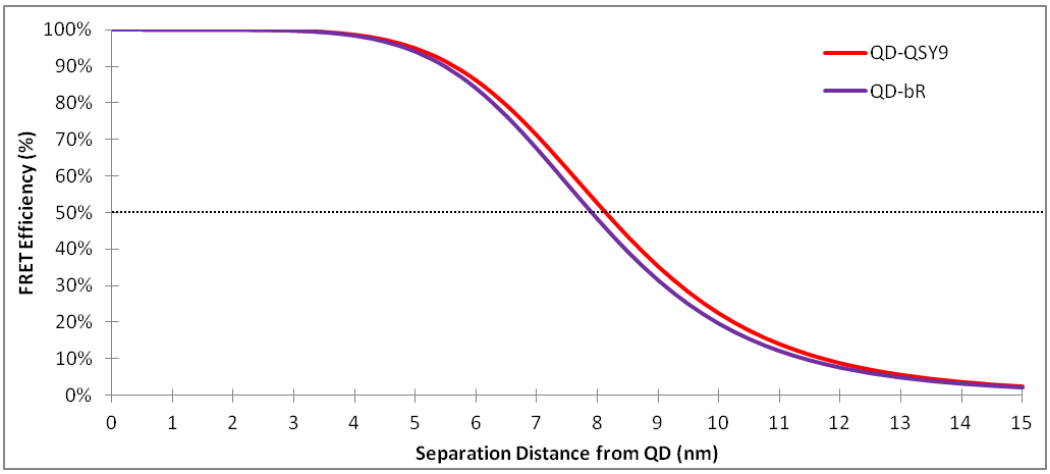

Fig. 67 Comparison of QD-bR and QD-QSY-9 FRET efficiency.

Table 11 Comparison of bR and QSY-9 FRET parameters.

Property	bR	QSY-9
Absorbance Peak Wavelength (nm)	570	562
Ext. Coeff. at Peak ($M^{-1}cm^{-1}$)	63000	88000
Forster Radius with 565nm Em. QD (nm)	7.82	8.13

5.0 QD-CB_2 Conjugates

As previously stated, in the control-state of the sensor system, the tagged cannabinoid ligand is bound to the CB_2 receptor on the QD. The dark quencher molecule and QD is in a direct fluorescent resonance energy transfer (FRET) coupling relationship. This FRET coupling relationship will quench the QD emission when the engineered ligand-dark quencher conjugate is bound to the CB_2 receptor. Utilizing the currently available CB_2 products, initial studies were performed on QD attachment and subsequent quenching with dark quencher addition. Stock solutions were prepared as follows:

- 450 nM CB2 in 50mM MOPS pH 7.5
- 200 nM Ni-NTA QDs in ddI
- 17.1 uM JWH-073 QSY7 in Methanol
- Reaction buffer: 10 mM MOPS pH 7.5 with 7.5mg/ml BSA

As shown in **figure 68**, attachment is achieved through the linkage of Ni-NTA functional groups on the CdSe/ZnS quantum dots with the His-tag expressed on the CB_2.

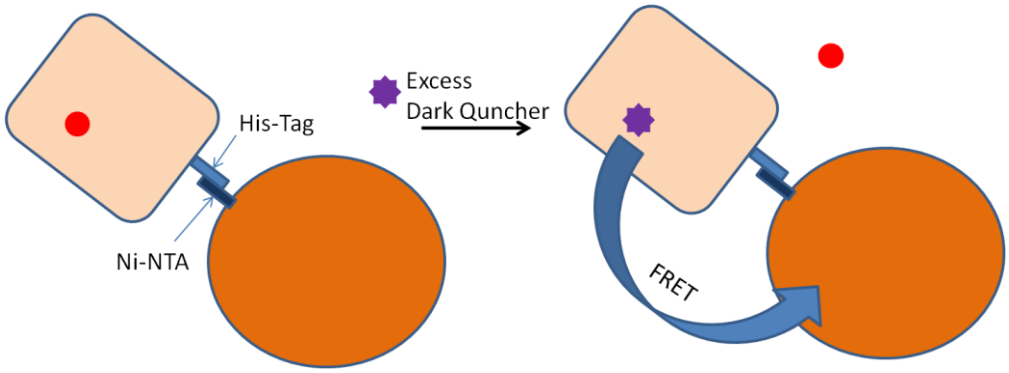

Fig. 68 Schematic of CP55,940 displacement with excess ligand-dark quencher conjugate.

An initial experiment was performed on a PTI flourospectrometer in a 100uL quartz cuvette and is shown in **figure 69**. Emission scan parameters were set for a 350nm excitation and 500-650nm emission measurement window. A 1:1 QD:CB_2 solution was prepared with a total of 5uL QDs and 2.25uL CB_2 stocks added to 90.5mL of the MOPS/BSA reaction buffer and mixed to facilitate binding. Upon addition to the cuvette, a control measurement was taken, followed by stepwise 1.155uL additions of the JWH-073 QSY7 stock. The dark quencher was applied in excess, with QD:CB_2:DQ solutions prepped at 1:1:200, 1:1:400, 1:1:600, and 1:1:800 molar ratios for samples DQ1-4. Emission quenching at the peak wavelengths is quantitatively presented in **table 12**.

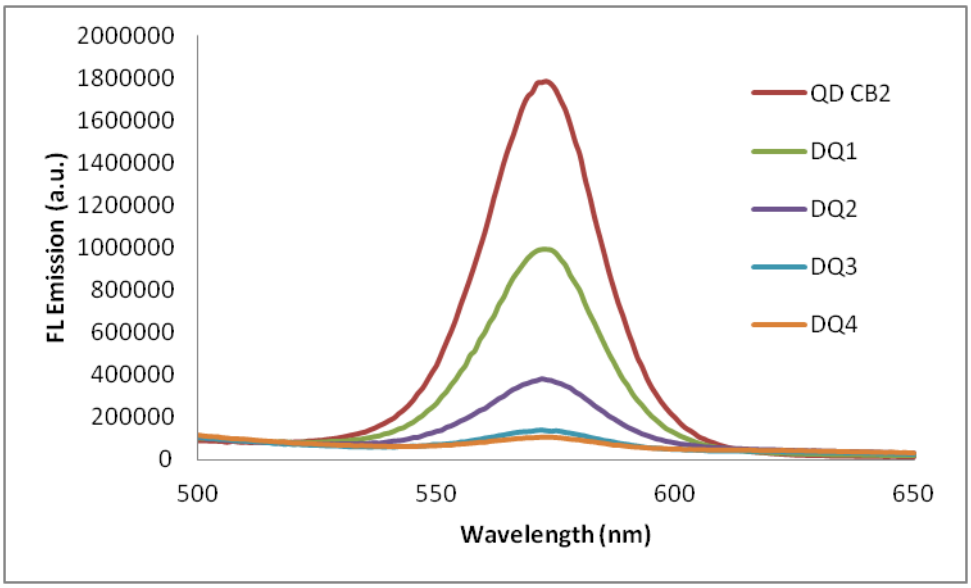

Fig. 69 Effect of JWH-073 – QSY7 addition to the emission of CB_2 bound QDs.

Table 12. Quenching effects of dark quencher addition to QD-CB_2 conjugate.

	QD CB_2	DQ1	DQ2	DQ3	DQ4
Em. Maxima	1783310	993206	382757	137996	115469
% quenching	0.00%	44.31%	78.54%	92.26%	93.53%

Initial results demonstrate a 44.3% quenching of the QD emission upon addition of the JWH-073 QSY7 dark quencher conjugate at a 200-fold molar excess. Further additions of the dark quencher continued the trend of QD emission reduction, with a plateau reached at over 90% quenching. The large quantities of dark quencher were utilized to competitively displace CP55,940 from the CB_2 binding site; however initial results demonstrate such high quantities might not be needed. Further studies are underway to optimize the dark quencher ratio's, ensure that the reaction buffer is not interfering with QD emission, and begin testing SC extracts on the fluoroanalytical system.

6.0 Hand-Held Platform

A senior design team at Michigan Technological University designed a sensor prototype. This platform designed to be handheld, need only one operator, provide present/not present result in under two minutes, and require no more than five minutes of training time. These design objectives were achieved by creating an intuitive user interface, an integrated sample cross contamination prevention system, and a redundant verification process of the results, as shown in **figure 70**. A disposable sensor chip cartridge, as shown in **figure 71**, is being printed and tested using bR chips prepared/delivered from ARL.

6.1 Physical Design

For any device to be desirable, it not only has to function well, but it must be user friendly. To meet this requirement, the usability goals for this device were comfort, ease of use, and an error proof usage process. In regards to physical form, anthropometry was used to design a device comfortable for most users (25th percentile female to 95th percentile male) [6]. It is 8"x 5"x1.5", uses 1" spacing on all light emitting diodes (LED) and buttons, and weighs 5.3 pounds (**figure 70**). Ease of use was quantified as less than 0.5% errors per operation with five minutes of training time. This target was achieved by using LEDs and text to prompt the user on the appropriate operation as well as having the microprocessor perform all the signal analysis.

Fig. 70 Virtual rendering of sensor platform body and user interface.

6.2 Detection Technology Interface

Two key issues needed to be addressed concerning the detection technology interface: (1) How to exchange the detection chip after each test as it is only good for one trial and (2) How to clean the system to prevent cross contamination between samples. Both of this issues were addressed by utilizing a disposable cartridge that houses detection technology as well as the test solution (**figure 72**). This cartridge consists of several key design features. Item one is an optically clear cast acrylic lid that allows light to pass to the detection technology, item two. Fluid is inserted through number three and fills chamber five, which then goes through six, filling chamber eight (**figure 71**). The channel at six is necessary to limit solution sloshing which adds noise to the device output. Item seven is a sealed chamber where the electrode makes contact with the chip. These contacts protrude out of the back of the device, item nine. Lastly, the ridge at four ensures the cartridge is inserted in the proper orientation.

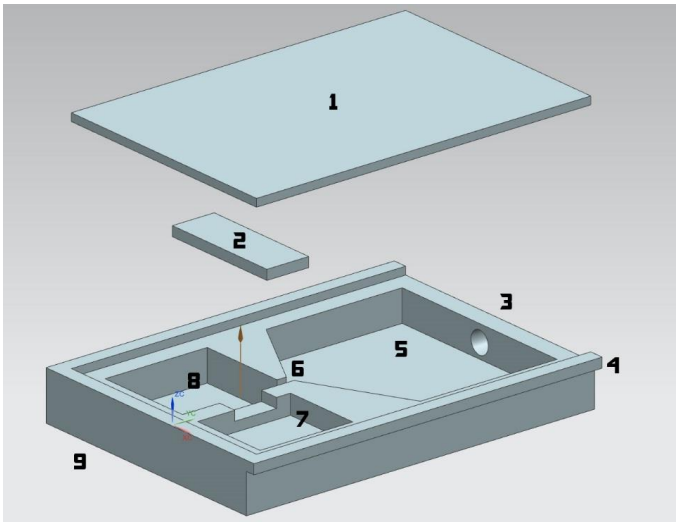

Fig. 71 Design of 3D printed disposable cartridge for sensor-chip housing.

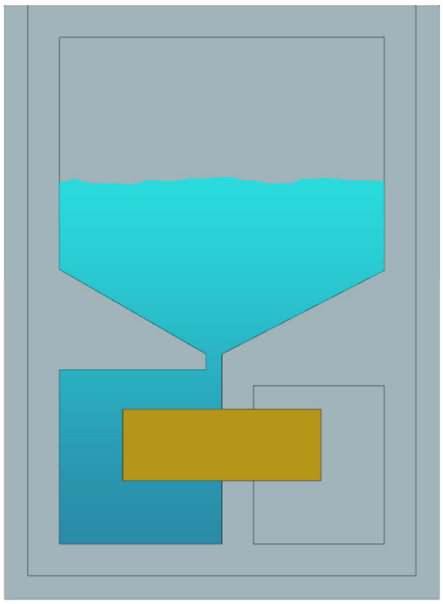

Fig. 72 The cartridge with test sample injected. Gold object represents sensor chip location.

6.3 Electronics

The electronics for this platform consists of the user interface/feedback, microprocessor, signal acquisition device, and operational amplifier. An Arduino Uno microprocessor was able to fulfill many of these roles: signal acquisition, signal processing, analyzing user input, and controlling user feedback (**figure 74**). The operational amplifier was necessary to increase the voltage of the detection technology, the difference between results being ~1 mV, as well as filtering out noise in

the signal. To further mitigate noise in the signal, aluminum was selected as the casing for this device to improve shielding (**figure 75**).

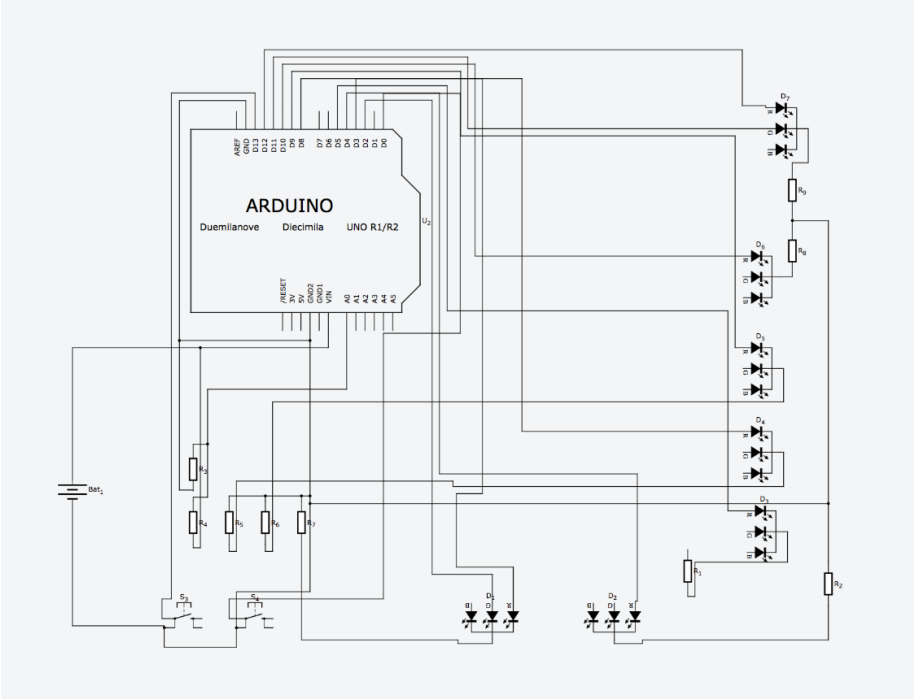

Fig. 73 Electronic wiring diagram.

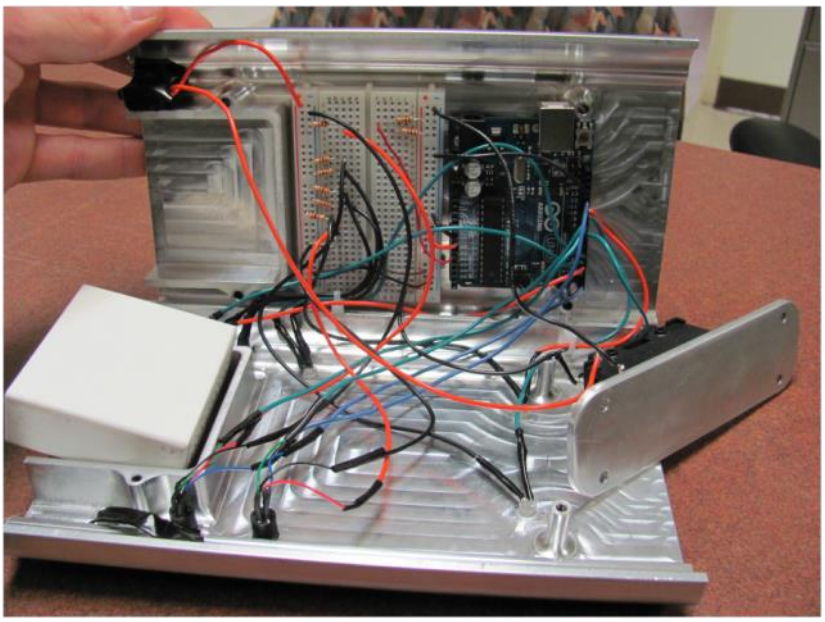

Fig. 74 The physical wiring of the platform. The power source (9V battery) is located in the right of picture and powers the Arduino Uno microprocessor (black and blue board). The white rectangle in the left of the picture is a slot for holding the cartridge and houses the electrical pins to connect to it.

6.4 Signal Processing

Voltage output from the detection technology varies with time, solute concentration, and SC presence. Therefore, the detection logic had to account for signal variance from any of these factors. A key discovery was that the signal increase due to SC presence is an absolute value, therefore the program had to simply look for an almost instantaneous increase is voltage output.

6.5 Manufacturing

6061 Aluminum was selected as the outer housing to provide a robust casing as well as to reduce external noise in the detection signal. The cartridge and its receiving unit were ABS plastic 3D printed, allowing for easy design change integration. Despite these advantages, the low dimensional precision and the layering process made solution tight gaps difficult and an interior sealant had to be used. Future manufacturing of these components should be performed via plastic injection to eliminate the need for sealant.

7.0 Synthetic Cannabinoid – Damiana Leaf Extracts

In order to add synthetic cannabinoid sample to the sensor, a reliable, simple, fast, and effective extraction method must be determined to extract the SC compound from the plant material that it is sprayed onto. Synthetic cannabinoid extraction efficacies of four solvents at two different concentrations, 2% and 100% solvent were tested. A low solvent concentration allows for a more environmentally friendly extraction procedure in addition to potentially reducing the level of extracted plant material. Furthermore, a concentration of 2% solvent is compatible with more biomolecules and thus would enable the extracts to be added directly to a biomolecule based sensing platform. To determine the success of each extraction protocol we consider the quantity of extracted synthetic cannabinoids and the total mass percentage of synthetic cannabinoid extract in comparison to contaminants. We also utilize three different incubation periods to determine the shortest time frame necessary to extract the most synthetic cannabinoid. The objective of these studies is to isolate the simplest and most efficient method of extracting synthetic cannabinoids from a synthetic cannabinoid substrate for further forensic investigation.

7.1 Preparation of Spice-Like Herbal Product

To create a spice-like product for synthetic cannabinoid extraction testing we used the damiana leaf (**figure 76A**) as a substrate for synthetic cannabinoid deposition, which is one of the more prevalent substrates used in spice products. The synthetic cannabinoid Win 55, 212-2 (**figure 76B**) was dissolved in ethanol and subsequently uniformly deposited on the damiana leaf substrate. Each extraction trial utilized 100 mg of the damiana leaf doped with 20 mg of the Win 55,212-2. Afterwards, the doped damiana leaves were allowed to dry at room temperature for approximately one hour and divided into 10 mg aliquots.

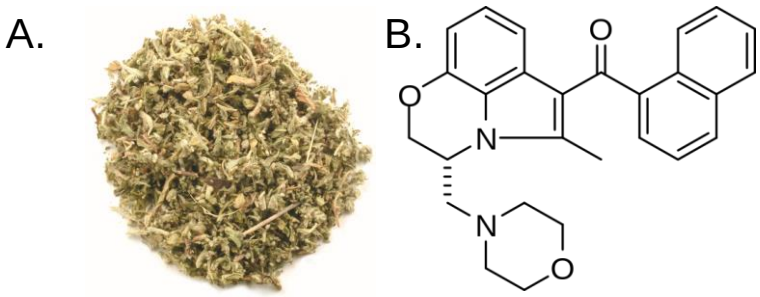

Fig. 75 Representative image of damiana leaves (A) and the chemical structure of Win 55, 212-2 (B) utilized in the study.

7.2 Synthetic Cannabinoid Extraction Studies

All studies were performed in triplicate.

7.2.1 Extraction Solvent Studies

Four different solvents: DMSO, chloroform, methanol, and ethanol, were tested for their ability to extract synthetic cannabinoids from doped damiana leaves. The CB receptor activation assay is known to only be accurate with up to 2% methanol or ethanol. Due to this, extractions were tested at a solvent concentration of 2% and 100%. The 2% solutions were made by adding 20ul of DMSO, chloroform, methanol, or ethanol, 880ul of DI H_2O, and 100ul of 1M KCl. The addition of the KCl allowed for an electrolytic final solution. Control extraction experiments were done with 10 mg of damiana leaves while the doped samples contained 10 mg of damiana leaves spiked with approximately 2 mg of Win 55, 212-2. All samples were sonicated with 1 ml of solvent for 30 minutes. The extract was then isolated from leaf fragments with pipette for further characterization via liquid chromatography mass spectroscopy (LC-MS). It is important to note that in order to be consistent with all of the solvents, a mixture containing 2% chloroform was tried. The chloroform did not mix with the water, but rather remained in emulsions.

7.2.2 Extraction Time Studies

Four different solvents, DMSO, chloroform, methanol, and ethanol, were tested for their ability to extract synthetic cannabinoids from doped damiana leaves at two additional time points, 30 seconds and 60 seconds. Each solvent also consists of 0.1 M KCl to allow for an ultimately electrolytic extraction solution. Control extraction experiments were done with 10 mg of damiana leaves while the doped samples contained 10 mg of damiana leaves spiked with approximately 2 mg of Win 55, 212-2. Leaf extracts were prepared via a manual hand shaking method with 1 ml of solvent for either 30 seconds or 60 seconds, which could be easily used in the field for quick extraction of spice products. The extract was then isolated from leaf fragments with a pipette for further characterization via LC-MS.

7.3 Liquid Chromatography Coupled Mass Spectrometry Analysis of the Damiana Leaf Extracts

The overall purity of the Win55, 212-2 extracts was analyzed via LC-MS. A single quadrupole Agilent 6130 mass spectrometer was used in conjunction with an Agilent 1200 series LC system (Agilent Technologies, Santa Clara California). The LC column was an Agilent Eclipse XDB C18

column (150 x 4.6 mm i.d., 5 μm particle size), maintained at 25˚C with a mobile phase flow rate of 0.6 ml/min. Gradient elution mobile phases consisted of A (0.1% formic acid in water) and B (0.1 % formic acid in acetonitrile) at pH 3.6. The gradient initially began at 30 % B and remained isocratic until 2 minutes. The gradient increased linearly to 50 % B from 2 to 6 minutes and held at that concentration until 12 minutes at which point the gradient again increased in a linear fashion to 100 % B at 26 minutes. Any remaining compounds were eluted from the column during a wash with 100 % B from 26 to 30 minutes. Detection wavelengths for the LC were 330, 219 and 246 nm as WIN 55, 212-2 has a max absorbance as these wavelengths and an expected mass of 427.2. Quantification of the analytes was undertaken using positive scan mode with a molecular mass scan from 100 to 800 g/mol.

Efficient and quick extraction of cannabinoids is critical to successful analysis of suspicious materials in the field. The efficiency of an extraction is determined by two factors; the amount of cannabinoid extracted (signal strength) and the purity of the extract (level of the intrinsic plant compounds in the extract). However, previous studies that developed protocols for the extraction of synthetic cannabinoids from leafy substrates have relied heavily on lab based techniques. These techniques usually require several steps including, grinding up the leafy substrate, sonication and long extraction times (>10 minutes).[1, 6, 7, 35, 37, 40, 88] This widely accepted laboratory based procedure is not advantageous for field use for two major reasons; (i) the use of sonication during solvent incubation and (ii) long extraction times. In this comprehensive extraction study we determined the optimal solvent and extraction time in order to develop a facile synthetic cannabinoid extraction method that could be easily conducted in the field. Four common solvents (DMSO, chloroform, methanol and ethanol) at two different concentrations (2 % and 100 %) were assessed for overall extraction efficiency. Furthermore, all solvents studied contained 0.1 M potassium chloride in order to make them electrolytic. Electrolytic solvents are conductive and therefore compatible with any electronic based sensing platform.[89]

WIN 55, 212-2 was chosen as the synthetic cannabinoid for use in this study as it has been widely characterized in the literature and because it is not scheduled by the Drug Enforcement Administration (DEA) and is therefore available for purchase without a permit.[32, 41, 45] WIN 55 212-2 has a max absorbance at 219, 246 and 330nm and an expected mass of 427.2. Damiana leaves are one of the most common substrates used in the preparation of “spice” like substances.[90] Thus, damiana was used as the substrate in our test extractions. **Figure 77** shows a set of plots for the control and Win55, 212-2 doped damiana leaf extracts with 100 % ethanol for 30 minutes. These plots are characteristic of the extraction data obtained for all four solvents. The peak that appears at approximately 3.6 minutes is the cannabinoid elution peak. Mass spec analysis of the 3.6 minute peak show pure WIN 55, 212-2 with very little other contaminants (**figure 78**).

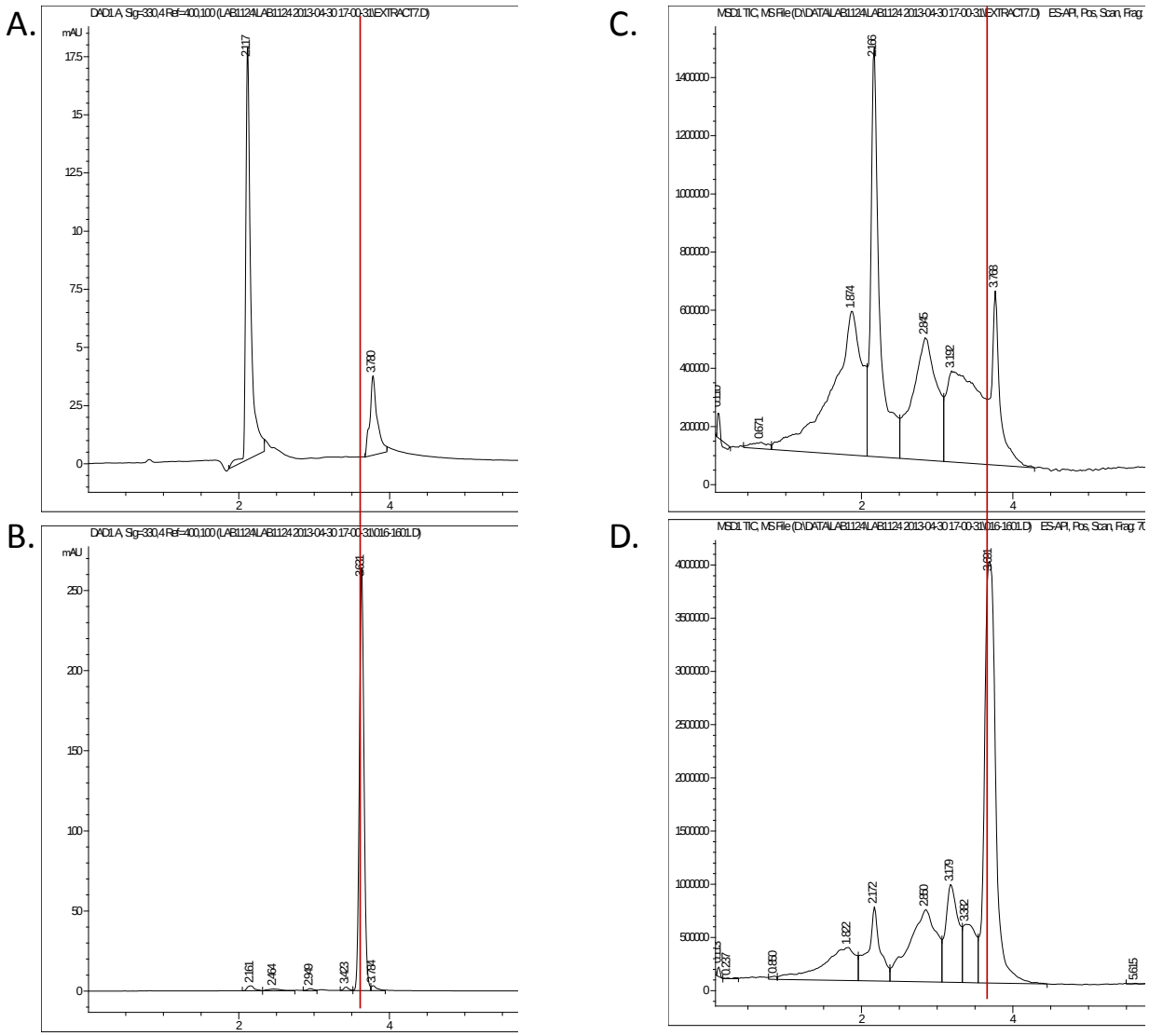

Fig. 76 LCMS Plots of 100% ethanol extracts of damiana leaves. Liquid chromatography spectra of control (A) and Win55, 212-2 doped (B) damiana leaf extracts monitored at 330 nm. Mass Spectral plots of control (C) and Win55, 212-2 doped (D) damiana leaf extracts.

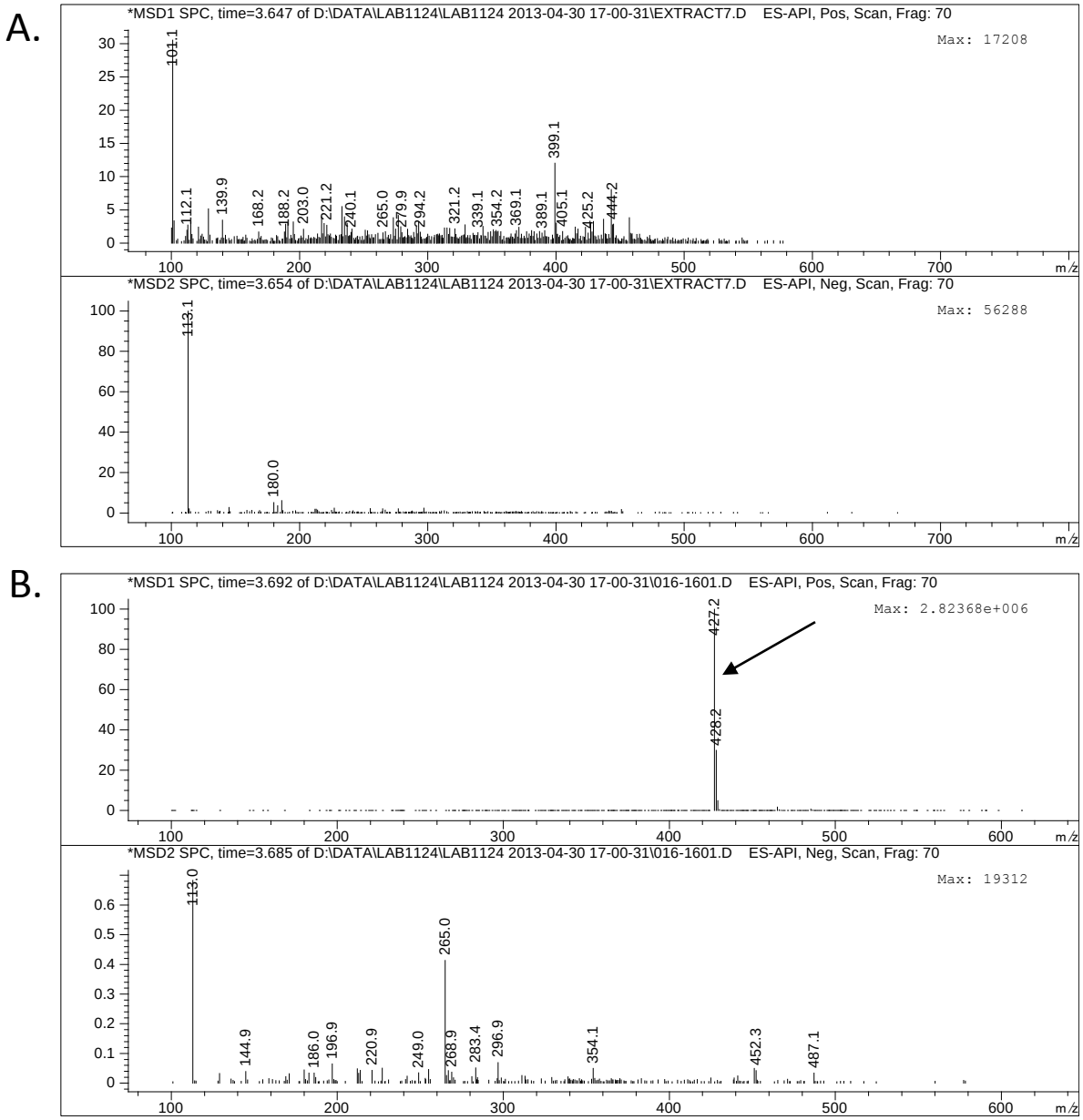

Fig. 77 Total extracted mass ion plots at 3.6 minutes of control (A) and Win 55, 212-2 doped (B) damiana leaf extracts with 100 % ethanol. Win55, 212-2 has an expected mass of 427.2 g/mol.

Initially, traditional solvent extraction methods were utilized to determine if a lower percentage of solvent could be sufficient in cannabinoid extraction. The use of a lower percentage of solvent allows for a more environmentally friendly process with less toxic waste produced. Solvent concentrations of 2 % were studied as this concentration is known to be compatible with several biomolecules including the cannabinoid receptor and thus extracts at this solvent concentration

could be directly used in any receptor based detection system. However, the samples with the low solvent concentration had very low efficiency. The LC chromatogram comparisons between 2 and 100 % solvent extractions with the four different solvents are highlighted in **figure 79**. Immediately evident is the large increase in Win55, 212-2 yield when 100 % solvent is used to prepare the leaf extracts. Peak area and total mass percentage comparisons for the WIN55 212-2 peak demonstrate that the amount of cannabinoid pulled off at 2 % solvent is 94 times less than the amount of cannabinoid extracted with 100 % solvent (**figure 79**). As it is only a 50 fold dilution to get from a 100 % solvent concentration to a 2 % solvent concentration, the more efficient method for extracting SC compounds from leafy substrates would be to extract with 100 % solvent and then dilute down to the concentration that is compatible with the assay of interest (*i.e.* 2 % for a receptor based detection platform).

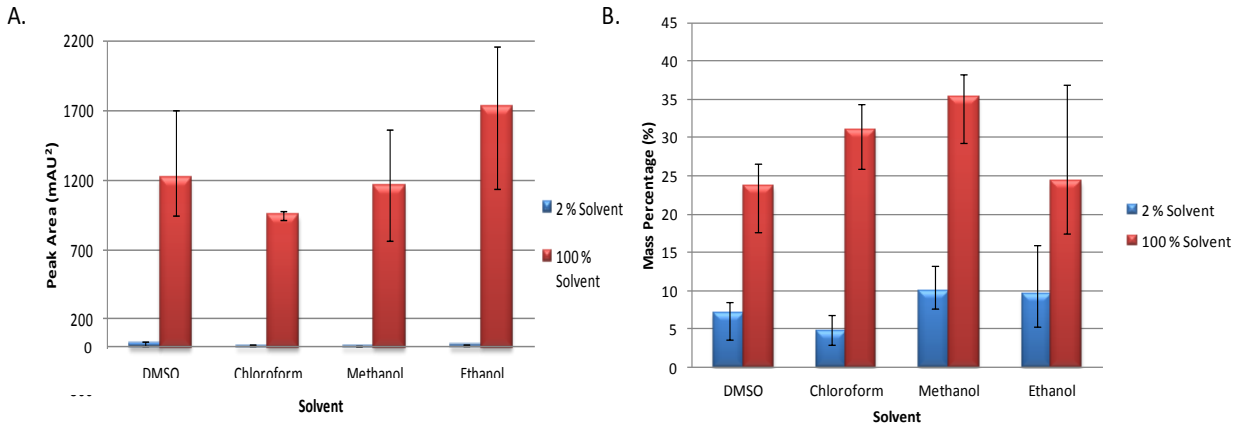

Fig. 78 Bar charts of peak area (A) and total mass percentage (B) comparisons of Win 55, 212-2 extraction with 2 % (blue) and 100 % (red) solvent concentration.

A fieldable extraction protocol must not only provide high quantity and purity of SC compounds post extraction; the total time requirements for the protocol must be low. Thus, it was then necessary to determine the shortest successful extraction time after determination of the ideal solvent concentration. It is not practical for one to perform an extraction in the field with a sonicator or related agitator instrument; consequently we chose to prepare the damiana leaf extracts with hand shaking. Furthermore, as extraction times greater than a few minutes are also impractical, we chose to study extraction efficacies at 30 second and 1 minute timepoints. Surprisingly, the data showed a higher overall mass percentage of WIN55, 212-2 in the extracts for both the 30 second and 1 minute extraction times with hand shaking (average 42 percent) when compared to the 30 minute extraction samples that were subject to sonication (average 28 percent, **figure 80**). The higher level of contaminants in the previous study could be attributed to the effects of a longer extraction time coupled with agitation via sonication. In conjunction, these two factors enable a higher amount of inherent damiana leaf compounds to be extracted

thus increasing the level of contamination in the Win55, 212-2 extracts. As the second protocol requires agitating for a shorter length of time with a much more gentle method (hand shaking) the only compounds extracted are those that are very easily removed, such as the synthetic cannabinoids that are sprayed on the leafy substrates. Notably, the peak area between the two extraction protocols (30 min sonication vs. ≤ 1 minute hand shaking) is highly similar with an average peak area of 1259 mAU^2 for the former and 1255 mAU^2 for the latter. These data lend further support to the observation that higher extraction efficiency is achieved with shorter incubation times and gentler agitation methods.

Also of interest was the result that there was no statistically significant difference in the overall extraction efficiency between the between the 30 second and 1 minute time points (**figure 80**). These results show that the easily extracted materials are lifted off leaves almost immediately upon solvent addition. Thus, the more intense extraction methodologies only serve to increase the level of contamination within the extract samples, not increase the amount of synthetic cannabinoid extracted from the leafy substrates.

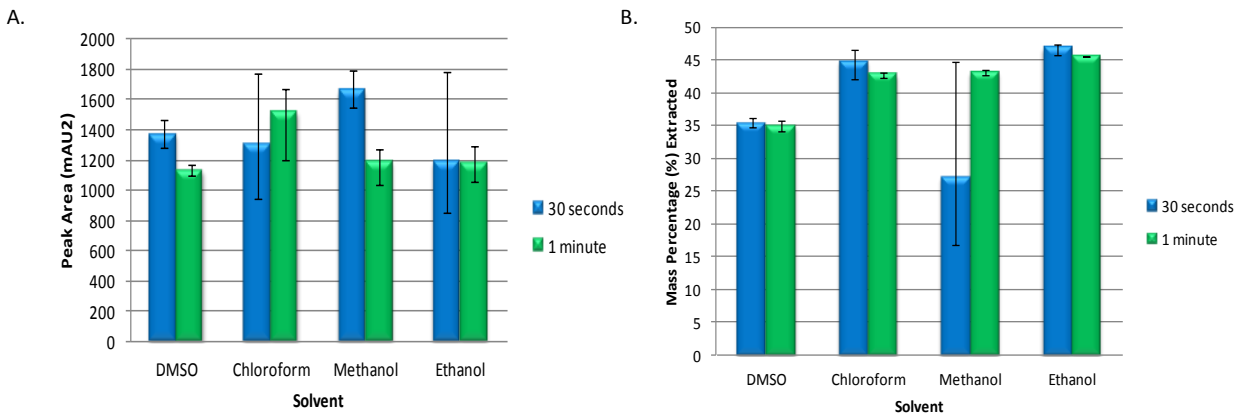

Fig. 79 Bar charts of peak area (A) and total mass percentage (B) comparisons of Win 55, 212-2 extraction with 30 second (blue) and 1 minute (green) shaking times.

7.4 Activation of CB_2 in Presence of Various Solvents

CB_2 was tested with various solvents. As shown in **figure 81**, CB_2 was able to detect the cannabinoid in all the solvents except chloroform; chloroform is not compatible with the receptor. Experiments have demonstrated that the presence of a cannabinoid agonist is detectable down to ~5,000 fold dilution using a [S^{35}]GTP-γ-S G protein-activation assay and bacterial membranes containing recombinant MBP-CB_2 fusion protein plus 10 mg of WIN 55,212-2 per dose of methanol extract with Spice confusants. Interference from the presence of confusants was not observed, as shown in **figure 82**. Spice simulated samples were prepared using a methanol extract from a typical Spice substrate (Damiana leaf) in combination with an unscheduled, strongly binding agonist such as CP-55,940, WIN 55,212-2 or similar.

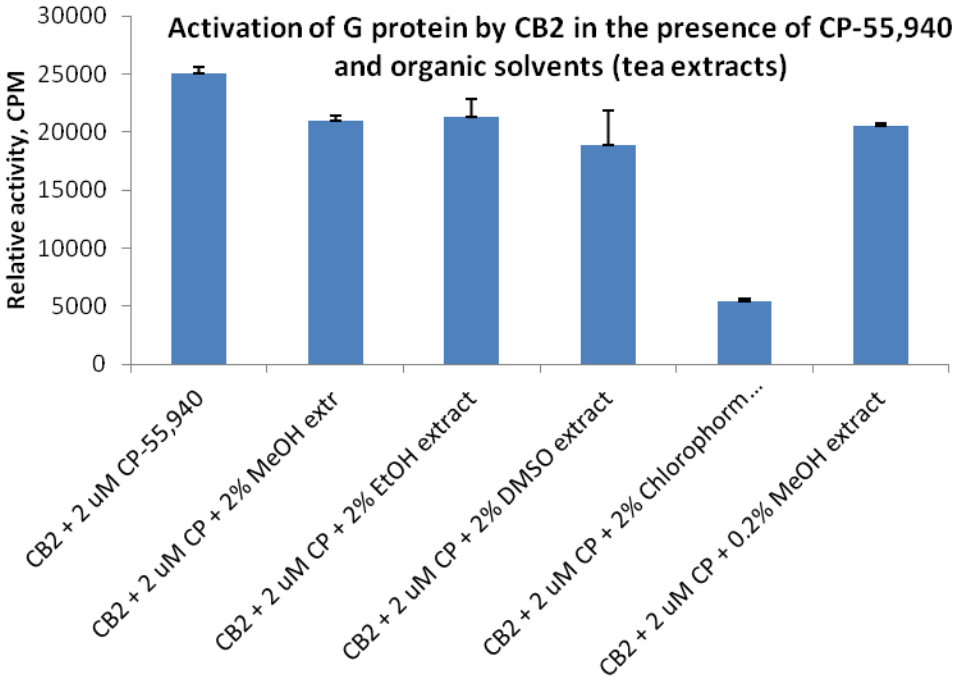

Fig. 80 Activations of CB_2 in the presence of varying ligand/solvent extract combinations.

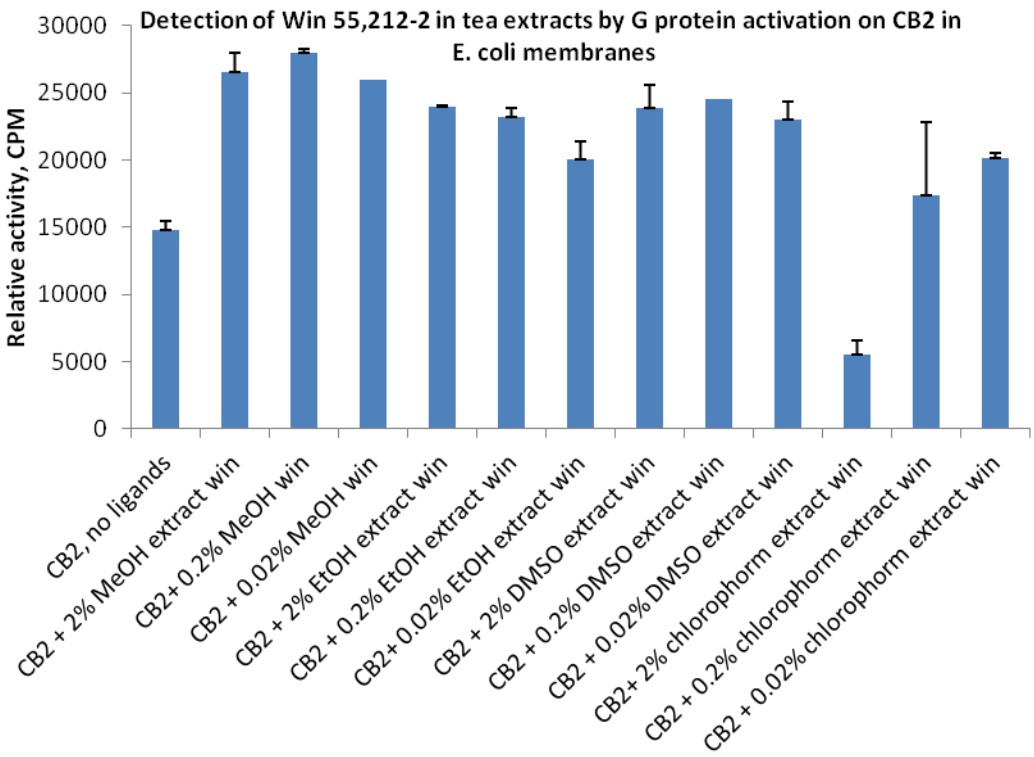

Fig. 81 Activation of CB_2 at 5000-fold dilutions of mock Spice extracts.

Based on these results, it was determined that chloroform at 2% is not compatible with the CB receptor. It also is not ideal due to the formations of emulsions, which may lead to inefficient extraction. 2% methanol, 2% ethanol, and 2% DMSO appear to be compatible with the receptor and also efficient at extraction of the cannabinoid from plant material in only 30 seconds of hand shaking. There are also a limited amount of impurities with that method. Due to the hazards of DMSO to the user, it seems that extraction with 2% methanol or ethanol for a total of 30 seconds of hand shaking is the best form of extraction.

8.0 Optical G-Protein Activation Assay

8.1 Europium GTP

Since the preparation of highly-purified CB receptor without a stabilizing ligand cannot be prepared to accommodate the SC-dark quencher model, a second approach for transferring photons to a BR sensor will be developed. In this approach the specific, selective binding of a cannabinoid agonist (test substances) to the human CB_1 receptor will drive the binding of a fluorescent GTP analog to the CB_1 receptor's cognate G-protein, Gi1. The first phase of this work

developed a plate-reader fluorometric method for the high-throughput screening of samples suitable for a forensic laboratory setting. A second phase of the project will couple the fluorescent GTP-bound G-protein to bacterial rhodopsin via a G-protein specific monoclonal antibody to be developed which will assemble Eu-GTP-Gi in proximity to bacterial rhodopsin for a voltage detection-based sensor.

8.1.1 Fluoroanalytical Assay Overview

We used the europium-GTP method marketed by Perkin-Elmer as the basis for the creation of a cannabinoid-triggered creation of a fluorescently labeled G-protein. This procedure is schematized in **figure 83**. For this purpose the GPCR is the human CB_1 receptor expressed in Sf9 cell membranes and the agonist is a synthetic cannabinoid ligand. As seen in this illustration, the ligand recognition by a GPCR results in a robust enhancement of the fluorescence signal detected.

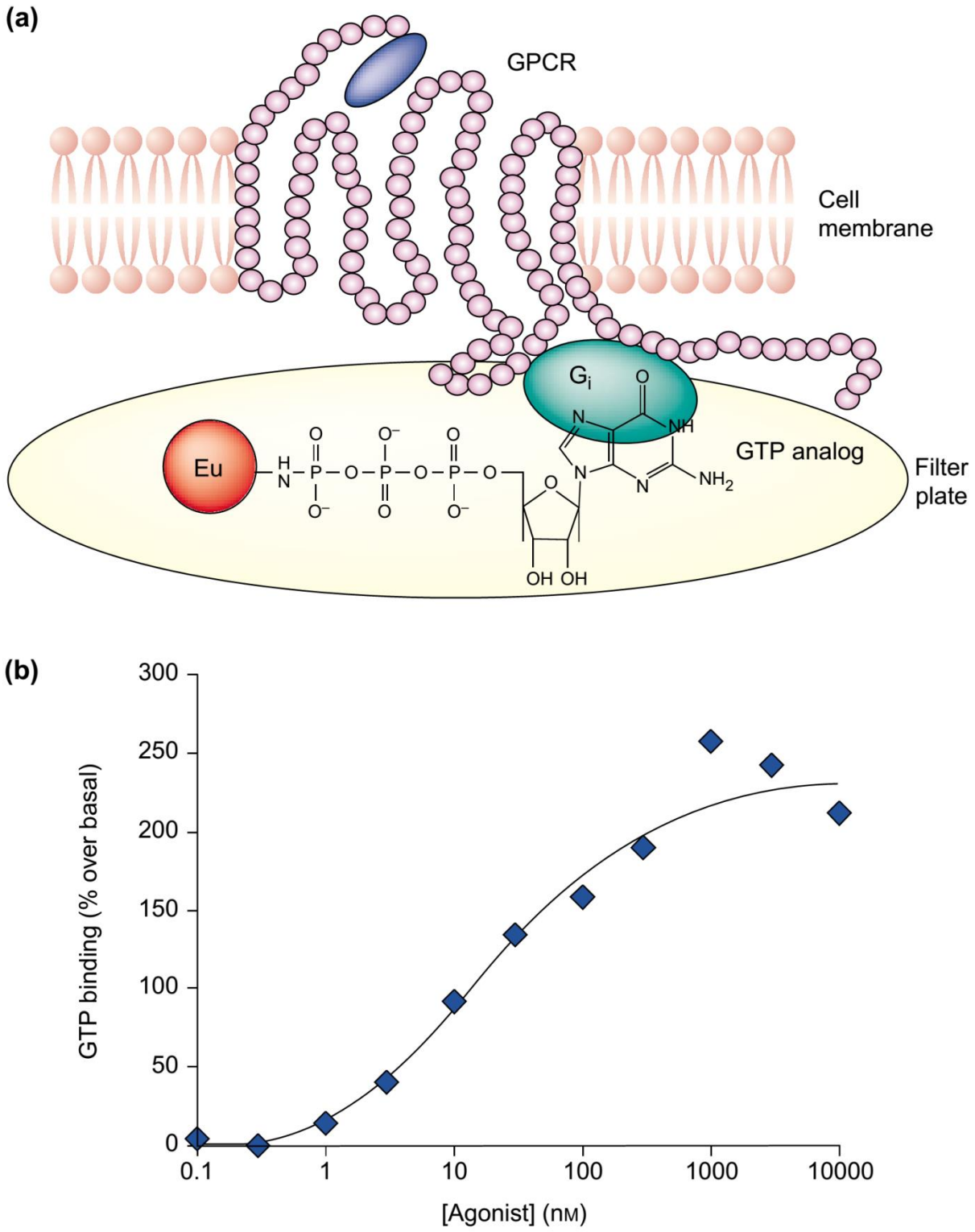

Fig. 82 GPCR Activity Schematic.

As marketed by Perkin-Elmer, the Eu-GTP method utilizes a plate filtration method to separate unbound Eu-GTP from the G-protein-bound product. We will utilize a quenching resonance energy transfer (QRET) approach by the addition of 1,1,3,3,3′,3′-hexamethylindodicarbocyanine to quench the fluorescence of Eu-GTP in aqueous environment which is relieved by the binding interactions with Gi shielding Eu-GTP from water. This allows a homogeneous plate reading approach to the detection of cannabinoids.

8.1.2 Eu-GTP Synthesis

Since initiating this project, we have learned that Perkin-Elmer has decided to discontinue the marketing of Eu-GTP. However, they have agreed to provide a sample of the product for our work. We expect this to be sufficient for some 500 experimental samples. Independently, we have been in contact with the laboratory responsible for developing the Eu-GTP and are in discussions regarding collaborating with them to synthesize and test additional Eu-GTP ligands which would be available for this research effort. Basically, the synthesis involves the conjugation of nona-dentate coordinated Eu^{3+} shown in B of **figure 84** below either as an amide-linkage through the γ-phosphate of GTP (the Perkin-Elmer product) or esterified to the 2’ or 3’ OH of the ribose (panel A). The challenges to our project are that the 4-[2-(4-isothiocyanatophenyl)ethynyl]-2,6,-bis([N,Nbis(carboxymethyl)-amino]methyl)pyridine chelator is not commercially available and involves a multistep synthetic path beyond our laboratory’s capacity. Further, the linkers spacing the Eu-chelate from GTP used in the Perkin-Elmer compound are proprietary information. Thus, purchasing the compound from Perkin-Elmer is the best option.

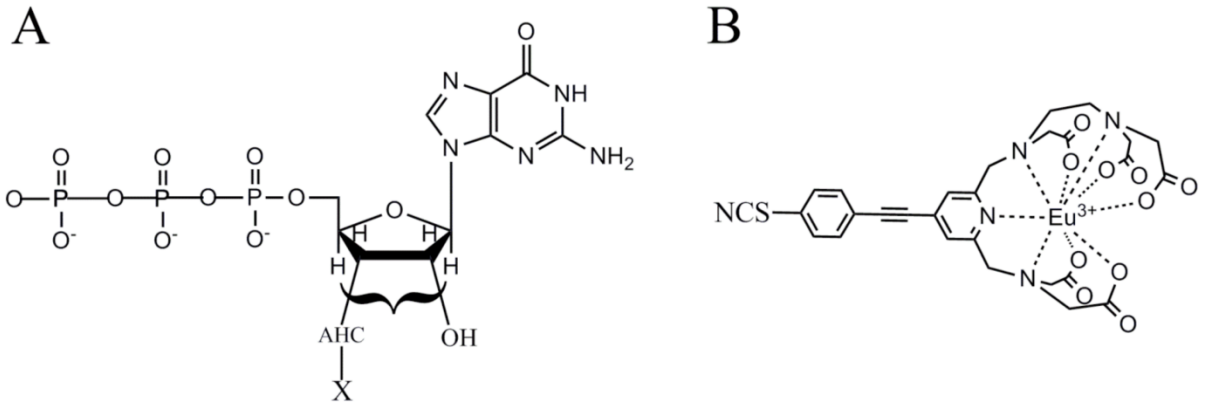

Fig. 83 Structures of GTP (A) and Eu-chelate (B).

8.1.3 Eu-GTP G-Protein Activation Plate Reader Assay

Experiments were modeled on established GTP-exchange assays using radioactive GTP analogs and are being optimized for maximum optical signals for Europium fluorescence including quencher 1,1,3,3,3,3-Hexamethylindodicarbocyanine iodide (diCy). Detection was based upon time resolved fluorescence (TRF) emissions with excitation at 340nm and emission at 612nm with a 400µs delay and integration for 400µs. Under these conditions the emission of Eu^{3+} is separated from all other fluorescence signals present in the sample. The solution emission of Eu-GTP is then quenched by resonance energy transfer to diCy (**figure 85**) and is only detected when Eu-GTP is bound to $G\alpha_{i1}$. The presence of cannabinoid can thus be detected by the CB_1 receptor catalyzed binding of Eu-GTP to $G\alpha_{i1}$ and the resultant fluorescence enhancement (**figure 86**).

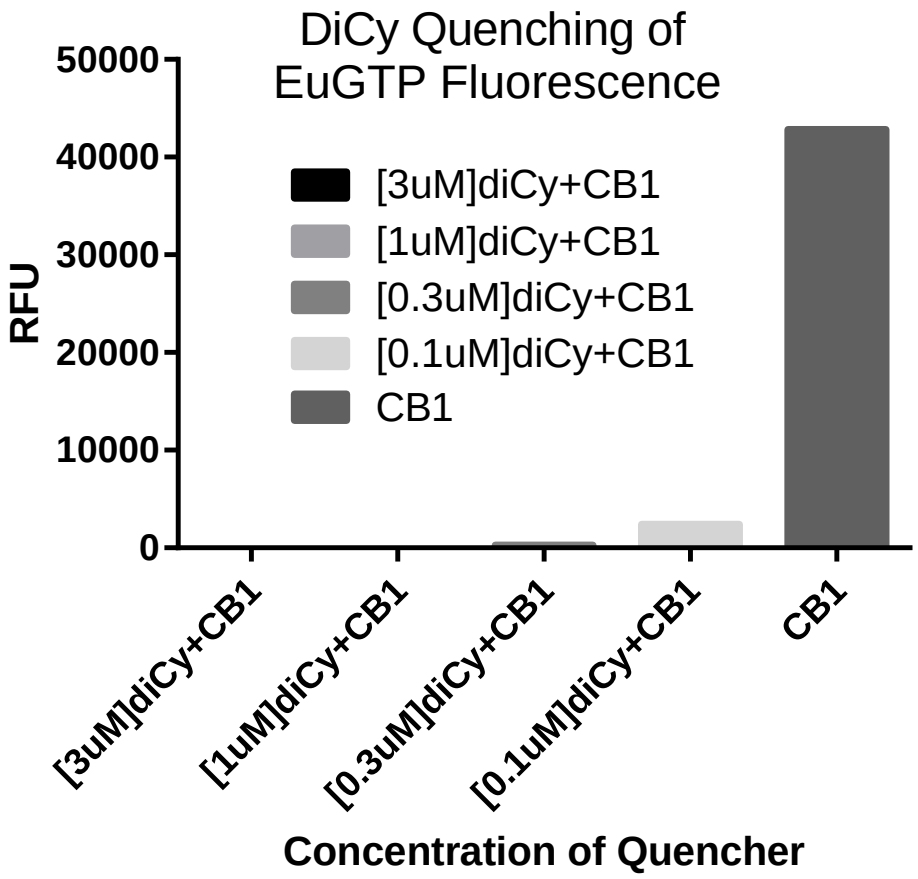

Fig. 84 Fluorescence signal from 40nM Eu-GTP with CB_1 receptor, in the presence of varying concentrations of quencher (diCy). The indicated concentrations of diCy were mixed in the presence of CB_1 containing membranes and 100nM Eu-GTP and TRF was measured.

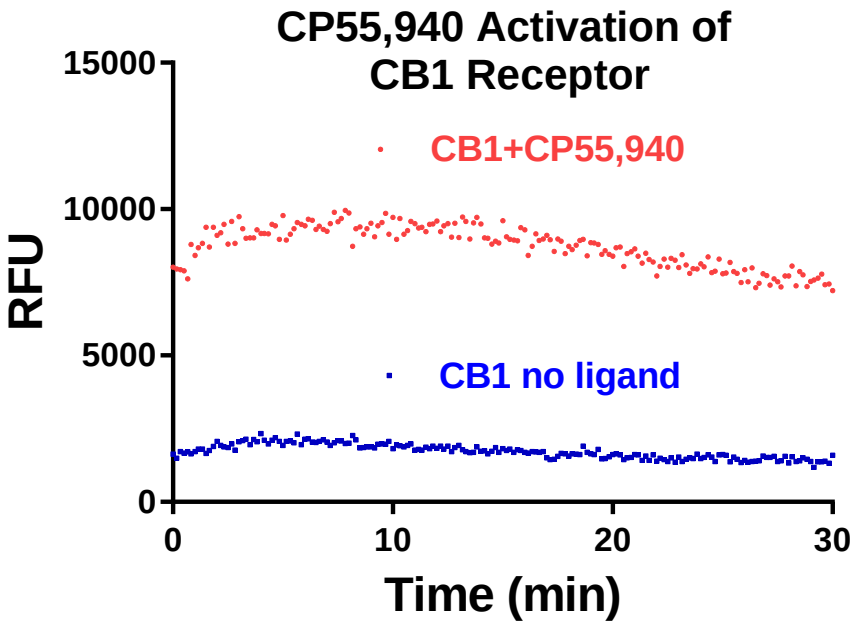

Fig. 85 CP55,940 activation of CB_1 receptor detected by TRF enhancement of Eu-GTP. CB_1 receptor containing membranes were mixed with $G\alpha_{i1}$ and $G\beta\gamma$ without and with the addition of CP55,940. Reactions were initiated by the addition of Eu-GTP and TRF monitored for three replicate samples each for 30 minutes.

These results utilized an extremely high concentration of CP55,940 as an activator. We were unable to consistently repeat these results with lower concentrations of CP. Upon getting such inconsistent results, further testing was done to verify the published data indicating that Europium-GTP was in fact binding with the $G_{\alpha i1}$ subunit.

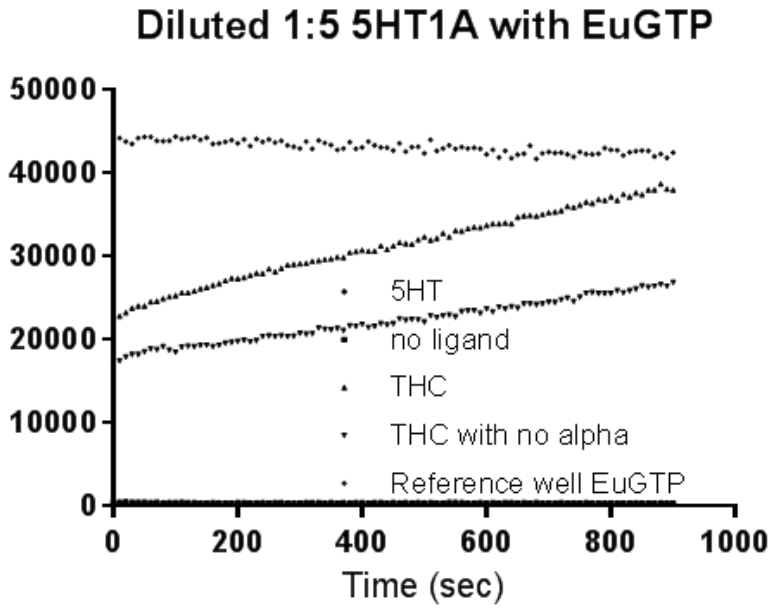

Fig. 86 Serotonin receptor (5HT, 5-hydroxytryptamine receptor) was used in place of CB_1 with THC as the activating ligand. 5HT is not activated by THC and should not show an increase in fluorescence. The graph shows a large increase in fluorescence when THC is added, indicating nonspecific interactions of EuGTP and THC.

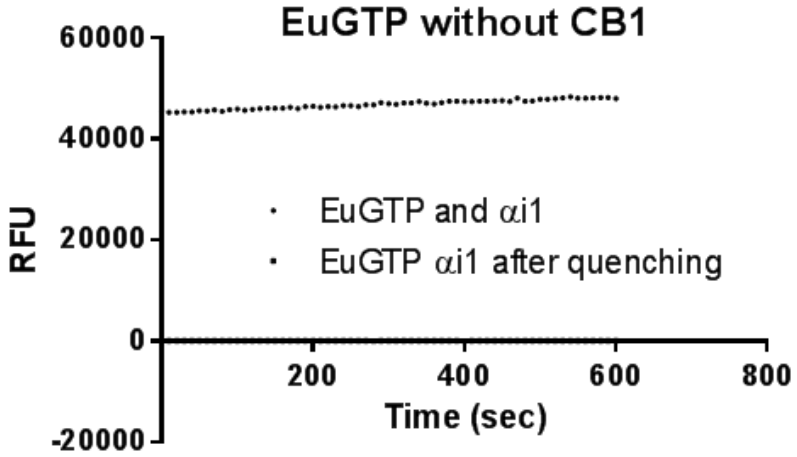

Fig. 87 $G\alpha_{i1}$ was incubated with EuGTP without a receptor present for one hour. Since $G\alpha_{i1}$ will bind GTP spontaneously at a slow rate, some EuGTP should remain bound after the addition of quencher.

A measurement was taken immediately before quencher addition and immediately after quencher addition. As can be seen, after the addition of quencher, all of the fluorescence is immediately quenched. This indicates that the Eu-GTP molecule is not binding with $G\alpha_{i1}$.

Based on the data from **figures 87 and 88**, it was determined that using the catalysis of GTP binding to $G\alpha_{i1}$ and the fluorescent guanine nucleotide analog Eu-GTP as a biosensor would not work.

8.2 BODIPY-Fl GTPγS CB_2

The CB_2 used in the current efforts is synthesized with a stabilizing ligand (CP55,940) in the binding pocket, thus assay experiments are performed with CB_2 in an 'activated' state. All experiments were performed in a 10mM MOPS pH7.5 buffer with a binding solution prepared with 50mM MOPS, 1mM Na-EDTA, 3mM MgSO4, 1mM DTT, and 100mM NaCl in ddI H2O. Assays were prepared by mixing the CB_2, G-protein subunits, buffer, and binding solution in a silanized glass tube for 30s at room temperature to facilitate GCPR coupling to the G-protein subunits. Reaction initiates upon addition of the BODIPY FL GTPgS compound. In a synthetic cannabinoid screening assay, the test sample is added prior to the BODIPY FL GTPγS; resulting in activated CB_2 as schematically represented in **figure 89**.

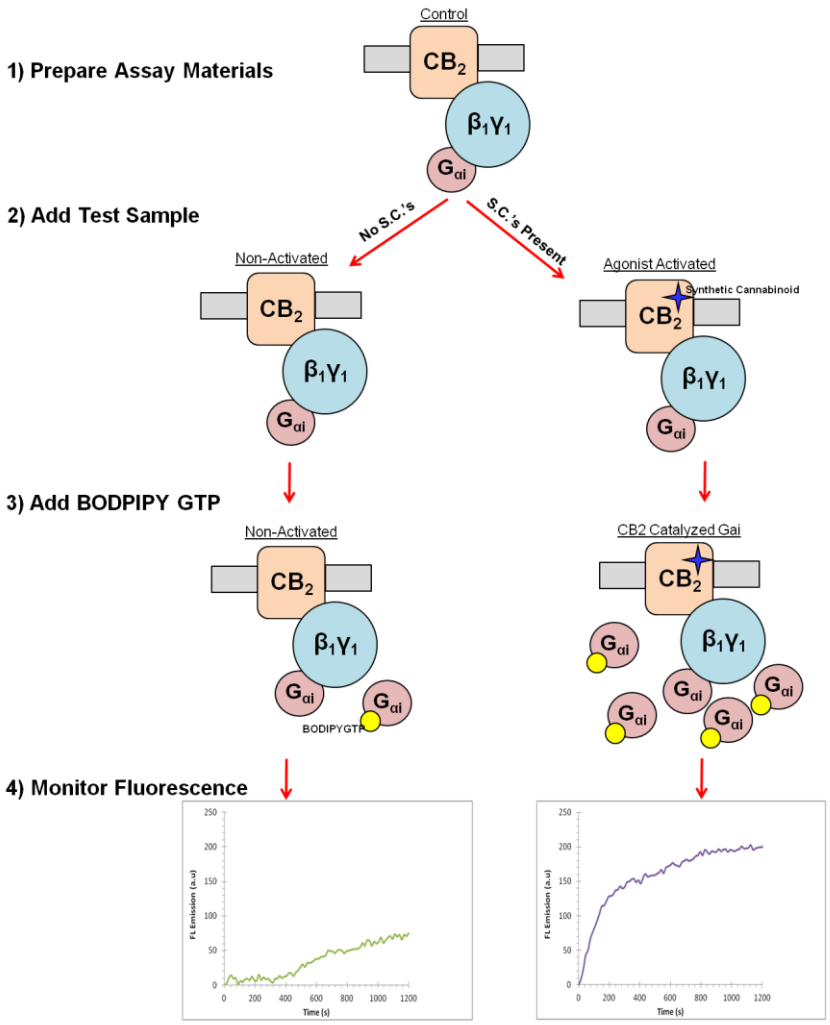

Fig. 88 Schematic of GPCR-G protein screening assay for synthetic cannabinoids.

Initial tests were performed on a PTI fluorospectrometer with the BODIPY FL GTPgS control, Gai/BODIPY FL GTPgs, and CB_2 catalyzed Gai in the presence of BODIPY FL GTPgs. The end fluorescence emission profiles after a 10 minute incubation is shown in **figure 90**, with the timebased evolution monitoring the 512nm BODIPY FL peak fluorescence shown in **figure 91**. The results demonstrate a 6-fold increase in fluorescence output in the presence of CP55,940 activated CB_2 compared to uncatalyzed Gai binding alone. From **figure 92** it can be estimated that the presence of a synthetic cannabinoid could be determined in under 5 minutes.

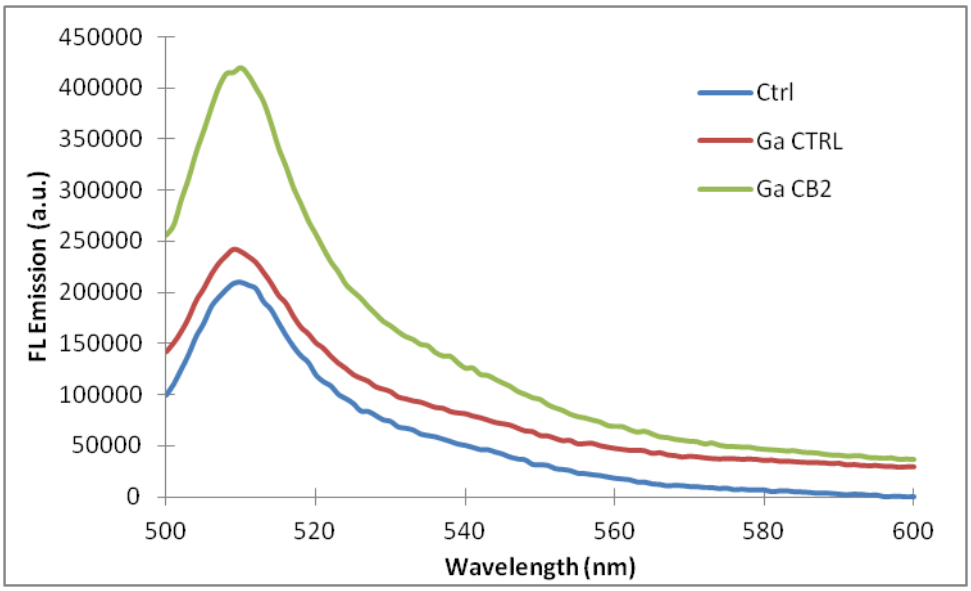

Fig. 89 Fluorescence emission of BODIPY FL GTPgS after 10 minute incubation in varying experimental configurations.

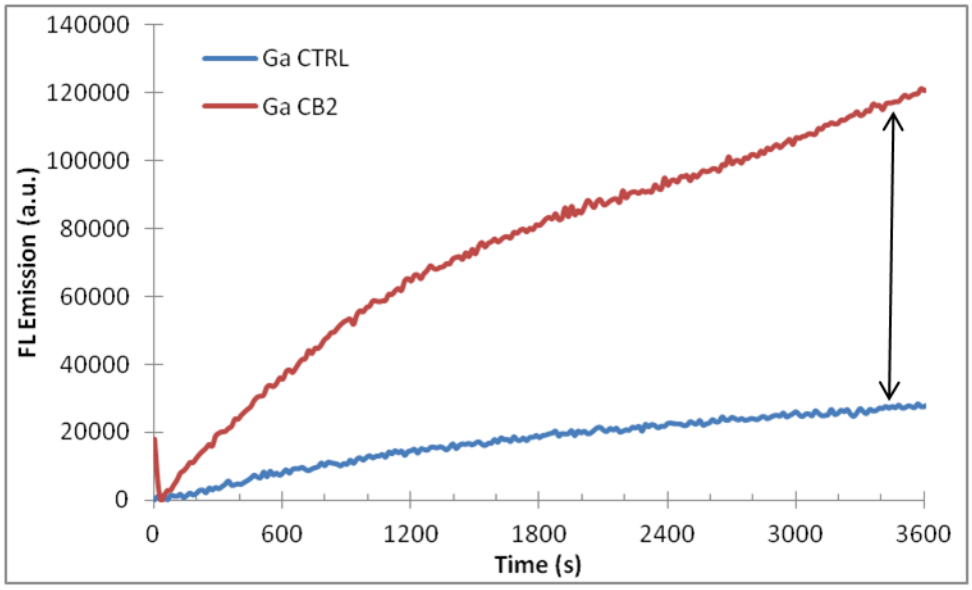

Fig. 90 Time based 512nm fluorescence monitoring of activated assay versus control.

To increase the screening through-put, the materials were also tested on a TECAN 96-well plate instrument. As shown in **figure 92**, the catalytic effect of synthetic cannabinoid activated CB_2 can be rapidly distinguished from inactivated samples. **table 13** lists the relative emission peak comparisons among the test group, with a clear 3-4 fold increase in emission intensity present in CB_2 catalyzed reactions over Gai controls.

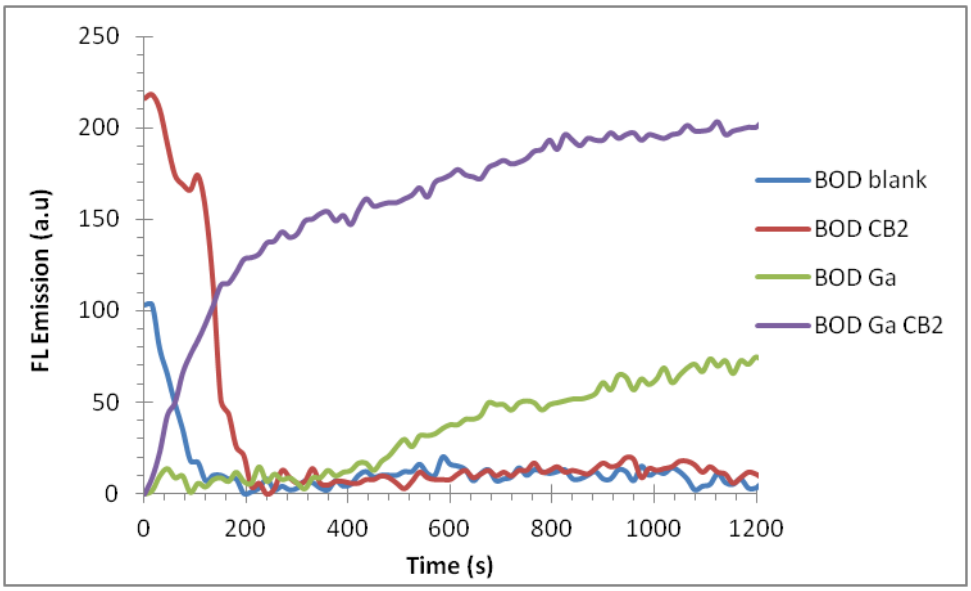

Fig. 91 Timebased 512nm fluorescence monitoring of activated assay components.

Table 13. Fluorescence emission comparisons at 5, 10, 15, and 20 minute timepoints.

Time (min)	BOD blank	BOD CB2	BOD Ga	BOD Ga CB2
5	3	6	6	142
10	16	8	38	174
15	8	17	61	193
20	3	11	75	200

8.3 BODIPY-Fl GTPγS CB_1

The above studies were done using CB_2 receptor. The receptor cannot be stabilized without the use of a strong binding stabilizing ligand. Studies were tested using CB_1 receptor and BODIPY-Fl-GTPγS. CP55,940 was used as the activating ligand for the CB_2 receptor. The Tecan plate reader was used to read the fluorescence over time. The results can be seen in **figure 93**.

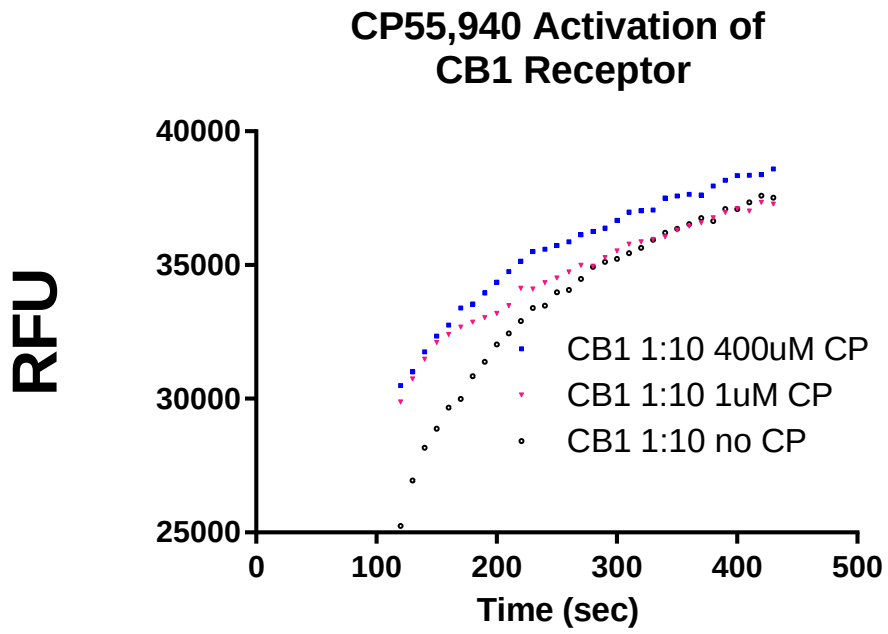

Fig. 92 Time based 512nm fluorescence monitoring of activated assay components CB_1, $G\alpha_{i1}$, and CP55,940 as the activating ligand. The catalysis can be seen between the activated and inactivated reaction.

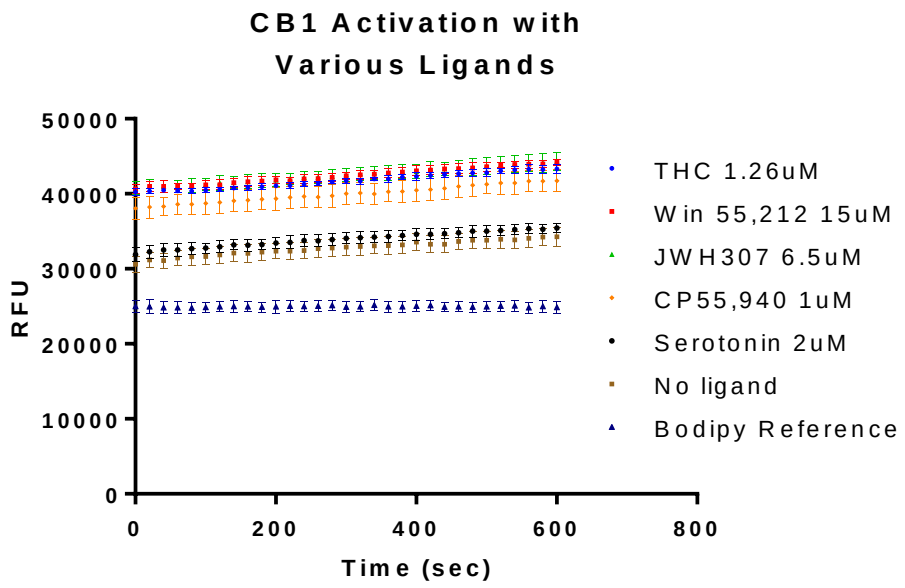

Fig. 93 BODIPY-Fl GTPγS emission in the presence of various ligands. Serotonin is not a CB activating ligand and was used as a negative control. Approximately a 30% increase in signal can be seen when activated.

With the use of BODIPY-Fl GTPγS, the bioelectronics platform described in Chapter 5 is not as straightforward. The BODIPY fluorophore emission does not overlap the absorbance of the bR. The emission can be tuned to align with bR absorbance in order to continue with this path. Another option would be to use a hand-held spectrometer to make optical readings. Such a device would require two channels, one to read the control fluorescence without the addition of a ligand and the other to read the fluorescence with the addition of the unknown sample. There are several obstacles that must be overcome; the temperature sensitivity of the reagents, addition of small microliter volumes, ease of use by personnel with limited training, and the hydrophobic nature of many of the components.

9.0 Summary, Conclusions, and Future Direction

Below is a summary of the key accomplishments of this project:

Experimental

- Optimized a rapid and facile method to extract synthetic cannabinoids from leafy substrates in the field
- Synthesized and purified three synthetic cannabinoid-dark quencher conjugates
- Demonstrated proof of concept for a biosensor for agonist cannabinoid agents using BODIPY-GTP
- First ever demonstration of a cannabinoid sensor independent of chemical structure

Computational

- Developed CHARMM parameters for the simulation of synthetic cannabinoid compounds
- Computed the solubility and diffusivity of synthetic cannabinoid compounds to describe behavior in the cell's bilayer
- Determined optimal DQ attachment location on cannabinoid and linker length
- Illustrated possible binding orientations of cannabinoid-DQ

Based on our studies, the results demonstrate that baculovirus encoded CB_1 receptor expressed in Sf9 cells can be used as the basis for a biosensor for agonist cannabinoid agents by using the catalysis of GTP binding to $G\alpha_{i1}$ and the fluorescent guanine nucleotide analog BODIPY-Fl-GTPγS. The agents tested include, Δ9-tetrahydrocannabinol (THC), JWH307, Win55,212, and CP55,940. All of the tested cannabinoid agonists showed an increase in fluorescence under

test conditions. Further testing of cannabinoid agonists sprayed onto and extracted from plant material using the methods described in chapter 6.0, should be completed. Additionally, testing of street samples of synthetic cannabinoids with common additives and contaminants would be very productive in determining the accuracy and limits of detection for this assay under given test conditions. Currently, work is ongoing to optimize the separation of signal to noise. Further validation and verification studies must be completed.

Testing of the fluorescent guanine nucleotide analog Eu-GTP showed that under our test conditions, the Eu-GTP did not bind to $G\alpha_{i1}$. This could not be used as a basis for a biosensor for agonist cannabinoid agents. Nonspecific artifacts could be seen during this testing.

A rapid and facile method to extract synthetic cannabinoids from leafy substrates in the field has been optimized. Win 55, 212-2 was used as the model synthetic cannabinoid while damaina leaf cuttings were used as a representative substrate material. Both low (2 %) and high (100 %) solvent concentrations were assayed for overall extraction efficiency and it was determined that extraction with pure solvent leads to a much higher yield of cannabinoid with ethanol extracting the largest quantity of cannabinoid. Interestingly, there is no significant different between extraction times of 30 seconds and one minute with hand shaking. Thus, we have determined that extraction of a small amount of substance (~ 10 mg) with 100 % ethanol and 30 seconds of shaking will yield a sufficient amount of synthetic cannabinoid compounds for further analysis techniques. Further studies are needed to determine if these extraction parameters are compatible with both real world "spice" samples and a wide range of synthetic cannabinoid compounds.

Three synthetic cannabinoid-dark quencher conjugates were successfully synthesized and purified during this work, JWH-073:QSY-7 amine, JWH-018:$(PEG)_4$:QSY-7 amine, and JWH-018:QSY-7 amine. To our knowledge, these conjugates are the first successful attempt at linking a dye to a cannabinoid compound. Both of the conjugates eluted as intense and pure peaks with good separation from any contaminants remaining from the reaction. Further study is needed to resolve the cannabinoid receptor binding ability of the conjugates, as the results were often inconsistent. Investigations would suggest that the currently available DQ candidates have too low an affinity for CB_1 to be utilized for a cannabinoid biosensor.

The BODIPY-GTP results were promising for an improved assay to detect current and future synthetic cannabinoids rapidly in a high throughput lab based assay. We have begun discussions with Nanohmics for the development of a handheld,

lightweight, and fieldable sensor that requires minimal manual sample manipulation.

10.0 Appendix

10.1 Cannabinoid Receptor 2 (CB_2) Homology Model Details

SWISS-MODEL Homology Alignment

```
TITLE  SWISS-MODEL
EXPDTA    THEORETICAL MODEL (SWISS-MODEL SERVER)
AUTHOR    SWISS-MODEL WORKSPACE (SEE REFERENCE IN JRNL Records)
REVDAT   1   Tue Dec  6 16:56:08 2011
JRNL        AUTH   ARNOLD K., BORDOLI L., KOPP J., SCHWEDE T.,
JRNL        TITL   SWISS_MODEL WORKSPACE: A WEB-BASED ENVIRONMENT
FOR PROTEIN
JRNL        TITL 2 STRUCTURE HOMOLGY MODELING
JRNL        REF    BIOINFORMATIVS                V.  22  195-201
REMARK   1
REMARK   1 REFERENCE 1
REMARK   1  AUTH   M.C.PEITSCH
REMARK   1  TITL   PROTEIN MODELING BY EMAIL
REMARK   1  REF    BIO/TECHNOLOGY                V.  13   658
1995
REMARK   1  REFN   ISSN 0733-222X
REMARK   1 REFERENCE 2
REMARK   1  AUTH   M.C.PEITSCH,N.GUEX
REMARK   1  TITL   SWISS-MODEL AND THE SWISS-PDBVIEWER: AN
ENVIRONMENT
REMARK   1  TITL 2 FOR COMPARATIVE PROTEIN MODELLING
REMARK   1  REF    ELECTROPHORESIS               V.  18  2714
1997
REMARK   1 REFERENCE 3
REMARK   1  AUTH   T.SCHWEDE,J.KOPP,N.GUEX,M.C.PEITSCH
REMARK   1  TITL   SWISS_MODEL: AN AUTOMATED PROTEIN HOMOLOGY-
MODELING
REMARK   1  TITL 2 SERVER
REMARK   1  REF    NUCLEIC ACIDS RESEARCH        V.  31  3381
2003
REMARK   1  REFN   ASTM NARHAD  UK ISSN 0305-1048
REMARK   1 REFERENCE 4
REMARK   1  AUTH   ARNOLD K., BORDOLI L., KOPP J., SCHWEDE T.,
REMARK   1  TITL   SWISS-MODEL WORKSPACE: A WEB-BASED ENVIRONMENT
FOR PROTEIN
REMARK   1  TITL 2 STRUCTURE HOMOLOGY MODELING
REMARK   1  REF    BIOINFORMATIVS                V.  22  195-201
REMARK   1 ------------------------------------------------------
---------------
REMARK   1 DISCLAIMER
REMARK   1
```

```
REMARK   1 The SWISS-MODEL SERVER produces theoretical  models
for proteins.  The
REMARK   1 results of any  theoretical  modelling  procedure is
NON-EXPERIMENTAL
REMARK   1 and MUST be considered with care. These models may
contain significant
REMARK   1 errors. This  is  especially true  for  automated
modeling since there
REMARK   1 is no human intervention during model building.
REMARK   1 Please read the header section and the logfile
carefully to  know what
REMARK   1 templates and alignments were used during the model
building  process.
REMARK   1 All information by the SWISS-MODEL SERVER is provided
"AS-IS", without
REMARK   1 any warranty, expressed or implied.
REMARK   1
REMARK   1 -------------------------------------------------------
---------------
REMARK   2 -------------------------------------------------------
---------------
REMARK   2 COPYRIGHT NOTICE
REMARK   2
REMARK   2 This  SWISS-MODEL protein model is  copyright. It is
produced by the
REMARK   2 SWISS-MODEL Server Group at Swiss Institute of
Bioinformatics.
REMARK   2 There are no restrictions on the use of individual
models  for your
REMARK   2 or your employer's research projects. If you publish
or patent any
REMARK   2 results obtained from this model, please cite the
papers mentioned
REMARK   2 under JRNL.
REMARK   2
REMARK   2 FAIR USE NOTICE
REMARK   2 Downloading the entire data-base or substantial
portions of it,
REMARK   2 systematic or automatic submission of data, mirroring
the repository,
REMARK   2 or further redistribution of substantial portions data
obtained from
REMARK   2 SWISS-MODEL is prohibited and requires written
permission from the
REMARK   2 SWISS-MODEL Server Group at Swiss Institute of
Bioinformatics.
REMARK   2 -------------------------------------------------------
---------------
```

CLUSTAL O(1.1.0) multiple sequence alignment

```
sp|P34972|CNR2_HUMAN       ----MEECWVTEIANGS----KDGLDSNPMK----
DYMILSGPQKTAV-AVLCTLLGLLS
sp|P07700|ADRB1_MELGA      ----
MGDGWLPPDCGPHNRSGGGGATAAPTGSRQVSAELLSQQWEAGM-SLLMALVVLLI
```

```
sp|P02699|OPSD_BOVIN       MNGTEGPNFYVPF------SNKTGVVRSPFEA---
PQYYLAEPWQFSMLAAYMFLLIMLG
sp|P29274|AA2AR_HUMAN      -----------------------------------
MPIMGSSVY--I-T-VELAIAVLA

:.      : :     : :*

sp|P34972|CNR2_HUMAN
ALENVAVLYLILSSHQLRRKPSYLFIGSLAGADFLASVVFACSFVNFHVFHGVDSKAVFL
sp|P07700|ADRB1_MELGA      VAGNVLVIAAIGRTQRLQT-
LTNLFITSLACADLVMGLLVV-PFGATLVVRGTWLWGSFL
sp|P02699|OPSD_BOVIN       FPINFLTLYVTVQHKKLRT-PLNYILLNLAVADLFMV-
-----FGGFTTTLYTSLHGYFV
sp|P29274|AA2AR_HUMAN      ILGNVLVCWAVWLNSNLQN-
VTNYFVVSLAAADIAVGVLAI-PFAITISTG-------FC
                              *. .        .*:      :: .** **:
*             *

sp|P34972|CNR2_HUMAN       -------
LKIGSVTMTFTASVGSLLLTAIDRYLCLRYPPSYKALLTRGRALVTLGIMWVL
sp|P07700|ADRB1_MELGA      CECWTSLDV-----
LCVTASIETLCVIAIDRYLAITSPFRYQSLMTRARAKVIICTVWAI
sp|P02699|OPSD_BOVIN
FGPTGCNLEGFFATLGGEIALWSLVVLAIERYVVVCKPMSNFRF-GENHAIMGVAFTWVM
sp|P29274|AA2AR_HUMAN
AACHGCLFIACFVLVLTQSSIFSLLAIAIDRYIAIRIPLRYNGLVTGTRAKGIIAICWVL
                                          :    :: :*   **:**: :  *
:    :*   :   *.:

sp|P34972|CNR2_HUMAN       SALVSYLPL-MGWTCCPRPCSE---------------
LFPLIPNDYLLSWLLFIAFLFSG
sp|P07700|ADRB1_MELGA      SALVSFLPIMMHWWRDEDPQAL-----
KCYQDPGCCDFVTNR--AYA-IASSIISFYIPL
sp|P02699|OPSD_BOVIN       ALACAAPPL-VGWSRYIPEGMQ----CSCGIDY--
YTPHEETNNESFVIYMFVVHFIIPL
sp|P29274|AA2AR_HUMAN      SFAIGLTPM-
LGWNNCGQPKEGKNHSQGCGEGQVACLFEDVVPMNYMVYFNFFACVLVPL
                           :   .  *: : *
.  . .

sp|P34972|CNR2_HUMAN       --IIYTYGHVLWKAHQHVASLS-------GHQDR----
----------------QVPGMA
sp|P07700|ADRB1_MELGA
LIMIFVYLRVYREAKEQIRKIDRCEGRFYGSQEQPQPPPLPQHQPILGNGRASKRKTSRV
sp|P02699|OPSD_BOVIN       IVIFFCYGQLVFTVKEAAAQQQE---------------
-------------------SAT
sp|P29274|AA2AR_HUMAN      LLMLGVYLRIFLAARRQLKQMES--------------
QPLP------GE-------RARS
                             ::  * ::   .:.   . .
.

sp|P34972|CNR2_HUMAN       RMRLDVRLAKTLGLVLAVLLICWFPVLALMAHSL-
ATTLSDQVKKAFAFCSMLCLINSMV
sp|P07700|ADRB1_MELGA
MAMREHKALKTLGIIMGVFTLCWLPFFLVNIVNVFNRDL--VPDWLFVFFNWLGYANSAF
sp|P02699|OPSD_BOVIN       TQKAEKEVTRMVIIMVIAFLICWLPYAGVAFYIF-
THQGSDFGPIFMTIPAFFAKTSAVY
```

```
sp|P29274|AA2AR_HUMAN
TLQKEVHAAKSLAIIVGLFALCWLPLHIINCFTFFCPDCSHAPLWLMYLAIVLSHTNSVV
                              : .  : : :::  : :**:*   :    .
: :   :   .:

sp|P34972|CNR2_HUMAN       NPVIYALRSGEIRSSAHHCLAHWKKCV----
RGLGSEAKEEAPRSSVTETEADGKI----
sp|P07700|ADRB1_MELGA      NPIIYCR-SPDFRKAFKRLLCFPRKA-
DRRLHAGGQPAPLP-----------GGFISTLG
sp|P02699|OPSD_BOVIN       NPVIYIMMNKQFRNCMVTTLCCGKNP----
LGDDEASTTVSKTETSQV------------
sp|P29274|AA2AR_HUMAN
NPFIYAYRIREFRQTFRKIIRSHVLRQQEPFKAAGTSARVL------AAHGSDGEQVSLR
                           **.**     ::*.     :                :

sp|P34972|CNR2_HUMAN       -------TPWPDSRDLD-----------LSDC------
----------------------
sp|P07700|ADRB1_MELGA      SPEHSPGGTWSDCNGGT-------------
RGGSESSLEERHSKTSRSESKMEREKNILA
sp|P02699|OPSD_BOVIN       ----APA------------------------------
----------------------
sp|P29274|AA2AR_HUMAN      -LNGHPPGVWANGSAPHPERRPNGYALGLVSGGSAQE-
--SQGNTGLPDVE---------


sp|P34972|CNR2_HUMAN       --------------------------------------
----------------
sp|P07700|ADRB1_MELGA
TTRFYCTFLGNGDKAVFCTVLRIVKLFEDATCTCPHTHKLKMKWRFKQHQA---
sp|P02699|OPSD_BOVIN       --------------------------------------
----------------
sp|P29274|AA2AR_HUMAN      ------------------------
LLSHELKGVCPEPPGLDDPL--AQDGAGVS
```

10.2 CHARMM Parameters (ParamChem) for Select Cannabinoids

CHARMM Charge Parameters for Virodhamine

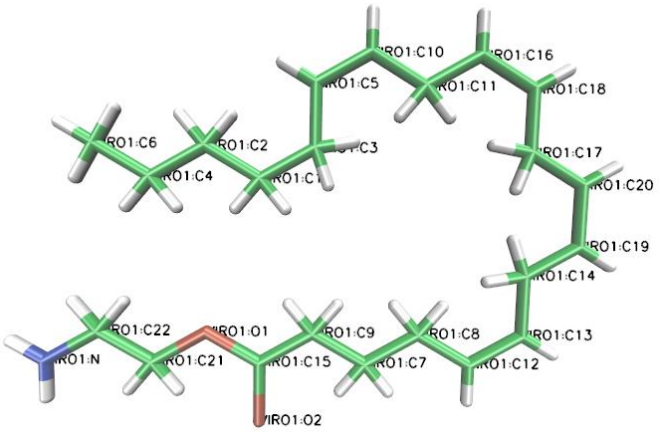

```
RESI VIRO        0.000 ! param penalty=  17.800 ; charge
penalty=   5.566
GROUP            ! CHARGE   CH_PENALTY
ATOM O1     OG302  -0.491 !    1.675
ATOM O2     OG2D1  -0.629 !    0.000
ATOM N      NG321  -0.975 !    5.045
ATOM C1     CG321  -0.179 !    0.000
ATOM C2     CG321  -0.178 !    0.000
ATOM C3     CG321  -0.181 !    0.000
ATOM C4     CG321  -0.183 !    0.000
ATOM C5     CG2D1  -0.150 !    0.000
ATOM C6     CG331  -0.269 !    0.000
ATOM C7     CG321  -0.178 !    0.000
ATOM C8     CG321  -0.181 !    0.000
ATOM C9     CG321  -0.221 !    0.000
ATOM C10    CG2D1  -0.149 !    0.000
ATOM C11    CG321  -0.182 !    0.000
ATOM C12    CG2D1  -0.150 !    0.000
ATOM C13    CG2D1  -0.149 !    0.000
ATOM C14    CG321  -0.182 !    0.000
ATOM C15    CG2O2   0.900 !    0.000
ATOM C16    CG2D1  -0.149 !    0.000
ATOM C17    CG321  -0.182 !    0.000
ATOM C18    CG2D1  -0.149 !    0.000
ATOM C19    CG2D1  -0.149 !    0.000
ATOM C20    CG2D1  -0.149 !    0.000
ATOM C21    CG321   0.075 !    5.029
ATOM C22    CG321   0.118 !    5.566
ATOM H1     HGA2    0.090 !    0.000
ATOM H2     HGA2    0.090 !    0.000
ATOM H3     HGA2    0.090 !    0.000
ATOM H4     HGA2    0.090 !    0.000
ATOM H5     HGA2    0.090 !    0.000
ATOM H6     HGA2    0.090 !    0.000
ATOM H7     HGA2    0.090 !    0.000
ATOM H8     HGA2    0.090 !    0.000
ATOM H9     HGA4    0.150 !    0.000
ATOM H10    HGA3    0.090 !    0.000
ATOM H11    HGA3    0.090 !    0.000
ATOM H12    HGA3    0.090 !    0.000
ATOM H13    HGA2    0.090 !    0.000
ATOM H14    HGA2    0.090 !    0.000
ATOM H15    HGA2    0.090 !    0.000
ATOM H16    HGA2    0.090 !    0.000
ATOM H17    HGA2    0.090 !    0.000
ATOM H18    HGA2    0.090 !    0.000
ATOM H19    HGA4    0.150 !    0.000
ATOM H20    HGA2    0.090 !    0.000
ATOM H21    HGA2    0.090 !    0.000
ATOM H22    HGA4    0.150 !    0.000
ATOM H23    HGA4    0.150 !    0.000
ATOM H24    HGA2    0.090 !    0.000
```

```
ATOM H25    HGA2    0.090 !    0.000
ATOM H26    HGA4    0.150 !    0.000
ATOM H27    HGA2    0.090 !    0.000
ATOM H28    HGA2    0.090 !    0.000
ATOM H29    HGA4    0.150 !    0.000
ATOM H30    HGA4    0.150 !    0.000
ATOM H31    HGA4    0.150 !    0.000
ATOM H32    HGA2    0.090 !    0.510
ATOM H33    HGA2    0.090 !    0.510
ATOM H34    HGA2    0.090 !    0.000
ATOM H35    HGA2    0.090 !    0.000
ATOM H36    HGPAM2  0.341 !    0.720
ATOM H37    HGPAM2  0.341 !    0.720
```

CHARMM Charge Parameters for AM2201

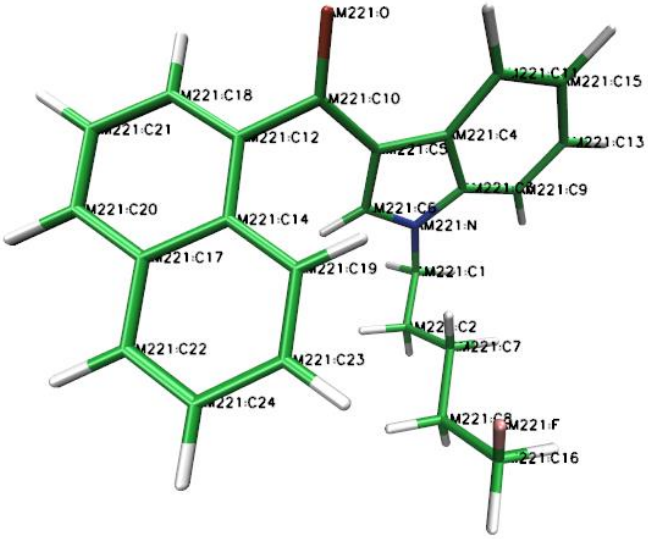


```
RESI AM22   0.000
GROUP            ! CHARGE
ATOM F      FGA1   -1.908
ATOM O      OG2D3  -0.462
ATOM N      NG2R51 -0.952
ATOM C1     CG321  -0.278
ATOM C2     CG321   0.606
ATOM C3     CG2RC0 -0.528
ATOM C4     CG2RC0 -0.290
ATOM C5     CG2R51 -0.862
ATOM C6     CG2R51  0.854
ATOM C7     CG321  -0.145
ATOM C8     CG321  -0.774
ATOM C9     CG2R61 -0.277
ATOM C10    CG2O5  -0.684
ATOM C11    CG2R61 -0.393
ATOM C12    CG2R61 -0.470
ATOM C13    CG2R61  0.513
ATOM C14    CG2R61  0.396
```

```
ATOM C15    CG2R61  0.092
ATOM C16    CG322  -0.397
ATOM C17    CG2R61 -0.344
ATOM C18    CG2R61 -0.093
ATOM C19    CG2R61 -0.869
ATOM C20    CG2R61 -0.271
ATOM C21    CG2R61  0.081
ATOM C22    CG2R61 -0.271
ATOM C23    CG2R61 -0.493
ATOM C24    CG2R61 -0.973
ATOM H1     HGA2    0.377
ATOM H2     HGA2    0.377
ATOM H3     HGA2    0.264
ATOM H4     HGA2    0.264
ATOM H5     HGR52   0.294
ATOM H6     HGA2    0.862
ATOM H7     HGA2    0.862
ATOM H8     HGA2    0.541
ATOM H9     HGA2    0.541
ATOM H10    HGR61   0.065
ATOM H11    HGR61   0.067
ATOM H12    HGR61   0.187
ATOM H13    HGR61   0.740
ATOM H14    HGA6    0.591
ATOM H15    HGA6    0.591
ATOM H16    HGR61   0.105
ATOM H17    HGR61   0.310
ATOM H18    HGR61   0.244
ATOM H19    HGR61   0.287
ATOM H20    HGR61   0.244
ATOM H21    HGR61   0.592
ATOM H22    HGR61   0.519
```

SWISS-MODEL Workspace

Workunit: P000008 Title:cb2-align_B1ARTU_RHODSQ_AA2RHU

Model Summary:

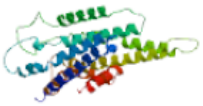

Model information:

Modelled residue range: 1 to 291

Based on template:

Quality information:

QMEAN Z-Score: -7.183

Quaternary structure information:

Ligand information:

Global Model Quality Estimation:

QMEAN4 global scores:

QMEANscore4: 0.292

Estimated absolute model quality:

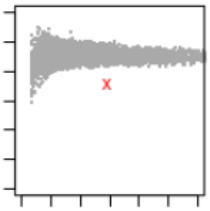

Z-Score: -7.183

Score components:

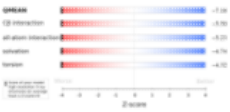

Local scores:

Coloring by residue error:

Residue error plot:

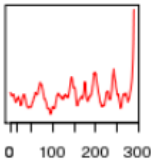

QMEAN4 global scores:

The QMEAN4 score is a composite score consisting of a linear combination of 4 statistical potential terms (estimated model reliability between 0-1). The pseudo-energies of the contributing terms are given below together with their Z-scores with respect to scores obtained for high-resolution experimental structures of similar size solved by X-ray crystallography:

Scoring function term	Raw score	Z-score
C_beta interaction energy	134.77	-5.50
All-atom pairwise energy	2399.24	-5.23
Solvation energy	17.23	-4.74
Torsion angle energy	0.25	-4.32
QMEAN4 score	0.292	-7.18

If you publish results from QMEAN, please cite the following paper:

Benkert P, Biasini M, Schwede T. (2011). "Toward the estimation of the absolute quality of individual protein structure models." Bioinformatics, 27(3):343-50.

11.0 References

1. Penn, H.J., et al., *Detection of synthetic cannabinoids in herbal incense products.* Clin Biochem, 2011. **44**(13): p. 1163-5.

2. Zuba, D. and B. Byrska, *Analysis of the prevalence and coexistence of synthetic cannabinoids in "herbal high" products in Poland.* Forensic Toxicology, 2013. **31**(1): p. 21-30.

3. Gerona, R.R.L., E. Birsdall, and A.H. Wu, *Non-targeted Analysis of Synthetic Cannabinoids in Two Intoxication Cases Involving Herbal Incense Products.* American Journal of Clinical Pathology, 2011. **136**(3): p. 474-475.

4. Langman, L.J., et al., *Synthetic cannabinoids detected in select "herbal incense" products.* Therapeutic Drug Monitoring, 2011. **33**(4): p. 471-471.

5. Uchiyama, N., et al., *Chemical analysis of synthetic cannabinoids as designer drugs in herbal products.* Forensic Science International, 2010. **198**(1-3): p. 31-38.

6. Oyemade, A., *Adverse effects and detection of synthetic cannabinoids.* Am J Addict, 2012. **21**(6): p. 568-9.

7. Simolka, K., et al., *Analysis of synthetic cannabinoids in "spice-like" herbal highs: snapshot of the German market in summer 2011.* Anal Bioanal Chem, 2012. **404**(1): p. 157-71.

8. Uchiyama, N., et al., *Chemical analysis of synthetic cannabinoids as designer drugs in herbal products.* Forensic Sci Int, 2010. **198**(1-3): p. 31-8.

9. Hudson, S. and J. Ramsey, *The emergence and analysis of synthetic cannabinoids.* Drug Test Anal, 2011. **3**(7-8): p. 466-78.

10. Logan, B.K., et al., *Identification of synthetic cannabinoids in herbal incense blends in the United States.* J Forensic Sci, 2012. **57**(5): p. 1168-80.

11. Piggee, C., *Investigating a not-so-natural high Researchers identify synthetic cannabinoids in herbal incense.* Analytical Chemistry, 2009. **81**(9): p. 3205-3207.

12. Camp, N.E., *Synthetic cannabinoids.* J Emerg Nurs, 2011. **37**(3): p. 292-3.

13. Penders, T. and S. Saeed, *Synthetic cannabinoids and "bath salts" should be considered drugs of abuse.* Am Fam Physician, 2012. **85**(9): p. 852.

14. Ashton, J.C., *Synthetic cannabinoids as drugs of abuse.* Curr Drug Abuse Rev, 2012. **5**(2): p. 158-68.

15. Platteborze, P.L. and T.M. Martin, *Re: "Spice, bath salts, and the U.S. Military: the emergence of synthetic cannabinoid receptor agonists and cathinones in the U.S. Armed Forces"*. Mil Med, 2013. **178**(1): p. v.

16. Loeffler, G., et al., *Spice, bath salts, and the U.S. military: the emergence of synthetic cannabinoid receptor agonists and cathinones in the U.S. Armed Forces.* Mil Med, 2012. **177**(9): p. 1041-8.

17. Crime, U.N.O.o.D.a., *Synthetic cannabinoids in herbal products.* UN Document, 2011(SCITEC/24): p. 24.

18. McGuinness, T.M. and D. Newell, *Risky recreation: synthetic cannabinoids have dangerous effects.* J Psychosoc Nurs Ment Health Serv, 2012. **50**(8): p. 16-8.

19. Seely, K.A., et al., *Spice drugs are more than harmless herbal blends: A review of the pharmacology and toxicology of synthetic cannabinoids.* Prog Neuropsychopharmacol Biol Psychiatry, 2012. **39**(2): p. 234-43.

20. Ashton, C.H. and P.B. Moore, *Regulation of synthetic cannabinoids.* Lancet, 2009. **374**(9701): p. 1595.

21. Psychoyos, D. and K.Y. Vinod, *Marijuana, Spice 'herbal high', and early neural development: implications for rescheduling and legalization.* Drug Testing and Analysis, 2013. **5**(1): p. 27-45.

22. Lindigkeit, R., et al., *Spice: a never ending story?* Forensic Sci Int, 2009. **191**(1-3): p. 58-63.

23. King, L.A., *Legal controls on cannabimimetics: An international dilemma?* Drug Test Anal, 2013.

24. Darmani, N.A., *Delta(9)-tetrahydrocannabinol and synthetic cannabinoids prevent emesis produced by the cannabinoid CB(1) receptor antagonist/inverse agonist SR 141716A.* Neuropsychopharmacology, 2001. **24**(2): p. 198-203.

25. Console-Bram, L., J. Marcu, and M.E. Abood, *Cannabinoid receptors: nomenclature and pharmacological principles.* Prog Neuropsychopharmacol Biol Psychiatry, 2012. **38**(1): p. 4-15.

26. Svizenska, I., P. Dubovy, and A. Sulcova, *Cannabinoid receptors 1 and 2 (CB1 and CB2), their distribution, ligands and functional involvement in nervous system structures - A short review.* Pharmacology Biochemistry and Behavior, 2008. **90**(4): p. 501-511.

27. Grotenhermen, F. and K. Muller-Vahl, *The Therapeutic Potential of Cannabis and Cannabinoids.* Deutsches Arzteblatt International, 2012. **109**(29-30): p. 495-U39.

28. Hermanns-Clausen, M., et al., *Acute toxicity due to the confirmed consumption of synthetic cannabinoids: Clinical and laboratory findings.* Addiction, 2012.

29. Cohen, J., et al., *Clinical presentation of intoxication due to synthetic cannabinoids.* Pediatrics, 2012. **129**(4): p. e1064-7.

30. Tomiyama, K. and M. Funada, *Cytotoxicity of synthetic cannabinoids found in "Spice" products: the role of cannabinoid receptors and the caspase cascade in the NG 108-15 cell line.* Toxicol Lett, 2011. **207**(1): p. 12-7.

31. Brakoulias, V., *Products containing synthetic cannabinoids and psychosis.* Aust N Z J Psychiatry, 2012. **46**(3): p. 281-2.

32. Ginsburg, B.C., et al., *Purity of synthetic cannabinoids sold online for recreational use.* J Anal Toxicol, 2012. **36**(1): p. 66-8.

33. Nutt, D., *Consideration of the major cannabinoid agonists.* Advisory Council on the Misuse of Drugs Report, 2009: p. 29.

34. Kneisel, S., V. Auwarter, and J. Kempf, *Analysis of 30 synthetic cannabinoids in oral fluid using liquid chromatography-electrospray ionization tandem mass spectrometry.* Drug Test Anal, 2012.

35. Kneisel, S. and V. Auwarter, *Analysis of 30 synthetic cannabinoids in serum by liquid chromatography-electrospray ionization tandem mass spectrometry after liquid-liquid extraction.* J Mass Spectrom, 2012. **47**(7): p. 825-35.

36. Merola, G., et al., *Analysis of synthetic cannabinoids in herbal blends by means of nano-liquid chromatography.* J Pharm Biomed Anal, 2012. **71**: p. 45-53.

37. Grabenauer, M., et al., *Analysis of synthetic cannabinoids using high-resolution mass spectrometry and mass defect filtering: implications for nontargeted screening of designer drugs.* Anal Chem, 2012. **84**(13): p. 5574-81.

38. Ammann, J., et al., *Detection and quantification of new designer drugs in human blood: Part 1 - Synthetic cannabinoids.* J Anal Toxicol, 2012. **36**(6): p. 372-80.

39. Sobolevsky, T., I. Prasolov, and G. Rodchenkov, *Detection of urinary metabolites of AM-2201 and UR-144, two novel synthetic cannabinoids.* Drug Test Anal, 2012.

40. Hutter, M., et al., *Determination of 22 synthetic cannabinoids in human hair by liquid chromatography-tandem mass spectrometry.* J Chromatogr B Analyt Technol Biomed Life Sci, 2012. **903**: p. 95-101.

41. Dresen, S., et al., *Development and validation of a liquid chromatography-tandem mass spectrometry method for the quantitation of synthetic cannabinoids of the aminoalkylindole type and methanandamide in serum and its application to forensic samples.* J Mass Spectrom, 2011. **46**(2): p. 163-71.

42. Musah, R.A., et al., *Direct analysis in real time mass spectrometry with collision-induced dissociation for structural analysis of synthetic cannabinoids.* Rapid Commun Mass Spectrom, 2012. **26**(19): p. 2335-42.

43. Moosmann, B., et al., *A fast and inexpensive procedure for the isolation of synthetic cannabinoids from 'Spice' products using a flash chromatography system.* Anal Bioanal Chem, 2012.

44. Bailey, K., D. Legault, and D. Verner, *Identification of synthetic cannabinoids by gas chromatography.* J Chromatogr, 1973. **87**(1): p. 263-6.

45. Hutter, M., et al., *Identification of the major urinary metabolites in man of seven synthetic cannabinoids of the aminoalkylindole type present as adulterants in 'herbal mixtures' using LC-MS/MS techniques.* J Mass Spectrom, 2012. **47**(1): p. 54-65.

46. de Jager, A.D., et al., *LC-MS/MS method for the quantitation of metabolites of eight commonly-used synthetic cannabinoids in human urine--an Australian perspective.* J Chromatogr B Analyt Technol Biomed Life Sci, 2012. **897**: p. 22-31.

47. Musah, R.A., et al., *Rapid identification of synthetic cannabinoids in herbal samples via direct analysis in real time mass spectrometry.* Rapid Commun Mass Spectrom, 2012. **26**(9): p. 1109-14.

48. Cox, A.O., et al., *Use of SPME-HS-GC-MS for the analysis of herbal products containing synthetic cannabinoids.* J Anal Toxicol, 2012. **36**(5): p. 293-302.

49. Griep, M.H., et al., *Quantum dot enhancement of bacteriorhodopsin-based electrodes.* Biosensors and Bioelectronics, 2010. **25**(6): p. 1493-1497.

50. Griep, M.H., et al., *Optical Protein Modulation via Quantum Dot Coupling and Use of a Hybrid Sensor Protein.* Journal of Nanoscience and Nanotechnology, 2010. **10**: p. 6029-6035.

51. Griep, M.H., et al., *Forster Resonance Energy Transfer Between Quantum Dots and Bacteriorhodopsin.* Molecular Biology International, 2012. **2012**(910707): p. 7.

52. Sellers, M.S. and M.M. Hurley, *XPairIt Docking Protocol for peptide docking and analysis.* Molecular Simulation, 2015(ahead-of-print): p. 1-13.

53. Schmidt, M.W., et al., *General atomic and molecular electronic structure system.* Journal of Computational Chemistry, 1993. **14**(11): p. 1347-1363.

54. Jiang, W., et al., *High-performance scalable molecular dynamics simulations of a polarizable force field based on classical Drude oscillators in NAMD.* J Phys Chem Lett, 2011. **2**(2): p. 87-92.

55. Phillips, J.C., et al., *Scalable molecular dynamics with NAMD.* J Comput Chem, 2005. **26**(16): p. 1781-802.

56. Shim, J.-Y., *Understanding functional residues of the cannabinoid CB1 receptor for drug discovery.* Current topics in medicinal chemistry, 2010. **10**(8): p. 779.

57. Lynch, D.L. and P.H. Reggio, *Cannabinoid CB1 receptor recognition of endocannabinoids via the lipid bilayer: molecular dynamics simulations of CB1 transmembrane helix 6 and anandamide in a phospholipid bilayer.* J Comput Aided Mol Des, 2006. **20**(7-8): p. 495-509.

58. Nebane, N.M., et al., *Residues accessible in the binding-site crevice of transmembrane helix 6 of the CB2 cannabinoid receptor.* Biochemistry, 2008. **47**(52): p. 13811-21.

59. Hurst, D.P., et al., *A lipid pathway for ligand binding is necessary for a cannabinoid G protein-coupled receptor.* Journal of Biological Chemistry, 2010. **285**(23): p. 17954-17964.

60. Latek, D., et al., *Modeling of ligand binding to G protein coupled receptors: cannabinoid CB1, CB2 and adrenergic β2AR.* Journal of molecular modeling, 2011. **17**(9): p. 2353-2366.

61. Poso, A. and J. Huffman, *Targeting the cannabinoid CB2 receptor: modelling and structural determinants of CB2 selective ligands.* British journal of pharmacology, 2008. **153**(2): p. 335-346.

62. Raitio, K., et al., *Targeting the cannabinoid CB2 receptor: mutations, modeling and development of CB2 selective ligands.* Current medicinal chemistry, 2005. **12**(10): p. 1217-1237.

63. Tuccinardi, T., et al., *Cannabinoid CB2/CB1 selectivity. Receptor modeling and automated docking analysis.* Journal of medicinal chemistry, 2006. **49**(3): p. 984-994.

64. Brooks, B.R., et al., *CHARMM: the biomolecular simulation program.* Journal of computational chemistry, 2009. **30**(10): p. 1545-1614.

65. Vanommeslaeghe, K., et al., *CHARMM general force field: A force field for drug-like molecules compatible with the CHARMM all-atom additive biological force fields.* Journal of computational chemistry, 2010. **31**(4): p. 671-690.

66. Mayne, C.G., et al., *Rapid parameterization of small molecules using the force field toolkit.* Journal of computational chemistry, 2013. **34**(32): p. 2757-2770.

67. Humphrey, W., A. Dalke, and K. Schulten, *VMD: visual molecular dynamics.* Journal of molecular graphics, 1996. **14**(1): p. 33-38.

68. Frisch, M., et al., *Gaussian 03, revision D. 01*. Gaussian Inc., Wallingford, CT, 2004. **26**.

69. Bhatnagar, N., et al., *Direct calculation of 1-octanol–water partition coefficients from adaptive biasing force molecular dynamics simulations.* The Journal of chemical physics, 2012. **137**(1): p. 014502.

70. Garrido, N.M., Queimada, A.J., Jorge, M., Macedo, E.A., Economou, I.G. , *1-Octanol/Water Partition Coefficients of n-Alkanes from Molecular Simulations of Absolute Solvation Free Energies.* J Chem. Theor. Comp., 2009. **5**: p. 2436-2446.

71. Tian, X., et al., *The conformation, location, and dynamic properties of the endocannabinoid ligand anandamide in a membrane bilayer.* Journal of Biological Chemistry, 2005. **280**(33): p. 29788-29795.

72. Yeliseev, A.A., et al., *Expression of human peripheral cannabinoid receptor for structural studies.* Protein Science, 2005. **14**(10): p. 2638-2653.

73. Ritchie, T.K., et al., *Chapter 11 Reconstitution of Membrane Proteins in Phospholipid Bilayer Nanodiscs*, in *Methods in Enzymology*, D. Nejat, Editor. 2009, Academic Press. p. 211-231.

74. Bayburt, T.H. and S.G. Sligar, *Membrane protein assembly into Nanodiscs.* FEBS Letters, 2010. **584**(9): p. 1721-1727.

75. Bayburt, T.H. and S.G. Sligar, *Self-assembly of single integral membrane proteins into soluble nanoscale phospholipid bilayers.* Protein Science, 2003. **12**(11): p. 2476-2481.

76. Porter, A.C., et al., *Characterization of a Novel Endocannabinoid, Virodhamine, with Antagonist Activity at the CB1 Receptor.* Journal of Pharmacology and Experimental Therapeutics, 2002. **301**(3): p. 1020-1024.

77. Sharir, H., et al., *The Endocannabinoids Anandamide and Virodhamine Modulate the Activity of the Candidate Cannabinoid Receptor GPR55.* Journal of Neuroimmune Pharmacology: p. 1-10.

78. Ryberg, E., et al., *The orphan receptor GPR55 is a novel cannabinoid receptor.* British Journal of Pharmacology, 2007. **152**(7): p. 1092-1101.

79. Medintz, I.L., et al., *Self-assembled nanoscale biosensors based on quantum dot FRET donors.* Nat Mater, 2003. **2**(9): p. 630-638.

80. Salomone, A., et al., *Simultaneous analysis of several synthetic cannabinoids, THC, CBD and CBN, in hair by ultra-high performance liquid chromatography tandem mass spectrometry. Method validation and application to real samples.* J Mass Spectrom, 2012. **47**(5): p. 604-10.

81. Heshmatolla, A.T., M and Mahdavi, N., *One Pot Reductive Amination of Carbonyl Compounds Using Sodium Borohydride-Amberlyst 15.* Chemical Communications, 2010. **40**: p. 951-956.

82. Forster, T., *Transfer mechanisms of electronic excitation.* Discuss Faraday Soc., 1959. **27**.

83. Medintz, I.L., et al., *A fluorescence resonance energy transfer-derived structure of a quantum dot-protein bioconjugate nanoassembly.* PNAS, 2004. **101**(26): p. 9612-9617.

84. Dennis, A.M. and G. Bao, *Quantum Dot-Fluorescent Protein Pairs as Novel Fluorescence Resonance Energy Transfer Probes.* Nano Lett., 2008. **8**(5): p. 1439-1445.

85. Clapp, A.R., et al., *Fluorescence resonance energy transfer between quantum dot donors and dye-labeled protein acceptors.* J. Am. Chem. Soc., 2004. **126**: p. 301-310.

86. Alivisatos, P., *The use of nanocrystals in biological detection.* Nature Biotechnology, 2004. **22**(1).

87. Weiss, S., *Fluorescence Spectroscopy of Single Biomolecules.* Science, 1999. **283**(5408): p. 1676-1683.

88. Jankovics, P., et al., *Detection and identification of the new potential synthetic cannabinoids 1-pentyl-3-(2-iodobenzoyl)indole and 1-pentyl-3-(1-adamantoyl)indole in seized bulk powders in Hungary.* Forensic Sci Int, 2012. **214**(1-3): p. 27-32.

89. Wu, Y.C. and W.F. Koch, *Absolute Determination of Electrolytic Conductivity for Primary Standard Kcl Solutions from 0-Degrees-C to 50-Degrees-C.* Journal of Solution Chemistry, 1991. **20**(4): p. 391-401.

90. Ogata, J., et al., *DNA sequence analyses of blended herbal products including synthetic cannabinoids as designer drugs.* Forensic Sci Int. **227**(1-3): p. 33-41.

List of Symbols, Abbreviations, and Acronyms

bR	Bacteriorhodopsin
BSA	Bovine Serum Albumin
CB	Cannabinoid receptor
CHARMM	Chemistry at HARvard Molecular Mechanics
DMSO	Dimethyl Sulfoxide
DQ	Dark Quencher
EDC	1-Ethyl-3-(3 dimethylaminopropyl) carbodimide
ESI	Electrospray Ionisation
Eu	Europium
FFTK	Force Field Tool Kit
FPLC	Fast Protein Liquid Chromatography
FRET	Förster Resonance Energy Transfer
ΔG	Gibbs free energy difference
GDP	Guanosine Diphosphate
GPCR	G-Protein Coupled Receptor
GRP	Guanosine Triphosphate
HPLC	High Performance Liquid Chromatography
LED	Light Emitting Diode
QD	Quantum Dots
MS	Mass Spectrometry
MSP	Membrane Scaffold Protein
NAMD	NAnoscale Molecular Dynamics
NMR	Nuclear Magnetic Resonance
PEG	Polyethylene Glycol
R	Ideal gas constant

SC	Synthetic Cannabinoid
Sulfo-NHS	N-hydroxysulfosuccinimide
T	Temperature
TEM	Transmission Electron Microscopy
THC	Tetrahydrocannabinol
TM	Transmembrane
UV-vis	Ultraviolet-Visible
VMD	Visual Molecular Dynamics

INTENTIONALLY LEFT BLANK.